Russian Original Vol. 39, No. 1, July, 1975
January, 1976

SATEAZ 39(1) 571-666 (1975)

SOVIET ATOMIC ENERGY

АТОМНАЯ ЭНЕРГИЯ
(ATOMNAYA ÉNERGIYA)

TRANSLATED FROM RUSSIAN

c/b CONSULTANTS BUREAU, NEW YORK

SOVIET ATOMIC ENERGY

Soviet Atomic Energy is a cover-to-cover translation of *Atomnaya Énergiya*, a publication of the Academy of Sciences of the USSR.

An agreement with the Copyright Agency of the USSR (VAAP) makes available both advance copies of the Russian journal and original glossy photographs and artwork. This serves to decrease the necessary time lag between publication of the original and publication of the translation and helps to improve the quality of the latter. The translation began with the first issue of the Russian journal.

Consultants Bureau journals appear about six months after the publication of the original Russian issue. For bibliographic accuracy, the English issue published by Consultants Bureau carries the same number and date as the original Russian from which it was translated. For example, a Russian issue published in December will appear in a Consultants Bureau English translation about the following June, but the translation issue will carry the December date. When ordering any volume or particular issue of a Consultants Bureau journal, please specify the date and, where applicable, the volume and issue numbers of the original Russian. The material you will receive will be a translation of that Russian volume or issue.

Subscription
$87.50 per volume (6 issues)

Single Issue: $50
Single Article: $15

Prices somewhat higher outside the United States.

CONSULTANTS BUREAU, NEW YORK AND LONDON

227 West 17th Street
New York, New York 10011

4a Lower John Street
London W1R 3PD
England

Published monthly. Second-class postage paid at Jamaica, New York 11431.

Soviet Atomic Energy is abstracted or indexed in *Applied Mechanics Reviews, Chemical Abstracts, Engineering Index, INSPEC—Physics Abstracts and Electrical and Electronics Abstracts, Current Contents,* and *Nuclear Science Abstracts.*

SOVIET ATOMIC ENERGY

A translation of *Atomnaya Énergiya*

January, 1976

Volume 39, Number 1 July, 1975

CONTENTS

CONTENTS

(continued)

CONTENTS

(continued)

The Russian press date (podpisano k pechati) of this issue was 6/26/1975. **Publication therefore did not occur prior to this date, but must be assumed to have taken place reasonably soon thereafter.**

INVESTIGATION OF THE PHYSICAL CHARACTERISTICS OF THE REACTOR DURING STARTUP OF THE FIRST UNIT OF THE BILIBINSK NUCLEAR POWER STATION

A. A. Vaimugin, V. V. Bondarenko, V. K. Goryunov, A. V. Gusev, B. G. Dubovskii, P. G. Dushin, A. N. Efeshin, L. D. Kirillovykh, I. M. Kisil', V. I. Kozlov, O. V. Komissarov, E. V. Koryagin, A. G. Kostromin, N. I. Lagosha, M. A. Lyutov, M. E. Minashin, K. N. Mokhnatkin, A. P. Pan'ko, Yu. F. Taskaev, V. N. Sharapov, and A. I. Shtyfurko.

UDC 621.039.524.2:621.039.519

As already reported [1], the Bilibinsk Nuclear Power Station will consist of four units with reactors of the same type. In the period from 10 to 31 December, 1973, physical startup of the reactor of the first unit was effected* and on January 12, 1974 the Bilibinsk Nuclear Power Station produced electric current for the first time.

During startup of the reactor of the first unit, detailed investigations were undertaken of the physical characteristics of the active zone in order to introduce, if required, any necessary changes in the loading of the reactors of subsequent units. The startup program, therefore, in addition to determining the characteristics of the reactor necessary for operation, provided for a number of other measurements, in particular, determination of the parameters of critical assemblies which was necessary for verification of the accuracy of the design procedures used in planning.

*The second unit of the nuclear power station was brought on stream at the end of 1974.

TABLE 1. Physical Characteristics of Assemblies

Assembly	Critical number of FC-3		Material parameter, m^{-2}	
	experiment	calculation	experiment	calculation
I	38,3±0,2	39	6,5±0,6	5,9
II	55,2±0,2	55	4,7±0,5	4,6
III	50,8±0,2	46	4,4±0,5	4,5
IV	63,5±0,2	58	—	3,9

TABLE 2. Change of Reactivity on Withdrawal of FC-3 with Water ($\Delta\rho^{FC}$) and with the Water Removed from It ($\Delta\rho_{H_2O}$)

Assembly	Coordinates of cell*	$\Delta\rho^{FC}\cdot 10^3$	$\Delta\rho_{H_2O}\cdot 10^4$
I	11—11	—4,4±0,2	—1,52±0,08
	11—10	—3,9±0,2	—
	11—08	—2,9±0,2	—0,41±0,02
III	11—11	—	—0,65±0,03
	11—10	—	—0,67±0,03
	11—14	—	—0,25±0,02
	12—07	—2,7±0,2	—

*Here and in future, the first two figures signify the number of the row and the next two figures signify the number of the cell in the row (see Fig. 1, a).

Translated from Atomnaya Énergiya, Vol. 39, No. 1, pp. 3-8. July, 1975. Original article submitted September 13, 1974.

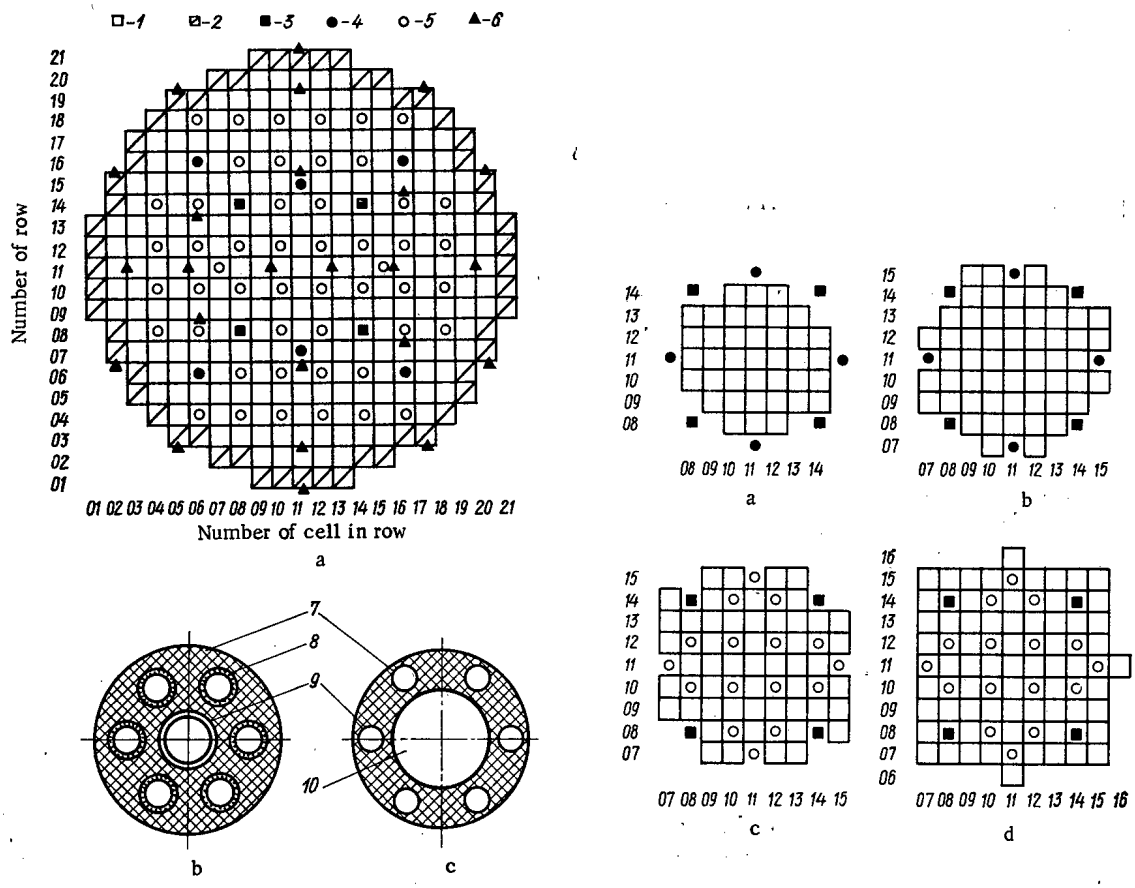

Fig. 1. Record chart of the reactor (a), transverse sections of a fuel channel (b) and a control and safety rod channel (c): 1, 2) Cells with fuel channels FC-3 and FC-3.3; 3, 4, 5) Automatic control rods (ACR), scram rods (SR) and manual control rods (MCR); 6) Neutron flux sensors; 7) Graphite brickwork; 8) Fuel element; 9) Steel tube; 10) Opening for control and safety rod.

Fig. 2. Record charts of critical assemblies I-IV (a-d): □) Cell with fuel channel FC-3; ●, ■, ○) Channels for scram rods, ACR and MCR.

TABLE 3. Change of Reactivity on Withdrawal of the Control and Safety Rod Channel with Water ($\Delta\rho^{CS}$), and the Graphite Plug ($\Delta\rho^{g}$) from cell 12-12

Assembly	$\Delta\rho^{CS}\cdot 10^3$	$\Delta\rho^{g}\cdot 10^3$
III	2,8±0,2	−0,74±0,04
IV	2,4±0,2	−0,87±0,04

The condition of the reactor and the emergency protection was monitored by means of a highly-sensitive startup equipment, the sensors of which were located in the peripheral cells of the active zone. This equipment, with the presence in the active zone of a startup neutron source with a strength of $\sim 10^7$ n/sec, enabled the neutron flux in the reactor to be monitored reliably from the instant of loading of the first fuel channels up to emergence at the power generating level. The effects of reactivity were measured by a "Pamir-M" analog reactimeter [2], whose kinetic simulator was made in accordance with the characteristics of the effective groups of delayed neutrons of the Bilibinsk Nuclear Power station reactor.

Measurements on critical assemblies were made for the purpose of investigating the physical properties separately of the central and peripheral parts of the active zone. The difference between the properties of these parts of the active zone is because the control and safety rod channels, which occupy separate cells, are located in the central part of the active zone and not in the peripheral section (Fig. 1). The following units were mounted in the center of the reactor for these measurements: assembly I represented the control lattice (200 x 200 mm) of fuel channels filled with water and there were no control and safety rods in the active zone of the assembly; assembly II was similar to assembly I, but without water in

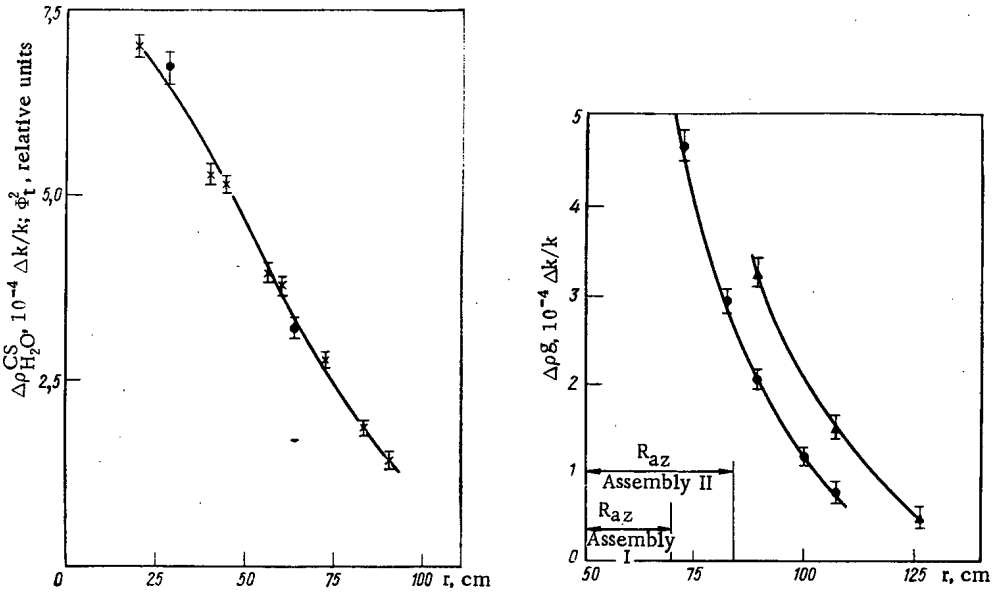

Fig. 3. Dependence of efficiency of water in the control and safety rod channels and the square of the neutron flux on the distance to the center of the assembly: •) $\Delta\rho^{CS}_{H_2O}$; ×) Φ^2_t.

Fig. 4. Dependence of change of reactivity $\Delta\rho^g_f$ by filling an opening for a fuel channel with graphite, on the distance to the center of the assembly: •, ▲) Assemblies I and II.

TABLE 4. Efficiency of Water in Control and Safety Rod Channels

Position of rod in control and safety rod channel	Presence of water in fuel channel	Average change of reactivity on removal
Fully withdrawn	Yes	6,1±0,3
	No	8,0±0,4
Fully inserted	Yes	4,3±0,2
	No	5,7±0,3

the fuel channels; assembly III represented the fuel channel lattice, evacuated, with control and safety rod channels and fuel channels filled with water; assembly IV was similar to assembly III, but without water in the fuel channels.

In order to form assemblies I and II, 12 regular control and safety rod channels were removed from the central part of the reactor and fuel channels were installed in their place. The entire assembly was loaded with fuel channels having a 3% uranium enrichment (FC-3).

During the measurements on the assemblies, the minimum kinetic loadings, fuel channel efficiency and the efficiency of the control and safety rod channels, and the neutron flux distribution along the radius and height of the assemblies were measured. The measurement results are shown in Tables 1 to 3 and the record chart of the assemblies is plotted in Fig. 2.

Comparison of the calculated and experimental data (see Table 1), shows their quite good agreement. The greatest difference (~ 9%) in the critical number of channels is observed for assemblies III and IV.

The effect of water in the cooling tubes of the control and safety rod channels on the reactivity of the assembly was determined. The data obtained (Fig. 3), show that the effectiveness of the water in the control and safety rod channels ($\Delta\rho^{CS}_{H_2O}$), positioned at a different distance from the center of the active zone, to a first approximation is proportional to the square of the thermal neutron flux (Φ^2_t). This confirms that the effect of the water in the control and safety rod channels is due mainly to an increase of thermal neutron absorption. The overall decrease in reactivity, when the cooling tubes of the 12 central control and safety rod channels of assembly III are filled with water, amounted to $5.2 \cdot 10^{-3}$.

In the experiments on the assemblies, the opening for the fuel channels, located outside the active zone, were not filled with graphite. In order to estimate the reduction of efficiency of the reflector due to the presence of these openings, the change of reactivity when certain openings were filled with graphite and located at a different distance from the boundary of the active zone (Fig. 4) was determined. The data showed that by filling all openings of the reflector with graphite, the reactivity is increased by $9.6 \cdot 10^{-3}$ and $7.6 \cdot 10^{-3}$ respectively for assemblies I and II.

TABLE 5. Efficiency of Fuel Channel and Control and Safety Rod Channels

Reactor change	Measurable effect	Change in reactivity, $\Delta k/k \cdot 10^4$				
		cell 11-11	cell 11-14	cell 11-17	cell 11-19	cell 11-21
269 FC with water	FC-3 with water	7,3±0,4	7,4±0,4	5,5±0,3	6,1±0,3	5,8±0,3
	FC-3.3 with water	9,0±0,5	8,8±0,4	6,6±0,3	7,8±0,4	7,5±0,4
	FC-3 filling with water	1,23±0,06	0,33±0,02	0,95±0,05	1,66±0,08	1,06±0,05
	FC-3.3 filling with water	1,66±0,08	0,60±0,03	1,26±0,06	2,3±0,1	1,52±0,08
	Removal of CSR channel with water	—	2,4±0,1	2,5±0,1	3,0±0,2	—
269 FC without water	FC-3 with water	10,0±0,5	10,2±0,5	5,6±0,3	4,6±0,2	4,2±0,2
	FC-3.3 with water	12,5±0,6	11,5±0,6	7,1±0,4	6,4±0,3	5,6±0,3
	FC-3 filling with water	2,5±0,1	0,40±0,02	1,39±0,07	2,2±0,1	1,13±0,06
	FC-3.3 filling with water	3,3±0,2	1,00±0,05	1,72±0,08	2,9±0,2	1,46±0,07
	Removal of CSR channel with water	—	3,4±0,2	3,0±0,2	3,5±0,2	—

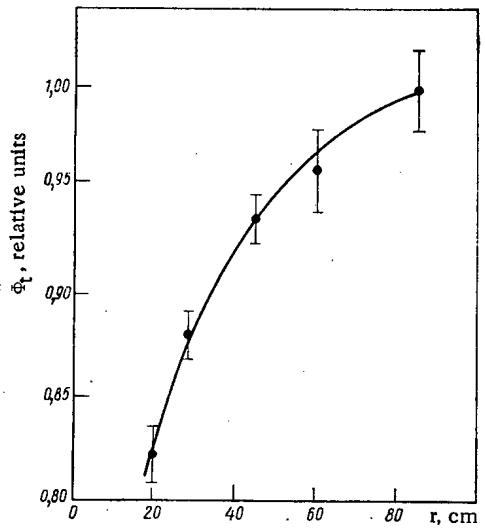

Fig. 5. Dependence of the neutron flux on the distance to the manual control rods.

Measurements with the Full Reactor Charge. After carrying out the experiments on the assemblies, the reactor was loaded completely with fuel channels filled with water. A total of 217 FC-3 and 56 channels with 3.3%-enriched uranium (FC-3.3), which were installed in the peripheral cells of the active zone, were loaded into the reactor. The reactor was compensated at a minimally controlled power level by the total insertion of 40 manual control rods (out of 48) and 4 automatic control rods were located in the central position. In this state of the reactor, the efficiency of all the standard scram rods (8 rods) was $\Delta k/k = 1.3 \cdot 10^{-2}$, which coincided satisfactorily with the design value of $1.24 \cdot 10^{-2}$. On raising the scram rods and all the inserted manual control and automatic control rods, the subcriticality of the reactor was equal to $\Delta k/k = -1.1 \cdot 10^{-2}$. The value obtained for the total reactivity reserve of the reactor ($\Delta k/k = 0.11 \pm 0.015$) coincided with the calculated value.

In the Bilibinsk Nuclear Power Station, reduction of the water density in the fuel channels leads to a drop in reactivity. It was determined in the experiments that the complete removal of water from all of the 273 fuel channels reduces the reactivity of the reactor by $3.1 \cdot 10^{-2}$. The corresponding calculated value is $\Delta k/k = 2.75 \cdot 10^{-2}$. The experiment showed that water in the fuel channels at 30-50 cm distant from the boundary of the active zone and located in regions where there are no control and safety rods, has the greatest efficiency. The change of reactivity on removal of water from the fuel channels is due mainly to an increase of neutron leakage from the reactor. Analysis of the results of measurements of the efficiency of the rods in the case of a complete loading of the reactor with fuel channels without and with water, shows that the efficiency of the first case is greater by a factor of 1.4 approximately than in the second case. The removal of water from the tubes of the control and safety rod channels leads to a small increase of reactivity of the reactor. This effect was measured when the reactor was loaded with fuel channels without water, and fuel channels filled with water (Table 4).

The data given show that the efficiency of water $\Delta k/k$ in the control and safety rod channels depends on the position of the absorbing rods in these channels and the presence of water in the fuel channels. In the control and safety rod channels, the efficiency of the water on withdrawal of the rods, is higher by a factor of 1.4 approximately than in channels with inserted rods.

During operation of the reactor at 100% power (62 MW), the average water density in the fuel channels is $\sim 0.6\ g/cm^3$ and $\sim 0.9\ g/cm^3$ in the tubes of the control and safety rod channels. As, at the start of the run, the number of control and safety rod channels with inserted rods is 30 (out of 60), the overall increase of reactivity as a result of the complete removal of water from the control and safety rod circuit in this case amounts to $3.5 \cdot 10^{-3}$.

The increase of reactivity by the removal of water from the control and safety rod channels is caused mainly by a change of the multiplication properties of the active zone. The efficiency of the rods in this case is changed only very insignificantly. The effect of water in the control and safety rod channels on the efficiency of the rods was investigated for both complete loading of the reactor and by the critical assembly II. With complete loading of the reactor, no effect of the water in the control and safety rod channels on the efficiency of the rods was detected, within the limits of measurement error (±5%). On assembly II, measurements were conducted in the control and safety rod channels (12-06 and 12-04), located in the reflector at distances of 40-80 cm from the boundary of the active zone of the assembly. The measurements showed that, in this case, the presence of water in the tubes of the control and safety rod channels reduces the efficiency of the rod by 8-10%.

The effects of reactivity on the setting up of the fuel channels (FC) and the control and safety rod channels were measured in cells of the eleventh row (see Fig. 1, a) for two states of the reactor: with the FC filled with water and without water (Table 5). The effects being considered are significantly different for different cells which is due, in the first place, to the shape of the neutron field and to the presence of lattice inhomogeneities created by the control and safety rod channels. On loading the reactor with fuel channels with water, the arrangement of fresh FC-3 (with water) increases the reactivity of the reactor on an average by $6.4 \cdot 10^{-4}$, and the arrangement of FC-3.3 by $7.9 \cdot 10^{-4}$. In this state of the reactor, the increase of reactivity on filling an FC-3.3 channel with water is greater by a factor of 1.4 approximately than on filling an FC-3 channel with it and the replacement of one manual control channel by an FC-3 channel increases the reactivity of the reactor by $9.2 \cdot 10^{-4}$ on an average. Replacement of FC-3 by FC-3.3 gives the least gain of reactivity in the cells located in the row with the control and safety rod channels and in the peripheral cells with two faces adjacent to the side of the reflector.

The neutron flux over the height of the reactor and along the radius near the manual control rods and the empty cell was measured with miniature fission chambers when the reactor was loaded with fuel channels without water. The measurements showed that when 8 absorbing rods are in the active zone in the central position (up to 4 scram rods and manual control rods), the neutron flux nonuniformity coefficient in the region of the active zone located around these rods and over the height K_z is equal to 1.50. Even when there is no rod in the intermediate position in the zone, $K_z = 1.34$. These results confirm the design data concerning the significant increase of K_z in the presence of eight or more absorbing rods in the intermediate position in the zone. Measurements on the reactor showed also that the insertion of manual control rods into the zone reduces the neutron flux in the fuel channels located in series with the rod approximately 18% (Fig. 5). The presence of an empty cell leads to an increase of the neutron flux in the fuel channel adjacent to it by 7± 3%.

The misalignment of the neutron flux in the fuel elements of the fuel channels located in a cell, which was situated between an empty cell and a cell with an inserted manual control rod, was determined experimentally. The maximum difference between the neutron fluxes in the fuel elements of this channel amounted to 8 ± 2%.

Monitoring of the Energy Release in the Fuel Element Channels. A system for monitoring the heat release in the fuel channels is provided in the Bilibinsk Nuclear Power station, consisting of 24 rhodium sensors for the neutron flux [3]. The sensors are connected to an interpolating device and their currents are recorded by a multipoint pen-recording potentiometer. In addition to this, the energy release in the fuel element channels can be determined by measuring the efficiency of identical sections of the manual control rods as described in [4]. In these methods, the energy release in each fuel element channel is determined by linear interpolation of the neutron flux values at the measurement points and by the introduction of coefficients which take into account the change of the neutron flux in the vicinity of the command and control rods, empty cells and at points of installation of peripheral sensors, and also the uranium enrichment in the fuel element channels. In determining the energy release by the efficiency of sections of the manual control rod, a coefficient defining the reduction of the neutron flux at the periphery of the active zone also is used. In order to refine the values of these coefficients, the neutron flux was measured in all fuel element channels and at points of location of the sensors for monitoring the heat release, with a full reactor charge of fuel element channels without water, by fission chambers. On the basis of these measurements, values of the coefficients were chosen for which the values of the neutron flux in the fuel element channels obtained by linear interpolation, differed to the minimum degree from the values obtained by direct measurement in these fuel element channels.

For the coefficients chosen in this way, the mean-square error in determining the energy release in the fuel element channels by means of the regular system of monitoring the energy release amounts to ±7%, and by measuring the efficiency of sections of the manual control rods it is ±5%. The small error is due to the fact that the number of manual control rods is greater by a factor of two than those of the energy release monitoring sensors. With the combined use of both procedures, the error is reduced to ±4%.

Measurements during startup showed that the principal physical characteristics of the reactor of the first unit of the Bilibinsk Nuclear Power Station correspond with the design values. The planned control and safety rods provide compensation of the reserve of reactivity equal to 11% and create the required subcriticality for the safe startup of the reactor. Therefore, the introduction of any corrections to the loading record chart of the active zone and to the reactivity compensation system is not required.

By means of the manual control rods, the energy release field along the radius of the reactor can be smoothed. The coefficient of nonuniformity does not exceed the design value of 1.5. The reactor has a negative steam reactivity effect, which makes its operation stable and safe.

In conclusion, the authors express their sincere thanks to all staff of the Bilibinsk Nuclear Power Station, participating in the preparation and execution of the physical startup.

LITERATURE CITED

1. V. M. Abramov et al, Atomnaya Énergiya, 35, No. 5, 299 (1973).
2. B. G. Dubovskii et al, Atomnaya Énergiya, 36, No. 2, 104 (1974).
3. E. N. Babulevich et al, Atomnaya Énergiya, 31, No. 5, 465 (1971).
4. I. Ya. Emel'yanov et al, Atomnaya Énergiya, 30, No. 5, 422 (1971).

BOOK REVIEWS

V. G. Zolotukhin, L. R. Kimel',
A. I. Ksenofontov, et al.
THE RADIATION FIELD FROM A POINT UNIDIRECTIONAL SOURCE OF GAMMA QUANTA*

Reviewed by B. R. Bergel'son

In order to calculate the effects due to the interaction of γ radiation with a substance, namely the quantity of energy released, dose intensity, instrument readings, biological effects, etc, it is necessary to have available comprehensive data on the space-energy and angular distribution of the radiation in every specific case. However, the problem of determining the γ-radiation spectrum presents considerable computational difficulties. Even modern computers, in many cases cannot provide the required volume of calculations. An alternative for carrying out the cumbersome calculations is a procedure in which the required spectra can be set up by means of tabular data obtained for elementary sources. A point unidirectional source can be considered as the most elementary source, the radiation field of which has maximum information content. In the light of this approach, and also taking into account the applied nature of the problem, the monograph by V. G. Zolotukhin et al. should be considered; this is devoted to the computational-experimental investigation and tabulation of spectral data from point, unidirectional γ-radiation sources in an infinite medium. The book consists of six chapters. In the first chapter, definitions are given of the principal characteristics of the sources and field and also methods of transforming the spectral distribution.

The methodology for the experimental study of the energy and angular radiation spectra of a point unidirectional source is described in the second chapter.

The authors pay particular attention to problems associated with the possibilities and special features of the use of the Monte Carlo method for calculating the transfer of γ radiation to large distances from the source. These sections are written in a condensed form and, in contrast from others, postulate defined skills and knowledge of the subject by the reader.

In the fourth chapter, the results are given of calculations of the differential characteristics of the radiation field of a point unidirectional source, and also data on the spectra, energy flux, absorbed energy and dose intensity for infinitely homogeneous media of H_2O, Al, Fe, Sn, W, Pb and U for source energies of 0.1 to 10 MeV.

The present monograph is a unique publication in the diversity of the information given in the section on the characteristics of the γ-radiation field of a point unidirectional source.

In the sixth chapter, data are given which are essential for engineering calculations on building factors of scattered γ radiation for anisotropic point sources. Unfortunately, the authors have confined themselves in this section to only a single medium — water, although the necessary data for other media also were available.

In conclusion, it should be emphasized that on the whole, the problem of finding the spectral distribution of scattered γ radiation can be solved only by improvement of the appropriate algorithms and programs for machine calculations. A knowledge of the entire problem for studying a unidirectional point source is scarcely feasible, in consequence of the diversity of the parameters of the source-medium-detector system, the complexity of presentation of the information in compact form and time consumption

*Atomizdat, Moscow, 1975.

Translated from Atomnaya Énergiya, Vol. 39, No. 1, p. 8, July, 1975.

for reconstruction of the spectra. However, for the simplest case of point and surface anisotropic sources and a homogeneous infinite medium, this approach is competent and undoubtedly useful.

The book reviewed will be used widely by engineers and scientific workers in their practical activities.

ARTICLES

SOME PROBLEMS OF THE ECONOMICS OF A RESEARCH NUCLEAR REACTOR

V. I. Zelenov, S. G. Karpechko, and A. D. Nikiforov

UDC 621.039.55:003.12

Recently, more attention is being paid everywhere to problems of the economics of a research nuclear reactor and the planning of experiments on it [1-6]. Procedures are considered in the papers for estimating the cost of an experiment on the reactor and certain efficiency indexes for its utilization. In determining the cost of the experiment, the total reactor costs are distributed between the experiments proportionally with the efficiency of the experimental apparatus [1], depending on the product of its volume and the neutron flux.

This approach to the distribution of expenditure, in our opinion, is in need of refinement. For example: part of the total reactor costs, depending slightly on the power, is more suitable distributed equally between all experiments and the remaining part, which is directly dependent on the reactor power, is more suitably distributed proportionally with the efficiency of the experimental facility.

In this paper, a procedure is proposed for assessing the cost of an experiment on a research nuclear reactor, taking account of this refinement. In addition, an attempt is made to explain the effect of the index of efficiency of utilization of a research reactor (in particular, the power utilization factor and the average operating power) on the cost of neutrons in the experimental facility.

Procedure for Assessing the Cost of Experiments on a Research Nuclear Reactor

We define the total costs on a research nuclear reactor in the following way:

$$E_{total}=E_{const}+E_{var} \quad (1)$$

where E_{total} is the total annual expenditure on the reactor; E_{const} is the constant component of the total expenditure and E_{var} is the variable component of the total expenditure.

We relate to the constant expenditure, those costs which depend only slightly on the reactor power :

$$E_{const}=E_{am}+E_{sal}+E_{int}+E_{adm}, \quad (2)$$

where E_{am} is the annual funding of amortization deductions on production buildings and power plant; E_{sal} is the annual funding of working salaries of the staff; E_{int} is the expenditure on the energy requirements for the intrinsic needs of the reactor and E_{adm} is the expenditure on salaries of the administration—management staff. We relate to the variable expenditure, the costs which depend directly on the power, in particular the fuel costs :

$$E_{var}=\frac{qC_f}{\varphi}\bar{N}k_{puf}8760, \quad (3)$$

where q is a coefficient which takes into account the consumption of fuel in the generation of one unit of thermal energy; C_f is the specific fuel costs in manufactured products; φ is the relative average burnup of the discharged fuel; $\bar{N}$ is the average operating power of the reactor and k_{puf} is the power utilization factor of the reactor, defined as the ratio of the time of operation of the reactor at any level of power to the calendar time.

Translated from Atomnaya Énergiya, Vol. 39, No. 1, pp. 9-11, July 1975. Original article submitted August 8, 1974.

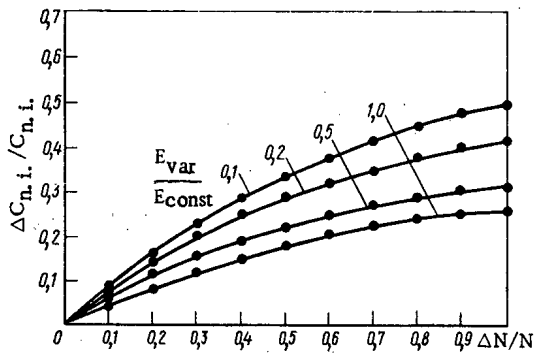

Fig. 1. Variation of cost of neutrons in experimental facilities with increase of average reactor power.

The cost of an experiment is determined by both the constant and variable components of the total expenditure on the reactor. As the constant component depends only slightly on the reactor power, then it should be distributed equally between the experiments without taking account of their individual characteristics (volume of the experimental facility, and the neutron flux in it). This distribution allows the minimum cost of an experiment in a given reactor to be obtained. We shall call it the support cost. The distribution of the variable component of the total costs between the experiments, which is proportional to their efficiency, allows individual special features of the experimental facility to be taken into account and the supplementary cost of the experiment to be obtained. We shall call this the physical cost. Thus, the total cost of the experiment will be determined by the support and physical costs.

Taking account of what has been said, we write the total cost of a specific experiment on the reactor in the following form:

$$C_{e.i.}=\frac{E_{const}}{n}+\frac{E_{var}}{n}\bar{\Phi}_i S_i, \tag{4}$$

where $C_{e.i.}$ is the annual cost of the i-th experiment; $\bar{\Phi}_i$ is the unperturbed specific neutron flux in the cell of the active zone, intended for installation of the experimental apparatus [1]; S_i is the working surface area of the experimental facility (immediately adjoining the active zone). Here, in place of the working volume in the expression for the efficiency of the experimental facility [1], the working surface is used, which equates the degree of effect of the physical (neutron flux) and geometric (diameter of the experimental facility) components of the efficiency, to the cost of the experiments.

Cost of Neutrons in Experimental Facilities

From the cost of an experiment in the reactor and the number of neutrons created by the reactor in the experimental facility during the year, it is easy to determine the cost of the neutrons for a given experimental facility:

$$C_{n.i.}=\frac{C_{e.i.}}{\bar{\Phi}_i S_i \bar{N} k_{puf} 8760}, \tag{5}$$

where $C_{n.i.}$ is the cost of neutrons in the i-th experimental facility. With calculation (4)

$$C_{n.i.}=\frac{E_{const}}{n\bar{N}k_{puf}8760\bar{\Phi}_i S_i}+\frac{qC_f}{\varphi}\frac{1}{\sum_{i=1}^{n}\bar{\Phi}_i S_i}. \tag{6}$$

The structure of the neutron cost is determined by the structure of the cost of the experiment. The cost of the neutrons also has two components:

$$C_{n.i.const}=\frac{E_{const}}{n\bar{N}k_{puf}8760\bar{\Phi}_i S_i}; \tag{7}$$

$$C_{n.i.var}=\frac{qC_f}{\varphi}\frac{1}{\sum_{i=1}^{n}\bar{\Phi}_i S_i}. \tag{8}$$

This definition of the neutron cost shows that, in experimental facilities of a different type (channel in a "catcher," in the heat release assembly, in the reflector and beyond the reflector), it is different. The constant component of the neutron cost in the i-th experimental facility depends on the utilization efficiency index of the reactor ($\bar{N}$, k_{puf}) and on the characteristics of the experimental facility ($\bar{\Phi}_i$, S_i) and the variable component depends on the productivity of the reactor $\sum_{i=1}^{n} \bar{\Phi}_i S_i$, on the fuel cost and the depth of burnup of the discharged fuel. Let us consider the effect of the utilization factor of the reactor on the cost of the neutrons in experimental facilities.

Simple mathematical transformations show that:

$$\frac{\Delta C_{n.i.}}{C_{n.i.}} = \frac{\frac{\Delta \bar{N}}{\bar{N}}}{1+\frac{\Delta \bar{N}}{\bar{N}}} \frac{1}{\left(1+\frac{E_{var}}{E_{const}}\frac{\bar{\Phi}_i S_i}{\bar{\Phi}_i S_i}\right)}, \tag{9}$$

where $\bar{\Phi}_i S_i$ is the efficiency averaged over the entire experimental facility; $\Delta C_{n.i.}/C_{n.i.}$ is the relative reduction of the neutron cost in the experimental facility for a relative increase of the average operating power of the reactor by $\Delta\bar{N}/\bar{N}$ with change of the other reactor characteristics.

Figure 1 shows the dependence of $\Delta C_{n.i.}/C_{n.i.}$ on $\Delta\bar{N}/\bar{N}$ for various ratios of E_{var}/E_{const} with constant value of $\bar{\Phi}_i S_i/\bar{\Phi}_i S_i = 1.0$. It follows from the figure that the maximum effect when the average reactor power is increased is achieved with small values of the ratio of these quantities.

The absolute magnitude of the economic effect, when the average power of the reactor is increased, amounts to

$$\Delta C = E_{const}\frac{\Delta\bar{N}/\bar{N}}{1+\frac{\Delta\bar{N}}{\bar{N}}}. \tag{10}$$

Consequently, the nature of the dependence of $\Delta C/E_{const}$ on $\Delta\bar{N}/\bar{N}$ is identical for all reactors, and the economic effect is determined by the constant component of the reactor costs, other parameters being constant (φ, C_f, $\bar{\Phi}_i$, S_i). It is obvious that an increase of the reactor utilization factor gives an economic effect which is determined by the expression:

$$\Delta C = E_{const}\frac{\Delta k_{puf}/k_{puf}}{1+\Delta k_{puf}/k_{puf}}.$$

The graph of the dependence of $\Delta C/E_{const}$ on $\Delta k_{puf}/k_{puf}$ for all reactors will also be identical.

Thus, in the case of costs distribution according to the proposed procedure, the concept of the support cost of the experiment is introduced (defined by the constant component of the cost and the number of experimental facilities), which is the minimum cost of the experiment in the reactor. It is obvious that the cost of any experiment on a research reactor cannot be lower than the support cost. It has been shown that the ratio of the variable and constant cost components on the reactor, depends strongly on the reduction of the cost of neutrons in the experimental facilities with an improvement of the utilization efficiency index of the reactor. In particular, it is most advantageous to increase the power characteristics of the reactor with respect to the variable and constant cost components within the limits of 0.1 to 0.5.

The economic effect, when the utilization efficiency index of the reactor is changed, depends only on the constant component of the costs and is independent of the other reactor characteristics (φ, C_f, $\bar{\Phi}_i$, S_i).

LITERATURE CITED

1. V. A. Tsykanov, Atomnaya Énergiya, 14, No. 5, 469 (1963).
2. A. S. Kochenov, Atomnaya Énergiya, 21, No. 2, 97 (1966).
3. A. N. Erykalov and Yu. V. Petrov, Atomnaya Énergiya, 25, No. 1, 52 (1968).
4. V. A. Tsykanov, Atomnaya Énergiya, 31, No. 1, 15 (1971).
5. G. A. Bat', A. S. Kochenov, and L. P. Kabanov, Research Nuclear Reactors [in Russian], Atomizdat, Moscow (1972).

6. V. V. Batov and Yu. I. Koryakin, Economics of Nuclear Power Generation [in Russian], Atomizdat, Moscow (1969).

BOOK REVIEWS

A. A. Vorob'ev, B. A. Kononov, and V. V. Evstigneev

BETATRON ELECTRON BEAMS*

Reviewed by P. S. Mikhalev

Interest in accelerators as radiation sources for medicine, biology and industry continues to grow. One of the simplest and cheapest of the accelerators in operation over the range of energies 5-50 MeV is the betatron, which has been in series production for many years. The authors have attempted to elucidate the buildup of experience in relation to the characteristics of electron beams during injection, acceleration and, mainly, their extraction and utilization.

There are five chapters in the book. The first two are devoted to the theory of the classical betatron with a time-variable azimuthal-symmetrical magnetic field, and the dynamics of electrons on injection and during acceleration.

In the third and fourth chapters, various methods are considered for extraction of the electron beam, problems of stabilization of the electron beam parameters and instruments used during operation with the beam.

Problems of the practical application of betatronelectron beams are described in the fifth chapter.

The authors have attempted to cover a quite wide circle of problems involving the motion of the electron beam in the betatron. The principal value, in our opinion, is the experimental data assembled during the construction and operation of the betatrons in the Tomsk Polytechnical Institute and the engineering approach developed for the construction of beam extraction devices. The third and fourth chapters comprise the basis of the book. However, these data are discussed very concisely and the theoretical part preceding it (chapters 1 to 3) is, in essence, an account of other well-known manuals on the theory of the betatron. It would be more valuable to give examples in more detail of the practical application of theory in approximate engineering calculations. The fourth chapter is overloaded with data which could be the subject of a separate and detailed consideration (this refers, first and foremost, to the sections on detection and spectrometry, where only a brief listing is given of the methods and instruments for beam diagnostics).

Unfortunately, future improvements of the betatron beam characteristics are considered almost not at all in the book. It is true, the authors make an attempt to describe, from their point of view, future trends in this order: a betatron with a constant guiding field, a betatron with a spiral magnetic field, the application of superconductors, linear induction accelerators and a plasma betatron. Consideration of the prospects, in essence, reduces to the listing mentioned. However, a linear induction accelerator has been used for a long time in a number of investigations and, on the basis of the experience built up, judgement on the prospects for its utilization can be justified; an induction cyclic accelerator with a constant field, well-studied theoretically and on model experiments, permits the beam intensity to be increased by comparison with the normal betatron by an order of two to three, and now it should be possible to assess the prospects for its utilization. The other trends listed are in the experimental stage (plasma betatron) and the first theoretical proposals (spiral field), and no reference would be made in this book.

Despite the shortcomings mentioned, the book can be useful to specialists in the development of beam extraction devices for betatrons of various applications. Moreover, the bibliography contained in the book

*Atomizdat, Moscow, 1974.

Translated from Atomnaya Énergiya, Vol. 39, No.1, p. 11, July, 1975.

(126 references) and the brief description of the experiments enables those so desiring to become acquainted in detail with the work carried out in this field.

ARTICLES

SYNTHESIS OF A DIGITAL SYSTEM FOR CONTROL OF NEUTRON FLUX DISTRIBUTION

E. V. Filipchuk, P. T. Potapenko,
V. G. Dunaev, N. A. Kuznetsov,
and V. V. Fedulov

UDC 621.039.515

In recent years, data-transmission and data-handling systems based on "objective" computers are being used ever more extensively at nuclear power stations. The traditional path for computer use is the creation of a system of centralized control followed by its use as an "adviser" with the possibility of performing certain control functions in proportion to the accumulation of operating experience. It is considered that one of the basic automatic control functions of such a system is control of the distribution of energy release in the core.

We discuss several problems involved in the construction of a control system for a neutron field using an objective computer.

Formulation of the Problem. For spatial control, we divide the reactor into m control zones with a detector and control rod in each zone. We introduce the local neutron fluxes φ_i and the settings φ_i^0. The aim of control is minimization of the quadratic quality index

$$I_N = \sum_{n=1}^{N} [\varphi^0(nT) - \varphi(nT)]^T [\varphi^0(nT) - \varphi(nT)].$$

In contrast to [1, 2], we consider here fast motions of the system for a reactor with a stable power distribution. For a formulation of the problem, one can assume that the iodine and xenon concentrations are independent of time and the dynamics are satisfactorily described by a one-group diffusion equation. It is further assumed that the total power is stabilized by a supplementary high-speed automatic control system or by internal effects.

A block diagram of the control system is shown in Fig. 1. Here, the D_i are intrazone neutron flux detectors; K are commutators which provide a connection between the computer and each channel; the DM_i are constant-velocity drive mechanisms.

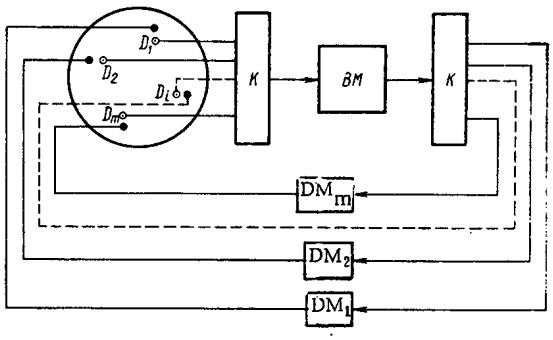

Fig. 1. Block diagram of control system.

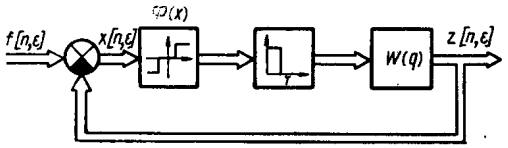

Fig. 2. Structural diagram of pulse-height system.

Translated from Atomnaya Énergiya, Vol. 39, No. 1, pp. 12-16, July, 1975. Original article submitted June 13, 1974.

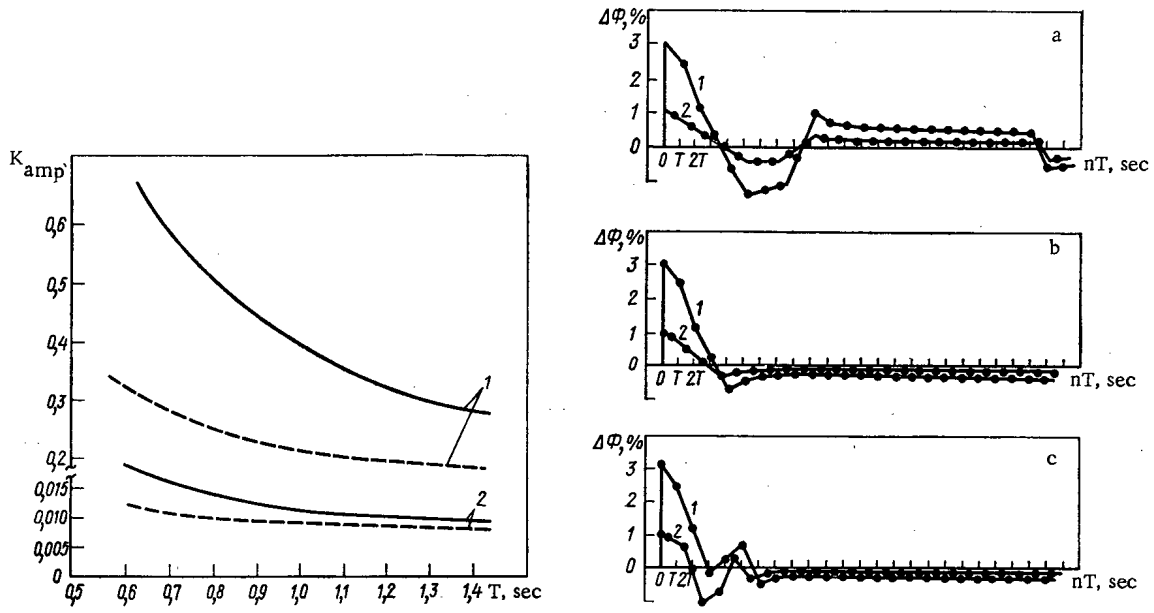

Fig. 3. Dependence of threshold amplification factor of an open circuit on quantization time: —) one channel; ---) two channels.

Fig. 4. Transitional processes in the system parameters: T = 1.4 sec; rate of introduction of reactivity, $1.7 \cdot 10^{-5}$ sec^{-1}; static accuracy, 0.5%; correction coefficient b = 0(a), 1 (b), and 2 (c).

A feature of this system is that the control computer, or machine for centralized control, is included in a closed control circuit, i.e., the controlled coordinates are quantized with respect to time and level.

Introducing the appropriate lattice functions and considering that each of the m control channels is connected by commutators to the computer in a definite time period $\varepsilon = T/m$ after the $(m-1)$-th channel (quantization time T is identical for all channels), we obtain a structural scheme for this multi-dimensional relay, pulse-height system (Fig. 2). Here, $W(q, \varepsilon)$ is a matrix of transfer functions for the continuous portion shown, which joins detectors, drive motors, and object of control; $\mathbf{x}$, $\mathbf{f}$, and Φ are m-dimensional vectors for error, external effect, and characteristics of nonlinear elements.

We assume that the digital control device, which is realized with a specialized or general-purpose computer, has a sufficiently large digital mesh and therefore quantization with respect to level in the computer can be neglected in the calculation.

Stability. Since the range of possible perturbations is ordinarily rather large, there is particular interest in a study of the absolute stability of this system.

We use theorems on absolute stability [3] for analysis of the stability of multiply-connected nonlinear pulsed systems. This method is similar to the well-known Popov method for the determination of the stability of continuous nonlinear automatic systems and yields results which are associated with the concept of frequency response; what is more important, the method yields general sufficient conditions for stability which are applicable to systems of arbitrary order in this class.

Note that the frequency criteria yield only sufficient conditions for absolute stability. However, these qualitative results are extremely useful in the initial design stage of the system.

We consider an autonomous multiply-connected pulsed system (see Fig. 2). The system has m nonlinear (in this case, relay) elements. $\Phi_i(x_i)$ is the output of the i-th nonlinear element; the input is the i-th component of the vector $\mathbf{x}[n, \varepsilon]$. We assume the nonlinear functions belong to the sector (0, K):

$$\Phi_i[0] = 0; \quad 0 \leqslant \Phi_i[x_i]\, x_i < K x_i^2.$$

The inputs and outputs of the nonlinear elements are connected through linear filters which, by assumption, are observed and controlled. Their transfer functions $W_{ij}(q, \varepsilon)$ are the elements of the trans-

fer matrix $\mathbf{W}(q, \varepsilon)$. For the class of systems being considered, each linear filter is assumed at least stable in the limit, i.e., having all poles within the unit circle in the plane of q with the exception of a simple pole at $|eq| = 1$ (q is a parameter of a discrete Laplace transformation).

It should be noted that the number and location of control rods ordinarily fixed and limited by safety considerations. For large reactors, the spacing between them is, as a rule, considerably greater than the neutron diffusion length and the coupling between control channels is weak. In practice, therefore, consideration can be limited to two neighboring control channels for localized and limited perturbations of reactivity.

We write an equation with respect to the output coordinates $z_i[n, \varepsilon]$ for a two-channel sytem with input disconnected in the form of a discrete Laplace transformation:

$$z_i[q, \varepsilon] = \sum_{j=1}^{2} W_{ij}[q, \varepsilon - \varepsilon_{j-1}]\,\Phi_j\{x_j[q, \varepsilon_{j-1}]\}, \quad i = 1, 2. \tag{1}$$

Here, $W_{ij}[q, \varepsilon]$ is a representation in the sense of a discrete Laplace transformation of the effect of the j-th input perturbation on the i-th output coordinate.

Setting $\varepsilon_0 = 0$, we write the transfer matrix of the system in the form

$$\mathbf{W}[q, \varepsilon] = \begin{vmatrix} W_{11}[q, 0] & W_{12}[q, -\varepsilon] \\ W_{21}[q, \varepsilon] & W_{22}[q, 0] \end{vmatrix}, \quad \varepsilon = 1, 2. \tag{2}$$

As an example, we assume the neutron flux is measured by direct charge detectors with known dynamic properties; reactor dynamics and internal coupling characteristics were determined on the basis of the nodal adiabatic model [5]. Because of channel identity, we have

$$W_{11}[q, 0] = W_{22}[q, 0] = W_1[q, 0]; \; W_{12}[q, -\varepsilon] = e^{-q}W_{21}[q, \varepsilon] = e^{-q}W_2[q, \varepsilon]. \tag{3}$$

On the basis of [3] one can then formulate the following sufficient conditions for absolute stability of this system:

$$\operatorname{Re}\left(1 + \frac{e^{j\bar{\omega}} - 1}{e^{j\bar{\omega}}}\alpha\right) W_1^*(j\bar{\omega}, 0) + \frac{1}{k} > 0; \tag{4}$$

$$\left[\operatorname{Re}\left(1 + \frac{e^{j\bar{\omega}} - 1}{e^{j\bar{\omega}}}\alpha\right) W_1^*(j\bar{\omega}, 0)\right]^2 -$$

$$-0{,}25\left|\left(1 + \frac{e^{j\bar{\omega}} - 1}{e^{j\bar{\omega}}}\alpha\right) e^{-j\bar{\omega}} W_2^*(j\bar{\omega}, \varepsilon) + \right.$$

$$\left. + [1 + (1 - e^{j\bar{\omega}})\alpha]\, W_2^*(-j\bar{\omega}, \varepsilon)\right|^2 > 0,$$

$$\forall\, (0 \leqslant \bar{\omega} \leqslant \pi). \tag{4a}$$

Setting $\alpha = 0$ (see [4]), we obtain the simpler forms

$$\operatorname{Re} W_1^*(j\bar{\omega}, 0) + \frac{1}{k} > 0; \tag{5}$$

$$\left[\operatorname{Re} W_1^*(j\bar{\omega}, 0) + \frac{1}{k}\right]^2 - 0{,}25\,|W_2^*(j\bar{\omega}, \varepsilon)\, e^{-j\bar{\omega}} +$$

$$+ W_2^*(-j\bar{\omega}, \varepsilon)|^2 > 0, \quad \forall\, (0 \leqslant \bar{\omega} \leqslant \pi). \tag{5a}$$

Criteria of the form (4)-(5a) are reference criteria for the analysis of the absolute stability of this two-channel system.

The algorithm for the determination of the sector of absolute stability (0, K) is the following: on the set $0 \leq \bar{\omega} \leq \pi$, we seek $\min_{\bar{\omega}} \operatorname{Re} W_1^*(j\omega)$ with $\min_{\bar{\omega}} \operatorname{Re} W_1^*(j\bar{\omega}) = 1/K$ when $\alpha = 0$ according to Eq. (5), where K is the upper bound of the sector of absolute stability. The next step is to check for satisfaction of condition (5a); if it is not satisfied, the sector of stability is reduced by an amount Δ and the procedure repeated. After a boundary K for the sector of stability which satisfies the criterion for $\alpha = 0$ is found (this result corresponds to the Tsypkin criterion), the computational process is repeated for a series of values of α.

From the resultant set of values $K(\alpha)$, a maximum is selected which is also the desired value for the upper bound of the sector of absolute stability [3].

For given parameters of relay response, the quantity K is defined as the ratio between amplification factor and static accuracy. Thus, for a given static control accuracy, the value of the amplification factor for an open circuit is associated with the upper limit of the sector of stability by the obvious relation $K_{amp} = K\delta$.

Figure 3 shows the region of stability in the space of the parameters K_{amp} (amplification factor for an open circuit) and T (time quantization) for the curves 1 and 2 plotted with respect to the criteria (4)-(5a) respectively. The numerical values of the parameters of the reactor model are: power feedback factor $K_M = -\beta$, time constant $T_M = 3$ sec, and coupling coefficient $K_c = 0.3$. A system is absolutely stable for parameter values falling below the corresponding curves. The figure also shows results calculated for a single channel in this system.

It should be noted that the results obtained with the first criterion give less stringent limitations on the characteristics of the part shown because of consideration of additional limitations on nonlinearity. At the same time, however, improvement of the criterion considerably increases the computational difficulties.

The curves obtained not only make it possible to compare the two criteria with respect to accuracy and volume of computation but are also important reference data for further system design.

Quality of Processes. It is of interest to consider the quality of the processes in the system, i.e., to establish a relation between the parameters of the selected control law and the process indicators (control time, degree of hunting).

Correction in pulsed systems which is used for improvement of the accuracy and qualtiy of control processes is achieved in various ways. Correction based on first differences, which is equivalent to correction with respect to the derivative in continuous systems, is quite effective.

In this case, the computer control device forms the following sequence of signals in the drive mechanism,

$$m_i[nT] = x_i[nT] + b\{x_i[nT] - x_i[(n-1)T]\},$$

where b is the amplification factor with respect to first differences.

Process quality is ordinarily studied approximately by means of indirect evaluations. Another, and very cumbersome, method is the construction of an exact solution of the equations describing a given control system. The method of state space, which is the basis of modern control theory, permits algorithmization of the problem and considerably simplifies the solution procedure.

We consider a linear stationary discrete system described by a set of linear differential equations of first order with constant coefficients in vector form [6],

$$\frac{d\mathbf{V}(\lambda)}{d\lambda} = \mathbf{A}\mathbf{V}(\lambda), \tag{6}$$

where $\lambda = t - nT$ and $0 < \lambda \leq T$.

The state vector includes input variables and process variables as components. The initial conditions for the differential equation of state (6) can be written in vector form,

$$\mathbf{V}(nT^*) = \mathbf{B}\mathbf{V}(nT). \tag{7}$$

This equation describes the change of variable states at the time of quantization.

Applying the direct Laplace transformation to Eq. (6), we obtain

$$\begin{aligned} s\mathbf{V}(s) &= \mathbf{A}\mathbf{V}(s) + \mathbf{V}(0^+); \\ \mathbf{V}(s) &= [s\mathbf{E} - \mathbf{A}]^{-1}\mathbf{V}(0^+). \end{aligned} \tag{8}$$

We then obtain a solution of the differential equation of state in the form

$$\mathbf{V}(\lambda) = \Phi(\lambda)\mathbf{V}(0^+), \tag{9}$$

where

$$\Phi(\lambda) = \mathcal{L}^{-1}[s\mathbf{E} - \mathbf{A}]^{-1}. \tag{10}$$

In the interval $nT < t \leq (n+1)T$,

$$\mathbf{V}(t) = \Phi(t - nT)\,\mathbf{V}(nT^{+}) \tag{11}$$

and, consequently, at the time $t = (n+1)T$

$$\mathbf{V}(t) = \Phi(t - nT)\,\mathbf{BV}(nT). \tag{12}$$

Considering Eq. (7), we obtain the state vector **V**

$$\begin{aligned} \mathbf{V}(t) &= \Phi(t - nT)\mathbf{BV}(nT); \\ \mathbf{V}[(n+1)T] &= \Phi(T)\,\mathbf{BV}(nT). \end{aligned} \tag{13}$$

This last equation is a recurrence relation which is used for calculation of successive values of the variable states of the system at the time of quantization.

It should be noted that in a relay system the elements of the transition matrix $\Phi(T)$ differ depending upon whether or not a control pulse exceeds the insensitivity zone of the relay (i.e., the static error).

Use of the nodal adiabatic model makes it possible to reduce this system in the general case to an assembly of m uniform channels [5] with noninertial internal coupling. We use the principle of superposition and consider that in the interval $nT < t \leq (n+1)T$ all variables are continuous functions and that the change in the magnitude of the control action occurs at the time of interruption. It is then possible to consider the interrelation of the channels at discrete times, which, in turn, makes it possible to build up processes in this multichannel system by using the variable states for a single channel. For example, the computational procedure is broken down in the following manner for a two-channel system.

1. The initial-condition vector $\mathbf{V}_1(nT^{+})$ for the first channel is determined from the given value of the vector $V_1(nT)$. Depending on the value of the control action, the corresponding transition matrix is then chosen and $V_1[(n+1/2)T]$ and $V_1[(n+1)T]$ are calculated with allowance for the phase shift between channels.
2. The state vector $V_2[(n+1/2)T]$ of the second channel is corrected in accordance with the value of the vector $V_1[(n+1/2)T]$ and the static coupling coefficient. $V_2[(n+1)T]$ and $V_2[(n+3/2)T]$ are found in a manner similar to that used in the first channel using the appropriate transition matrix.
3. The state vector $\mathbf{V}_1[(n+1)T]$ for the first channel is corrected and the procedure then repeated cyclically.

From the processes constructed in this manner, the quality index of the system is determined and, if necessary, the parameters of the control law changed. Transitional processes in this two-channel system are shown in Fig. 4 for input of a perturbation into channel 1.

In general form, the algorithm for synthesis of this system is the following. For given dynamic properties of the system, the region of stability in the space of the parameters K and T is constructed. Acceptable values of K_{amp} and T in the region of stability are selected in accordance with the required static accuracy and imposed limitations.

Depending on the value of the correction coefficient, a family of transitional processes in the system is then constructed. As a rule, the criterion for the required process quality in the system is the provision of the necessary control time with minimum number of motor startups. The parameters K_{amp}, T, and B of the control law are determined through the iterative procedure.

CONCLUSIONS

A method for calculation of a control system for a neutron field based on an objective computer is proposed in general form.

The criteria used for the study of absolute stability are applicable to systems of any dimensionality and of arbitrary structure. The Tsypkin criterion is mainly used in the analysis of multidimensional systems in order to reduce computational difficulties.

The method described for the study of process quality in a system, which is based on the method of state space, in conjunction with the nodal adiabatic model of a reactor makes it possible to take into account precisely the various limitations thereby preserving the low computational order of the problem.

The proposed method for synthesis of multidimensional pulsed systems for reactor control can easily be put in algorithm form and does not require a large amount of machine time.

LITERATURE CITED

1. O. B. Ronzhin and E. F. Sabaev, At. Énerg., 24, No. 2, 269 (1968).
2. I. S. Postnikov and E. F. Sabaev, At. Énerg., 30, No. 5, 445 (1971).
3. E. Jury and B. Lee, Avtomatika i Telemekhanika, 26, No. 6, 945 (1967).
4. Ya. Z. Tsypkin, Kybernetik, 6, No. 1, 524 (1965).
5. E. V. Filipchuk, P. T. Potapenko, and A. N. Kosilov, At. Énerg., 35, No. 5, 317 (1973).
6. J. T. Tou, Modern Control Theory, McGraw-Hill, New York (1964).

ABSOLUTE MEASUREMENT OF THE RADIATIVE CAPTURE CROSS SECTION OF ^{238}U FOR 30 keV NEUTRONS

Yu. G. Panitkin and L. E. Sherman

UDC 539.125.17

The radiative capture cross section of ^{238}U for neutrons is interesting because it is one of the most important nuclear constants in the design of fast breeder reactors. It is especially important to make an absolute measurement of the radiative capture cross section of ^{238}U for neutrons. However, the discrepancies between the results of different authors sometimes exceed the error limits cited in [1-3]. The aim of the present article is to describe an absolute measurement of the radiative capture cross section of ^{238}U for 30 keV neutrons.

The source of neutrons was the reaction $^{7}Li(p, n)^{7}Be$. The measurements were made in an electrostatic accelerator with maximum proton energy of 2.5 MeV. The radiative capture cross section for neutrons was determined by an activation method, and the neutron flux by the method of concomitant activity for 477 keV gamma quanta produced by the decay of ^{7}Be formed by the reaction $^{7}Li(p, n)^{7}Be$. The induced activity of the ^{238}U specimen was measured by means of the 74 keV gamma quanta produced by the decay of ^{239}U. The neutron beam was kinematically collimated into a narrow cone directed forward relative to the direction of incidence of the proton beam on the target. The energy of the protons was 2 keV higher than the threshold energy of the reaction $^{7}Li(p, n)^{7}Be$. The mean energy of the neutrons thus produced was 30 keV.

A specimen of uranoso-uranic oxide of ^{238}U, 300 mg/cm^2 in thickness, was aligned at an angle of zero degrees to a beam of incident protons and shielded from neutrons scattered in the target chamber of the accelerator by a cadmium jacket.

To monitor the neutron beam passing through the specimen we used a telescopic system consisting of flat and coaxial fission chambers with layers of ^{235}U (Fig. 1). This system permits operative monitoring

TABLE 1. Results of Absolute Measurements of Radiative Capture Cross Section of ^{238}U for 30 keV Neutrons

E_n, keV	σ_c ^{238}U, mbarn	Notes
30±8	375±77 [12]	Activation method. Neutron flux measured by concomitant activity in reaction $^{7}Li(p, n)^{7}Be$.
30±7	473±47 [7]	Time-of-flight method. Results normalized for indium, of which the capture cross section was measured absolutely with an Sb-Be photoneutron source [15].
30,0	430±43 [13]	Spherical experimental geometry. Measured with photoneutron source with neutron energy of 24 keV. Experimental value of 467 ± 46 mbarn was extrapolated to 30 keV using shape of curve in [1]. Correction made as described in [16].
30±8	479±15 [2]	See first note.
30±8	425±31 [1]	Time-of-flight method. Normalized by 6.7 eV resonance.
30±8	462±55 [14]	Time-of-flight method. Normalized by means of resonances in the energy range of a few electron volts.
30±8	528±36 [3]	Time-of-flight method. Normalized by 6.7 eV resonance.
30±6	465±23 (Present authors)	See first note.

Translated from Atomnaya Énergiya, Vol. 39, No. 1, pp. 17-19, July, 1975. Original article submitted September 9, 1974.

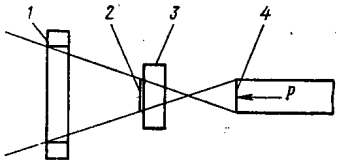

Fig. 1

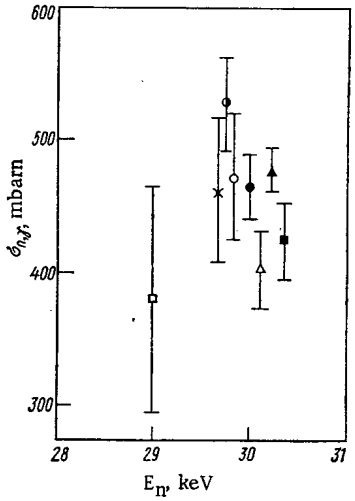

Fig. 2

Fig. 1. Geometry of absolute measurements: 1) coaxial fission chamber; 2) ^{238}U specimen; 3) flat fission chamber; 4) LiF target.

Fig. 2. Results of absolute measurements of radiative capture cross section of ^{238}U for 30 keV neutrons: ●) present authors; ■) [1]; ▲) [2]; ◐) [3]; ○) [7]; □) [12]; Δ) [13]; ×) [14].

TABLE 2. Radiative Capture Cross Section of ^{238}U for Neutrons

E_n, keV	σ_c, mbarn	E_n, keV	σ_c, mbarn
24±8	500±27		
30±6	465±23		
35±8	426±24	1 200±43	91±4,8
45±8,5	371±19	1 300±45	80±4,3
55±9	357±19	1 500±49	60±3,2
65±10	300±15	1 800±54	47±2,6
75±10,5	276±14	2 000±57	39±2,1
85±11	240±13	2 200±61	32±1,8
105±11,5	205±10	2 500±67	26±1,5
125±12,5	18f±9	2 800±73	21±1,3
145±13,5	165±8,5	3 000±78	18±1,1
200±18	145±7,5	3 500±94	16±1,5
250±19	132±6,8	4 000±110	13±1,1
300±19	122±6,3	5 000±115	8±1,1
400±19,5	114±6	6 000±136	6,8±1,0
500±22	108±5,6	7 000±160	5,8±1,1
600±34	108±5,6	15 000±150	3,3±1,47
700±35	114±5,9	16 000±200	3,0±1,3
800±36	116±6	17 000±260	3,7±1,3
900±36	116±6	18 000±235	3,3±1,2
1000±39	109±5,7	19 000±250	2,9±1,4
1100±41	106±5,5	20 000±285	3,4±1,9

of the passage of the neutron beam through the specimen during irradiation. A "long" BF_3 counter was used as an additional neutron flux monitor. The target current was monitored by a current integrator.

We investigated the sputtering of the target material under the influence of the beam of incident protons, and chose measurement conditions in which no sputtering could be observed within the experimental error (< 0.5%).

The background of neutrons which were scattered in the accelerator target chamber was measured by putting the specimen in the flat fission chamber outside the cone of neutrons, and was found to be about 0.1% of the measured effects.

The activity of the target and the activity induced in the ^{238}U specimen by neutron capture were measured by means of a Ge(Li) detector. The efficiency of the detector for measuring the induced activity of ^{238}U was determined by means of a $4\pi\beta$-counter. For this purpose, specimens of impoverished ^{238}U were irradiated in the neutron flux from the thermal column of a BR-10 reactor. To avoid possible resonance self-blocking and self-screening, we used a specimen of "zero" thickness, i.e., one for which these effects are negligible(< 0.6%). Specimens of zero thickness (defined in this way) were irradiated and then measured with a Ge(Li) detector in the $4\pi\beta$-counter. For the measurements with the Ge(Li) detector the specimen thickness was 0.66 mg/cm^2, and for the measurements with the $4\pi\beta$-counter it was 0.2 mg/cm^2.

To convert the measured activity of the zero-thickness specimen to that of a specimen 300 mg/cm^2 thick, we experimentally determined the absorption coefficient of the ^{238}U specimen for 74 keV gamma quanta; as a result of the measurements we made the appropriate correction.

The measurement geometry for the zero-thickness specimens was the same as for the 300 mg/cm^2 specimens.

The results of the determinations in the $4\pi\beta$-counter were processed with the following principal corrections: a correction for the count from the fission products of ^{235}U (0.05%), corrections for self-absorption of beta particles in the specimen (0.1%), and corrections for accumulation of ^{239}Np in the test specimen (1.2%).

To measure the activity of the LiF target, the efficiency of the Ge(Li) detector was determined with a $4\pi\beta$-counter for 412 keV gamma quanta due to decay of ^{198}Au. The geometry for measuring the activity of ^{198}Au in a Ge(Li) detector was the same as for measuring the activity of the LiF target. The relative variation of the efficiency of the Ge(Li) detector with the gamma quantum energy was determined between 380 and 620 keV from the cascade of gamma quanta formed by decay of ^{71m}Zn. From the experimentally measured energy dependence of the detector efficiency we found a semiempirical relation between the efficiency of the Ge(Li) detector and the gamma quantum energy in the given range [4]. As a result, the efficiency of the Ge(Li) detector for 477 keV gamma quanta due to decay of ^{7}Be was calculated from the measured detector efficiency for 412 keV gamma quanta.

In processing the results we made a correction for self-absorption of gamma quanta in the ^{197}Au specimen (0.8%) and for self-absorption of beta particles in the specimen for the $4\pi\beta$-counter (0.1%).

The radiative capture cross section of ^{238}U for neutrons was determined with the following principal corrections: a correction for the increase in the effective specimen thickness due to the finite angle of the neutron cone (1.3%), a correction for resonance self-blocking (0.3%) [5, 6], a correction for scattering of neutrons by the structural materials of the apparatus (5%), a correction for the background of neutrons scattered in the target chamber of the accelerator (0.1%), and a correction for multiple scattering of neutrons in the specimen (0.3%) [7, 8]. The other corrections made in determining the detector efficiency are mentioned above.

The principal errors in the absolute measurement of the radiative capture cross section of ^{238}U for 30 keV neutrons are as follows: the statistical error of a single measurement (1.5%); the error in the value of the efficiency of the Ge(Li) detector in measuring the ^{238}U specimen (2.1%); the error in the efficiency of the Ge(Li) detector in measuring the LiF target (3.38%); the error in the number of gamma quanta from disintegrations (0.1% for ^{197}Au and 1.6% for ^{7}Be) [9, 10]; the error due to the correction for scattering of neutrons in the structure of the apparatus (0.15); the error due to indeterminacy in the half-lives of ^{239}U and ^{7}Be (0.5%); the rms scatter in the results of several series of measurements of the radiative capture cross section of ^{238}U for neutrons (0.8%); the error due to the correction for self-blocking (0.1%); the error due to indeterminancy in the spectrum of the neutrons incident on the specimen (0.2%); and the error due to indeterminancy in the energy dependence of the radiative capture cross section of ^{238}U for neutrons (0.8%).

From the measurements we obtained the radiative capture cross section of ^{238}U for neutrons: it was found to be 465 ± 23 mbarn for 30 ± 6 keV neutrons. In Table 1 (taken from [11] and Fig. 2 we give measurements of the radiative capture cross section of ^{238}U for 30 keV neutrons as found by us and other authors. As we see from Table 1, the results of most authors have errors of about 7-10% and agree with the present authors' results within the experimental error. (An exception is the results of De Saussure [3]. The cause of the marked discrepancy between his results and those of Gibbon [7] and Frike [14], also made by a time-of-flight method, is not clear at present.)

The results of the absolute measurements were used to normalize the energy dependences of the radiative capture cross section of ^{238}U for neutrons as measured previously [17-20]. The radiative capture cross sections are listed in Table 2 (for E_n = 30 keV the cross section was measured absolutely).

In conclusion we thank B. F. Samylin for helping with the measurements.

LITERATURE CITED

1. M. Moxon, Rep. AERE-R6074 (1969).
2. H. Menlove and W. Poënitz, Nucl. Sci. Engng, 33, 24 (1968).
3. G. de Saussure et al., Nucl. Sci. Engng, 51, 385 (1973).
4. T. Paradellis and S. Hontzeas, Nucl. Instrum. and Methods, 73, 210 (1969).
5. R. Macklin, Nucl. Instrum. and Methods, 26, 213 (1964).
6. L. Dresner, Nucl. Instrum. and Methods, 16, 176 (1962).
7. J. Gibbon et al., Phys. Rev., 122, 182 (1961).
8. V. S. Shorin, Preprint FÉI-288 (1971).

9. K. Way et al., Nuclear Data Sheets, National Academy of Sciences, National Research Council, Washington D.C. (1964).
10. J. Taylor and J. Merrit, Canad. J. Phys., 40, 926 (1962).
11. T. Beger and V. Konshin, IAER, Jul. (1971).
12. R. Hanna and B. Rose, J. Nucl. Energy, 8, 197 (1959).
13. T. S. Belanova et al., At. Énerg., 19, No. 1, 3 (1965).
14. M. Frike et al., in: Proc. Conf. of Nuclear Data, Helsinki, 1970, Vol. 2, IAEA (1970), p. 265; NASACR-72745, CA-10194 (1970).
15. H. Shmitt and C. Cook, Nucl. Phys., 20, 202 (1960).
16. Y. Stavisskii et al. [14], p. 51.
17. Yu. G. Panitkin et al., Second International Conference on Nuclear Data for Reactors, Helsinki, 1970, Report CN-26/77 [in Russian].
18. Yu. G. Panitkin and V. A. Tolstikov, At. Énerg., 33, no. 3, 782 (1972).
19. Yu. G. Panitkin et al., in: Proceedings of Conference on Neutron Physics [in Russian], Naukova Dumka, Kiev (1972).
20. Yu. G. Panitkin et al., At. Énerg., 33, No. 4, 825 (1972).

HEAT-TRANSFER CRISIS IN A STEAM-GENERATING TUBE ON HEATING WITH A LIQUID-METAL HEAT CARRIER (COOLANT)

A. V. Nekrasov, S. A. Logvinov, and I. N. Testov

UDC 621.181.021:621.039.517.5

In order to increase the reliability and operating safety of direct-flow steam generators using sodium as heat carrier (coolant), it is essential to make a careful study of the thermal state of the tube metal in the zone in which heat transfer worsens during the boiling of the water. The temperature pulsations of the wall in this zone may have a decisive influence on the life of the heat-emitting surface by accelerating corrosion and creating fatigue damage.

The aim of the present investigation was to study the worsening of heat transfer during the boiling of water in tubes heated by means of a liquid-metal heat carrier.

The experiments were carried out in installations of the direct-flow type (Fig. 1). The liquid-metal heat carrier was pumped through the circuit by means of a circulation pump. After passing the heaters, one flow of heat carrier was directed into a U-shaped evaporator and a second flow was directed through an additional heater into the experimental section. From the evaporator and the experimental section the heat carrier passed into a buffer vessel.

TABLE 1. Average Values of the Maximum Pulsation Intensities

ρw, kg/(m^2 · sec)	q_b, MW/m^2	δ, mm	σ_t, °C
730	0,67	1,6	2,9
730	0,67	0,44	1,3
375	0,73	1,6	3,5
375	0,73	0,44	1,5

The supply water was pumped from the deaerator through a heater to the evaporator inlet; the water-steam mixture (or underheated water) then passed along an unheated tube 20 mm in diameter, 4.5 m long, and reached the entrance into the experimental section. The water-steam mixture was taken out into a condenser through a throttle valve.

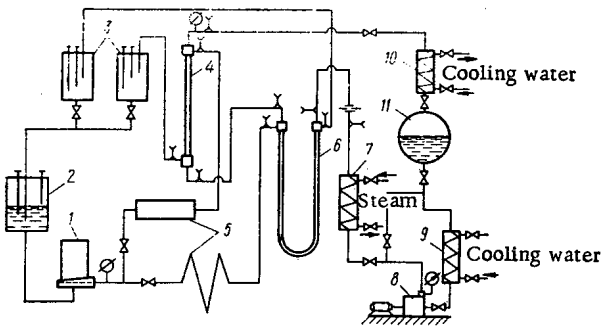

Fig. 1. Arrangement of the experimental apparatus: 1) pump ; 2) buffer vessel ; 3) measuring tanks ; 4) experimental section ; 5) heaters ; 6) evaporator ; 7) supply-water preheater ; 8) GB-351 pump ; 9) supply-water cooler ; 10) condenser ; 11) deaerator.

Translated from Atomnaya Énergiya, Vol. 39, No. 1, pp. 20-23, July, 1975. Original article submitted April 1, 1974.

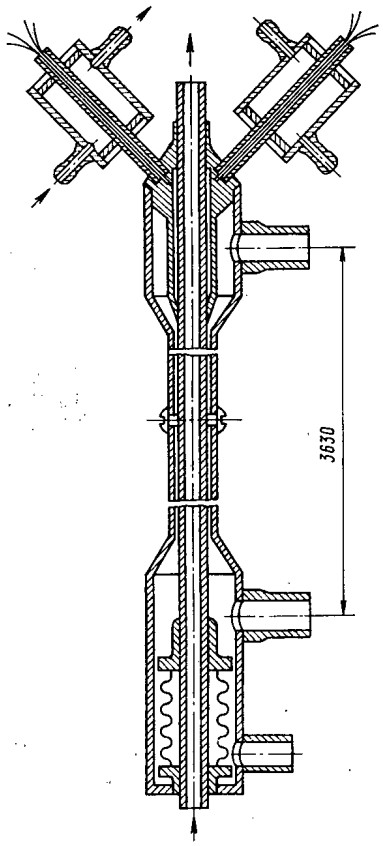

Fig. 2. Experimental section.

The experimental section (Fig. 2) was made in the form of a vertical straight-tube heat exchanger of the tube-in-tube type with counterflow motion of the heat carriers. The water-steam mixture passed from bottom to top along a tube of diameter 16 × 3 mm made from St. 20 steel. The liquid metal moved from top to bottom through an annular channel formed by the outer (diameter 32×3 mm) and inner tubes. The distance between the inlet and heat-carrier pipes was 3630 mm.

The temperature distribution of the liquid metal over the height of the experimental section was monitored by means of a set of surface thermocouples.

For studying the temperature pulsations in the wall of the inner tube, sixteen microthermocouples were fitted into the upper part of the experimental section; they were placed in such a way as to facilitate measurement of the temperature field along the perimeter, along the generator, and through the thickness of the tube wall.

The emf of the microthermocouples in the tube wall was measured with the aid of two single-range potentiometers having a scale of 0-150°C and a scanning time of 0.8 sec. The recording-paper pulling speeds were increased to 51200 mm/h. The pulling mechanisms of the two potentiometers were synchronized.

The experiments were carried out in the following way. The rate of heat-carrier flow through the experimental section, the temperature of the heat carrier at the inlet, the pressure, and the rate of water flow were kept constant, while the heat content of the water at the entrance into the experimental section was smoothly increased until signs of worsening heat transfer appeared in one of the thermocouple-monitored cross sections of the experimental section. On stabilizing the thermal conditions, all the parameters characterizing the latter were recorded, as well as the temperature pulsations of the heat-transfer surface.

Experiments were carried out at pressures of 29, 98, and 147 bar and mass velocities of 375-2100 kg/(m^2 · sec). In the region of developed bubble-type boiling the thermal flux varied in accordance with the law

$$q_b = k(t_b - t_s)\exp\left(-\frac{k\pi d}{GC_p}Z\right), \quad (1)$$

where k is the heat-transfer coefficient in the section of developed bubble-type boiling, t_b is the temperature of the liquid metal in the zone of worsening heat transfer (b = boundary), C_p is the specific heat, G is the flow of liquid metal, t_s is the boiling point, d is the diameter, and Z is the current coordinate.

An analysis of the results of these investigations shows that, in the range of specific heat flows characterizing the present experiments, and for a prespecified pressure and mass velocity, the steam content at which a worsening heat transfer begins is independent of the specific thermal flux (by way of example, Fig. 3b gives the results obtained for ρw = 700 kg/(m^2 · sec) and p = 147 bar). This means that, in the range of operating parameters under consideration, we are concerned with a heat-transfer crisis of the second kind [1], and the steam content at which a worsening heat transfer develops should be regarded as x_b^0.

Our present values of x_b^0, obtained under conditions in which the tube was heated by the liquid-metal heat carrier, may be compared with the results of calculations based on the equations derived in [1, 2]:

$$x_b^0 = \left[(0.92 - 0.00344P)\sqrt{\frac{1000}{\rho w}}\right]\left(\frac{8}{d}\right)^{0.15}; \quad (2)$$

$$x_b = 8.92P^{0.15}(\rho w)^{-0.45}. \quad (3)$$

The results of such a comparison are presented in Fig. 3. We see from these curves that for pressures of 98 and 147 bar our own data agree with the results of Eq. (2), and at 29 bar with those of Eq. (3). This means that x_b^0 does not depend on the form of heating or the manner in which the thermal flux varies along the tube axis.

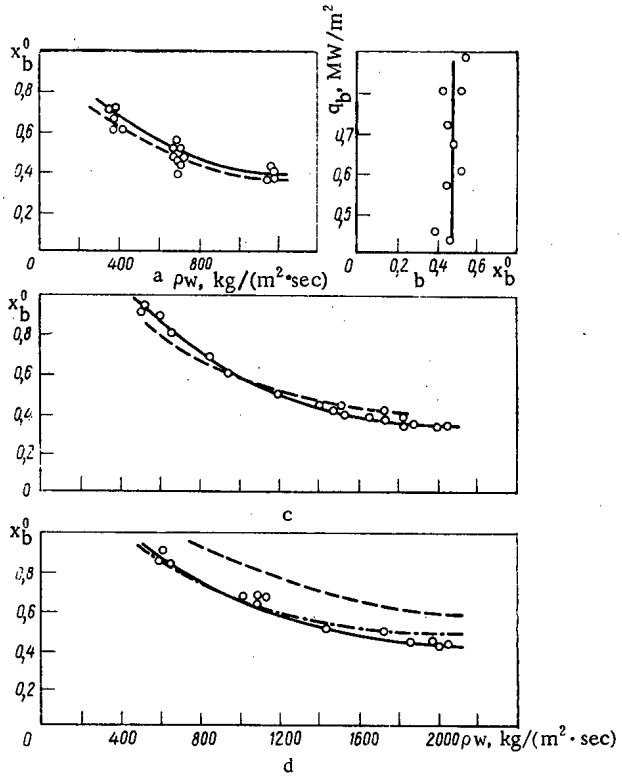

Fig. 3. Limiting (boundary) steam content as a function of mass velocity [—) this paper; ---) and -·-·) calculations based on Eqs. (2) and (3) respectively]: a) p = 147 bar; b) p = 147 bar, ρw = 700 kg/(m²·sec); c) p = 98 bar; d) p = 29 bar.

The pulsations of wall temperature accompanying the worsening heat transfer were studied at a pressure of 147 bar and mass velocities of 375, 700, and 1150 kg/(m²·sec). The experimental data relating to the pulsations were analyzed by methods of correlation analysis [3].

Using an electronic computer, we estimated the mathematical expectation t_{cp}, the dispersion, the mean square deviation (intensity) σ_t, the normalized autocorrelation time coefficient, and the normalized spectral density S (ω).

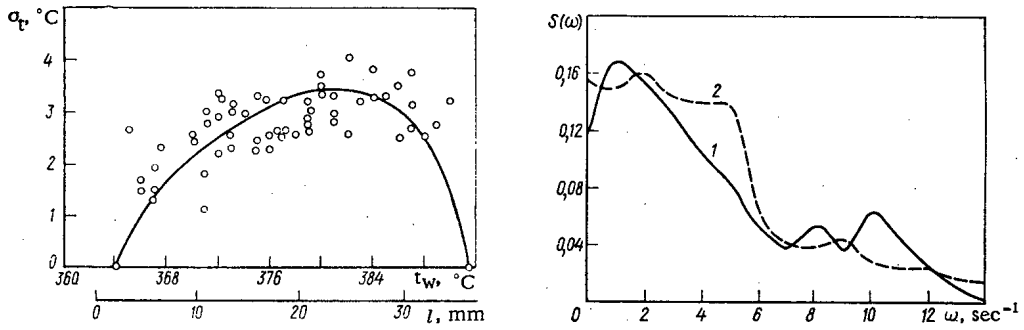

Fig. 4. Change in the intensity of the wall temperature pulsations along the tube for: pw = 375 kg/(m²·sec), p = 147 bar, q_b = 0.73 MW/m².

Fig. 5. Normalized spectral densities of the temperature pulsations at a distance of 1.6 mm from the outer surface of the tube for p = 147 bar: 1) pw = 730 kg/(m²·sec); q_b = 0.73 MW/m²; σ_t = 3.5°C.

The experiments showed that other conditions being equal the character and intensity of the pulsations differed according to whether water not quite heated to the boiling point or a water-steam mixture were fed into the inlet of the experimental section. In the first case the extent of the pulsation zone along the tube axis was no greater than 40 mm; different modes of heat transfer were able to take place at diametrically opposite points. This indicates that the liquid film wetting the tube wall breaks up into individual rivulets, alternating with dry spots, before vanishing altogether. For points lying at a distance of 1/4 of the circumference from each other, the results are ambiguous: sometimes the pulsations are sharply synchronized and of similar amplitudes, sometimes there is only a weak coupling between the pulsating processes. Apparently a distance equal to 1/4 of the circumference is close to the limiting correlation length.

The intensity of the pulsations and the average wall temperature differ in behavior along the pulsation zone. The pulsations are smallest when the wall temperature corresponds to the temperature in the mode of developed bubble-type boiling and in the mode of impaired heat transfer. The maximum intensity of the pulsations occurs for an intermediate value of the wall temperature (Fig. 4). The average values of the maximum pulsation intensities are shown in Table 1 (δ is the distance from the outer surface of the tube to the center of the hot junctions of the microthermocouples).

An analysis of the averaged curves of the normalized spectral densities shows that at a distance of 1.6 mm from the outer surface the greatest contribution comes from pulsations at a frequency of under 1 Hz (Fig. 5). On moving away from the inner surface the relative proportion of low frequencies in the spectrum increases.

On passing a water-steam mixture into the experimental section the intensity and spectral composition of the temperature pulsations change considerably. In this case the pulsations have a fairly ordered character; their intensity is much higher than on passing water not quite heated to the boiling point into the inlet. Thus, for example, for $\rho w = 700$ kg/(m^2·sec) and $q_b = 0.7$ MW/m^2 the intensity is ~ 9°C at 1.6 mm from the outer surface. The spectrum is dominated by frequencies of the order of 0.2-0.5 Hz. The temperature around the perimeter of the tube pulsates in synchronism; the length of the pulsation zone along the tube axis exceeds 80 mm.

Since water not quite heated to the boiling point is usually fed into the inlet of direct-flow steam generators using sodium as heat carrier, it is important when studying the temperature pulsations in the zone of impaired heat transfer either to avoid the supply of water-steam mixture to the inlet of the experimental section altogether or else to take special precautionary measures (shorten the feeding section to a minimum, make it conform to the geometry of the steam-generator tube, etc.).

LITERATURE CITED

1. V. E. Doroshchuk, Heat-Transfer Crisis for the Boiling of Water in Tubes [in Russian], Énergiya, Moscow (1970).
2. V. E. Doroshchuk and V. I. Nigmatullin, Teploénergetika, No. 3, 79 (1971).
3. E. S. Wentzel, Theory of Probabilities [Russian translation], Nauka, Moscow (1964).

X-RAY DIFFRACTION STUDY OF THE EFFECT OF THE TEMPERATURE OF DEFORMATION IN THE ALPHA PHASE ON THE QUENCH TEXTURE OF URANIUM RODS CONTAINING VARIOUS PROPORTIONS OF IRON AND SILICON

V. F. Zelenskii, V. V. Kunchenko,
V. S. Krasnorutskii, N. M. Roenko,
V. P. Ashikhmin, A. V. Azarenko,
and A. I. Stukalov

UDC 621.039.543:543.428.8

After deformation (working) at various temperatures uranium rods containing impurities in various initial states (e.g., in solid solution or in the form of dispersed inclusions) acquire certain characteristic forms of texture.

It was shown earlier that such impurities blocked {110} <100> slip processes during the plastic deformation of uranium at temperatures of over 450°C [1]. The slip effect only becomes appreciable at working temperatures of 600°C. Annealing at 600°C for 24 h after β quenching causes the impurities to coagulate. This has the effect that the contribution of {110} <110> slip processes, leading to the formation of (110) texture in the plastic deformation uranium, becomes appreciable even for working temperatures of 450°C. Such characteristics of work-induced texture formation may exert a considerable influence on the mechanism of texture formation after quenching from the β phase [2].

In this paper we shall study the effects of annealing, the temperature of deformation in the α phase, and changes in the iron and silicon content on the texture of uranium rods (bars) quenched from the β phase.

Materials and Experimental Method. In these experiments we used uranium of three types, differing in their iron/silicon impurity ratio. The first type of uranium contained twice as much iron as silicon; in the second type the impurity contents were equal, while in the third type the silicon content was twice as great as that of the iron.

The maximum content of each element was 0.03 wt.%. Other impurities amounted to the same percentage in each sample (carbon under 0.1 wt.%, aluminum 0.005 wt.%). According to the conditions of treatment the original samples may be divided into two groups. Group A comprised uranium bars obtained by extruding a 7 mm diameter rod from the γ phase, annealing at 800°C for 3 h, water-quenching from the β phase, and drawing at 250-600°C at a rate of 0.4 m/min, with a total reduction of 60% [1].

In contrast to group A the second group of samples (group B) were annealed at 600°C for 24 h after β quenching.* The uranium rods prepared in this manner were subjected to "transverse" quenching from the β phase.† The quenching texture was determined by calculating the inverse pole figures and the growth

*Deformation-texture data were presented in [1].

†The bar was passed at 7 mm/sec through the heating zone of the inductor of an hf generator, in which it was heated to 730-740°C, and remained at this temperature for 7-9 sec. On passing out of the heating zone the bar was cooled with a water spray.

Translated from Atomnaya Énergiya, Vol. 39, No. 1, pp. 24-27, July, 1975. Original article submitted June 3, 1974; revision submitted February 3, 1975.

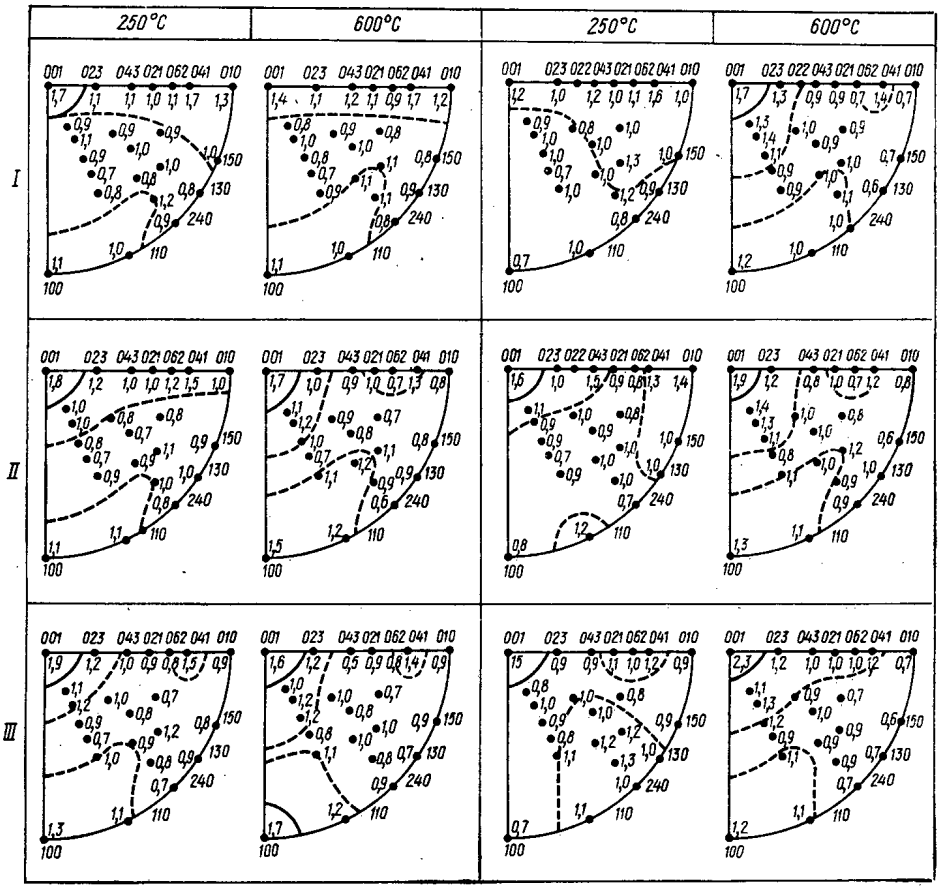

Fig. 1. Pole figures of unannealed (A) and annealed (B) uranium of various types (I, II, III) worked at various temperatures before β quenching (250 and 600°C).

index G_X [2]. In order to eliminate the influence of possible structural inhomogeneities in the bars, and also to increase the number of crystals taking part in x-ray diffraction, x-ray diffraction patterns were recorded from the surface of three microsections perpendicular to the axis of the rod [1]. We also determined the thermal expansion coefficient (α) at 20-100°C and the resistivity ρ of the uranium bars in the axial direction at 20°C.

Experimental Results and Discussion. For all three types of uranium (Figs. 1 and 2) the temperature of preliminary deformation has similar effects on the texture of the quenched samples. Group A uranium samples worked at 250°C have a complex texture in the direction of the rod axis. The main texture pole is (001), with considerable spreading in the (010) direction. The group of poles close to the (100) is poorly distinguished. A relative increase in the silicon content (samples of the second and third types) leads to a reduction in the density of poles close to the (010) and a slight increase in the density of the (001) poles and the poles close to the (100). The changes in texture caused a corresponding reduction in the growth index G_X and an increase in α and ρ (Fig. 2, curves A). With increasing deformation temperature of the uranium in the α phase this tendency to undergo changes in texture intensifies, but to different extents for the different types of metal.

Whereas for metal of the first type (Fe>Si) an increase in the prequench deformation temperature (to 600°C) leads to a very slight reduction in the density of the poles close to (010), for the second (Fe $\approx$ Si) and especially the third (Si > F) types these changes are very considerable. For uranium of the third type the group of poles close to the (010) gradually diminishes with increasing silicon content until it practically vanishes, while the (100) poles are correspondingly intensified. In this case the growth index assumes negative values, the linear thermal-expansion coefficient increases very slightly, while the resistivity remains constant.

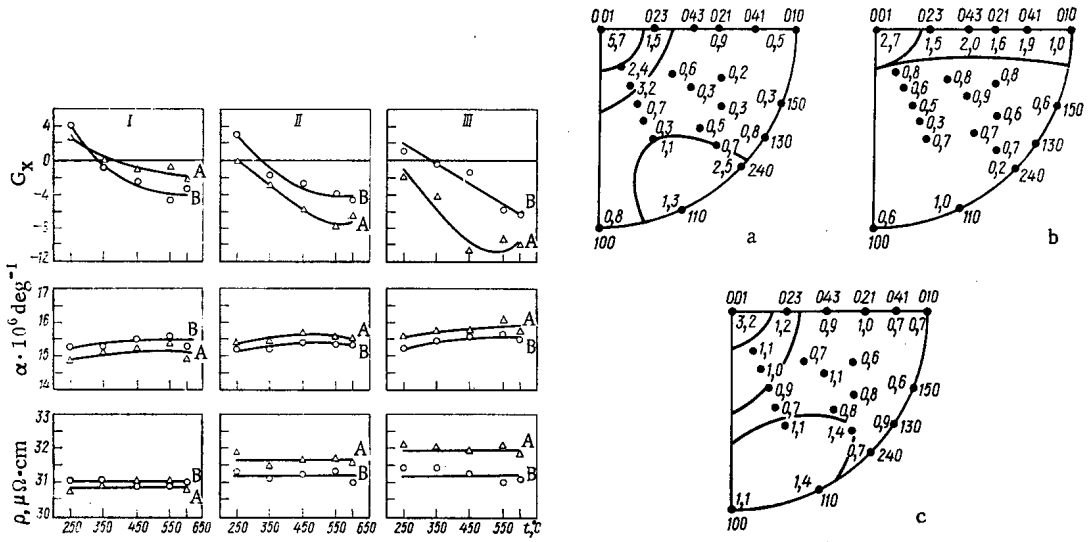

Fig. 2. Growth index G_x, thermal-expansion coefficient α, and resistivity ρ of unannealed (A) and annealed (B) uranium of various types as functions of the deformation temperature before quenching from the β phase.

Fig. 3. Quench textures of various types of uranium. a) Electrolytic uranium; b) Fe > Si; c) Si > Fe.

A change in silicon content has little effect on the quench texture of uranium annealed before deformation (Group B). On increasing the silicon content in quenched uranium previously worked at 250°C, there is a slight tendency for the (110) and (001) group of poles to become stronger. As deformation temperature increases, this tendency becomes rather more marked, the density of the poles close to (010) diminishing. However, the range of changes in the growth index due to changes in texture is smaller in this case than in the unannealed metal.

It was shown earlier [2] that the quench texture was determined by the character of the stress field (structural and thermal) acting on the β matrix. Under quenching conditions, the tensile forces at the phase boundary promote the formation of α crystals oriented with their [010] axis in the direction of action of these forces. Thus the geometry of the sample and the shape of the phase interface, determined by the quenching conditions, promote the development of characteristic texture [4, 5]. However, other factors may also act upon the texture of the quenched metal, especially factors changing the kinetics of the phase transformation (quench temperature [6], grain size, the presence of impurities [7, 8] and so on).

In the case under consideration samples differing in respect of their conditions of deformation, impurity state, and Fe/Si impurity ratio were subjected to β quenching.

It follows from experiments on the multiple quenching of uranium [9] that the earlier-observed [10] increase in the microstresses and the density of the randomly-distributed dislocations in uranium after three or four quenchings has no effect on the character and degree of perfection of the quench texture. We may thus reasonably assume that the changes in these characteristics caused by an increase in the deformation temperature in the α phase also have no decisive effect on the quench texture.

The dependence of the quench texture on the previous deformation temperature of the α uranium may arise from a change in the state of the impurities forming the supersaturated α solid solution (the state after β quenching). Increasing the deformation temperature to 600°C leads to the decomposition of the solid solution. The manner in which the impurities remaining in solution affect the kinetics of the $\alpha \rightleftarrows \beta$-transformation changes accordingly [8].

It is reasonable to assume that, as the deformation temperature and the silicon content increase, the decomposition of the supersaturated solid solution is accompanied by the formation of (U, Si, Fe) compounds which dissolve less readily in the β phase; this is equivalent to the "purification" of the uranium from iron and silicon. The texture of such β quenched uranium is similar in character to analogously quenched refined (electrolytic) uranium (Fig. 3); it follows that, on quenching the uranium, the excess

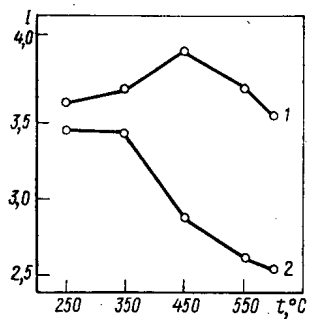

Fig. 4. Preliminary orientation parameter as a function of the deformation temperature of β-quenched (1) and post-quench-annealed (2) uranium bars [15].

(relative to silicon) iron in solid solution promotes the formation of texture with poles close to the (010). This evidently explains the kinetic characteristics of the redistribution of the texture poles in accordance with increasing silicon content and rising pre-β-quench deformation temperature.

However, the "purification" effect alone cannot explain the considerable dependence of the quench texture of the annealed samples on the preliminary deformation temperature. The annealing of β quenched samples at 600°C for 24 h leads not only to the decomposition of the solid solution but also to a considerable coagulation of the precipitating impurities. There are no grounds for considering that subsequent deformation at various temperatures will produce a further decomposition of the solid solution (or a renewed dissolution of the impurities). This is confirmed by the practically identical values of ρ after treating each of the three types of uranium in the same way (Fig. 2B).

The relationship in question may be associated with a change in the character of the uranium texture with increasing deformation temperature [1], if we allow for the possible formation of anisotropically-distributed two-dimensional dislocation and impurity-dislocation networks in the uranium α crystal [11-13]. In the case of iron alloys, impurity-dislocation networks remain stable with respect to phase transformations [14]. Such networks (constituting elements of the α-uranium substructure formed as a result of quenching or deformation) may serve as "memory" carriers in respect of the $\alpha \rightarrow \beta \rightarrow \alpha$ transformation associated with quenching.

Complexes of vacancies formed in specific crystallographic planes of strongly-textured uranium [13] may also serve as an orienting factor for the nucleating β crystal in the $\alpha \rightarrow \beta$ transformation.

A rise in the deformation temperature (especially when slip processes are active) leads to a reduction in the general anisotropy (Fig. 4), and hence to a reduction in the orienting effect of the factors under consideration.

Thus the quench texture of uranium bars is substantially influenced by changes in the deformation temperature of the uranium in the α phase, the quantitative relationship between the iron and silicon impurities, and also the state assumed by these impurities in the uranium before quenching.

LITERATURE CITED

1. V. E. Ivanov et al., At. Énerg., 24, No. 1, 87 (1968).
2. V. E. Ivanov et al., At. Énerg., 16, No. 4, 325 (1964).
3. G. Slattery and D. Connolly, Rep. TRG 360(S) (1963).
4. V. F. Zelenskii, V. S. Krasnorutskii, and V. V. Kunchenko, At. Énerg., 27, No. 5, 411 (1969).
5. V. F. Zelenskii and V. S. Krasnorutskii, At. Énerg., 31, No. 5, 449 (1971).
6. W. Donnell, Nucl. Sci. Engng., 12, 325 (1962).
7. J. Gittus et al., Preprint IAEA, NSM 25/83, Vienna (1962).
8. J. Gittus, Brit. Nucl. Energy Soc., 3, 106 (1964).
9. V. F. Zelenskii et al., At. Énerg., 33, No. 2, 677 (1972).
10. M. K. Asundi et al., J. Nucl. Materials, 6, No. 1, 123-126 (1962).
11. E. Ruedl and S. Amelinckx, J. Nucl. Materials, 9, No. 1, 116 (1963).
12. A. Crocker, J. Nucl. Materials, 15, No. 1, 121 (1965).
13. B. Sharma, R. Bharadmay, and K. Tangri, Phil. Mag., 8, No. 85, 1 (1963).
14. Metal Physics. Phase Transformations. Republican Interdepartmental Collection, Academy of Sciences of the Ukrainian SSR [in Russian], Naukova Dumka, Kiev (1970).
15. E. Sturcken and J. Croach, Trans. Met. Soc. AIME, 227, 934 (1963).

A LOOP CONVERTER CHANNEL FOR TESTING HIGHLY-ENRICHED FUEL ELEMENTS IN A RESEARCH REACTOR

V. G. Bobkov, V. B. Klimentov,
G. A. Kopchinskii, M. V. Mel'nikov,
and V. A. Nechiporuk

UDC 621.039.519

One of the most important problems of atomic technology is that of conducting loop tests on fuel elements made from highly-enriched fuel and developed for use in fast reactors. The possibilities of carrying out such tests in thermal research reactors are limited by the nonuniformities of energy evolution and burn-up in the fuel composition. An increase in the number of fuel elements in the fuel assemblies under test still further reduces the representative nature of the tests. One method of equalizing the energy evolution and burn-up in test fuel-element assemblies and making the test conditions approach those envisaged in the original design is to increase the hardness of the neutron spectrum in the loop channel. In support of this assertion, it is sufficient to remember that the range of thermal neutrons in highly-enriched uranium dioxide fuel is about 0.1 cm, while the mean range of superthermal neutrons is four times greater.

In order to equalize energy evolution in loop channels, a frequent practice is the use of absorbing (boron and cadmium) screens [1, 2]. However, the considerable negative reactivity involved limits the dimensions of the irradiating systems. The possibilities of using breeding materials for the screens have also been considered [3, 4]. The SOCRATE channel, with a uranium dioxide screen, was proposed in [4] for the mass irradiation of fuel elements in the BR-2 research reactor. Calculations indicated hopeful characteristics of this irradiating device. However, because of the thermal power of the channel, amounting to 10 MW, a complicated liquid-metal circuit had to be constructed.

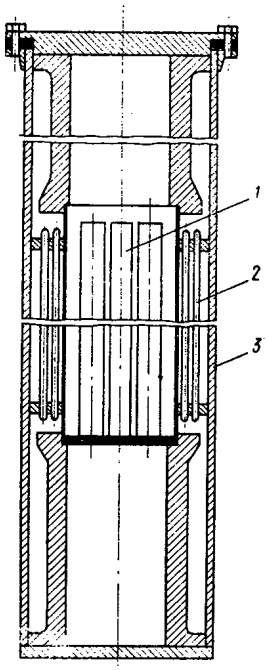

Fig. 1

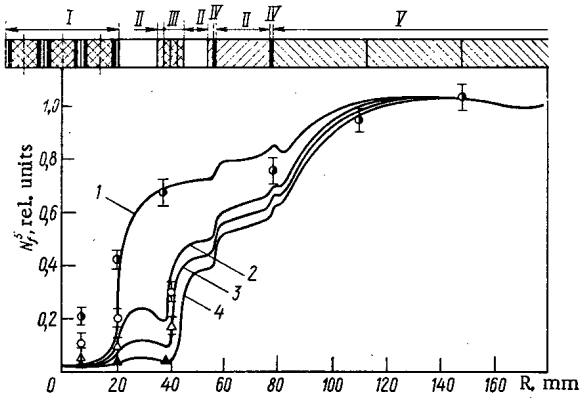

Fig. 2

Fig. 1. General view of the model loop converter channel : 1) Central assembly of highly-enriched fuel-element models; 2) converter screen; 3) body of channel.

Fig. 2. Fission density distribution (N_f^5) over the radius of the converter cell (1, 2, 3, 4 – $\Sigma_a \Delta l$, respectively equal to 0; 0.8; 1.6; 3.6): I) assembly of fuel element models; II) aluminum; III) screen; IV) water interlayers; V) active zone of the VVR-M.

Translated from Atomnaya Énergiya, Vol. 39, No. 1, pp. 28-32, July, 1975. Original article submitted August 9, 1974.

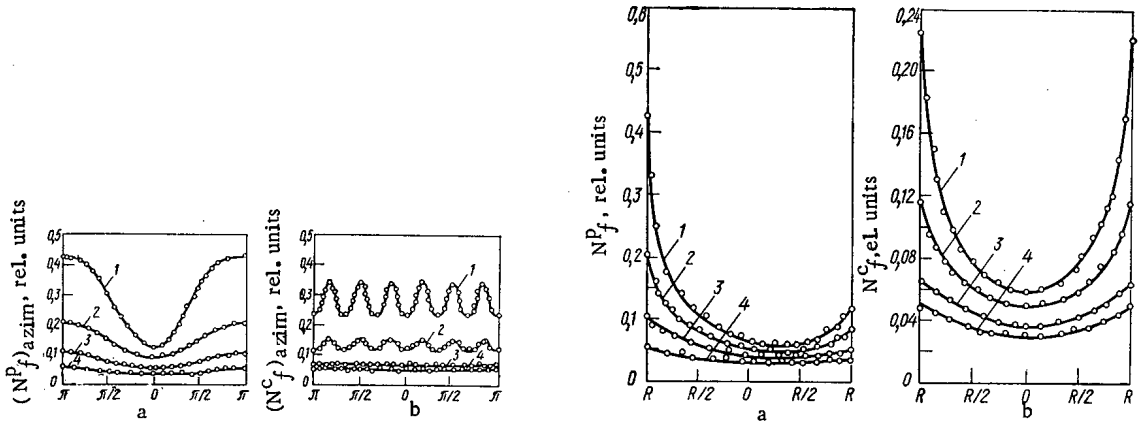

Fig. 3. Fission density distribution over the surface of the cores in the peripheral (a) and central (b) fuel elements (1, 2, 3, 4 — $\Sigma_a \Delta l$, respectively equal to 0; 0.8; 1.6; 3.6).

Fig. 4. Fission density distribution over the radius of the cores of the peripheral (a) and central (b) fuel elements (1, 2, 3, 4 — $\Sigma_a \Delta l$, respectively equal to 0; 0.8; 1.6; 3.6).

In 1965 experimental and theoretical research was started in connection with a model loop channel containing a breeding screen, intended for tests on assemblies of highly-enriched fuel elements in a thermal research reactor [5-7]. We shall present the main results of the tests in this paper.

Construction of the Channel, Basic Problems, and Research Methods

The model channel (Fig. 1) consisted of a cylindrical hermetic vessel, with a seven-element set of highly-enriched fuel-element models made from 90%-enriched UO_2 tablets 0.9 cm in diameter (2R) in the center; the fuel elements were held in a stainless steel tube with an external diameter of 1 cm and a wall thickness of 0.03 cm. The height of the tablets was variable (0.2-0.5 cm). The minimum height of the uranium in the tube varied from 3 to 6 cm. The test assembly was surrounded with a screen having an internal diameter of 7.5 cm. The screen was made up of rods. Each rod of the converter zone was a thin-walled nickel tube with an external diameter of 0.25 cm, an internal diameter of 0.23 cm, filled with 90%-enriched UO_2 over a length of 30 cm. The weight of the UO_2 in one rod was no less than 8.5 g for a ^{235}U content averaging 6.84 g. The rods were hermetized at the ends with nickel end-pieces 1.5 cm long. The number of rods prepared was 450. The optical thickness of the screen with respect to thermal neutrons varied from 0 to 3.6. The model of the channel was fixed in the middle of the active zone of the VVR-M critical assembly with an aluminum displacer [8].

The main problems of the investigation were : 1) To study the possibility of creating a uniform field of energy evolution in a seven-element assembly of highly-enriched fuel elements ; 2) to study the influence of screen thickness on the specific energy evolution in the fuel elements under test; 3) to study the converting effect of a breeding screen; 4) to study the spectral changes in the experimental volume of the channel; 5) to accumulate experimental data regarding the interaction of the fast microzone of the converter channel with the active zone of the thermal reactor; 6) to develop a method of neutron-physical calculations for the converter channel ; 7) to study the characteristics of various possible forms of the channel.

We studied the macro- and microdistribution of fission density in the assembly of fuel-element models. The macrodistribution was studied by using uranium detectors; these were made by depositing a layer of 90%-enriched UO_2 0.5 mg/cm^2 thick on an aluminum substrate. The diameter of the detectors equalled the diameter of the uranium tablets. The microdistribution of fission density over the radius and surface of the fuel-element models was studied by autoradiography [5]. As detectors we used paper disks and strips collecting the fission fragments during irradiation.

The relative distributions of the fast-neutron flux density were measured by using the $^{115}In(n\,n')^{115}In$ reaction. The detectors were made of metallic indium 112 mg/cm^2 thick; they were surrounded by a two-layer jacket : the outer layer, cadmium 0.05 cm thick, the inner layer, indium 40 mg/cm^2 thick. The activities of the detectors were measured in a γ spectrometer with a guard anticoincidence scintillator [6].

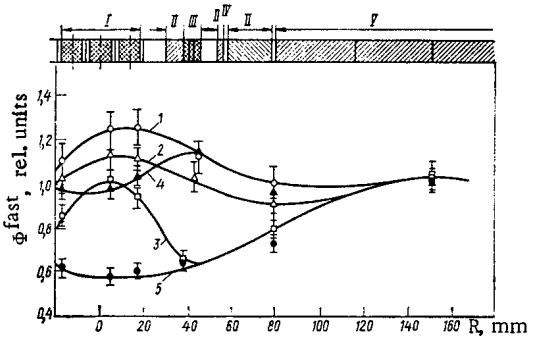

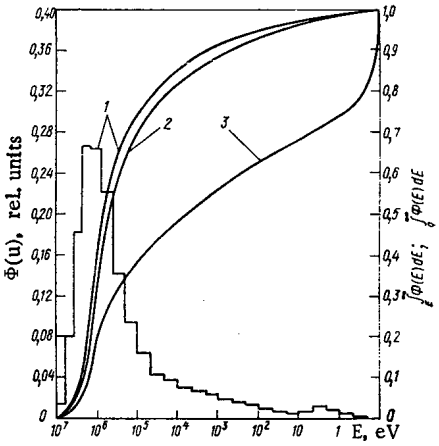

Fig. 5. Fast-neutron distributions (Φ), measured by reference to the activation of indium [1, 2, 3 — $\Sigma_a \Delta l$, respectively equal to 3.6; 1.6; 0; 4, 5 — without the assembly of fuel-element models (4 — $\Sigma_a \Delta l = 3,6$; 5 — without screen)]. The rest of the notation is as in Fig. 2.

Fig. 6. Neutron spectra in the converter cell with a screen 3.6 thick: 1) center of fuel-element model assembly; 2) periphery of fuel-element model assembly; 3) active zone of VVR-M reactor.

The test loop cells, consisting of the assemblies of fuel-element models, the screen, and the active zone of the thermal reactor were distinguished by a sharp inhomogeneity of their neutron-physical properties. The energy distributions of the neutrons within the cell may vary substantially, from the spectrum of the thermal reactor to spectra approaching those of fast systems. This necessitates using cumbersome methods for calculating such systems. In the present investigation we used the S_n method. The calculation was carried out in uniform cylindrical geometry using a 26-group system of constants [9] in the S_4 approximation, on the basis of a complex of programs developed in the Scientific-Research Institute of Atomic Reactors. The constants of the thermal group were averaged over the spectrum (previously calculated by the SI-5 program).

Results of the Investigations

Equalizing the Energy Evolution in the Assembly of Fuel Elements. The manner in which equalization progressed with increasing optical thickness of the screen is shown in Fig. 2, which presents the theoretical and experimental fission-density distributions in the converter cell. Whereas without the screen the ratio of the fission densities on the surfaces of the peripheral and central fuel-element models equalled 2.0, as the screen thickness increased to $\Sigma_a \Delta l = 3.6$ this fell to 1.06. The cadmium fission ratio on the surface of the fuel elements equalled 1.17±11%. For a small optical thickness of the screen there is a considerable difference between the experimental and calculated fission densities. This discrepancy may be explained by the heterogeneous structure of the screen and the assembly of fuel-element models, which creates a substantial inflow of thermal neutrons into the central zone. For the maximum screen thickness, corresponding to the pseudohomogeneous state, the calculated and experimental data are in satisfactory agreement.

The equalizing of the field of energy evolution in the fuel-element assembly is shown in more detail in Figs. 3 and 4. Figure 3 shows the measured azimuthal distributions of the fission density (obtained by autoradiography) on the surface of the peripheral and central fuel-element models, and Fig. 4 presents analogous data for the radial section of the models. The numerical data were characterized by fission-density "bias coefficients", defined as the ratio of the maximum to the minimum fission density in the corresponding section of the fuel-element model.

The fission-density distributions shown in Fig. 3 indicate a considerable azimuthal nonuniformity of energy evolution in the absence of the screen. The development of nonuniformity in the peripheral models may be attributed to the screening effect of neighboring fuel elements. As a result of this the energy evolution on the surface of the fuel element facing the active zone was 3.5 times greater than on that facing the center of the assembly. Clearly such conditions are not satisfactory for testing fuel elements. The

introduction of the converter screen greatly reduces the azimuthal nonuniformity in the peripheral fuel elements. For a screen 3.6 thick the corresponding fission-density bias coefficient falls to 1.57±5%.

A still more complicated picture of azimuthal nonuniformity occurs for the central fuel element. Without a screen the fission density distribution on the surface of the fuel element bears a sinuous character, due to the inflows of slow neutrons through the gaps between the peripheral fuel elements. The introduction of a screen 1.6 thick completely eliminates the azimuthal nonuniformity of energy evolution for the central fuel element.

It follows from Fig. 4 that without the screen the nonuniformity of energy evolution is also considerable over the radius of the fuel elements. Thus for a peripheral fuel element the radial bias coefficient of fission density reaches 7.00 ± 5%, and for a central element 3.00 ± 5%. After the introduction of a screen 3.6 thick the corresponding bias coefficients were 1.64 ±5% and 1.57 ±5%. If the bias coefficient for the whole seven-element assembly is defined as the ratio of the maximum to the minimum fission density, without the screen this equals 7.35 ± 5% and with the screen 3.6 thick it equals 1.67 ± 5%, the latter figure being confirmed by a calculation, which gave 1.71.

Average Specific Energy Evolution. The average specific energy evolution in a seven-element assembly was estimated on the basis of our experimental data, allowing for the relationship

$$\bar{q}_{sp} = \frac{\Phi_{th}\Sigma_f^{th} R_{Cd}^f \mu^f}{(R_{Cd}^f - 1)\,\bar{k}\,3.1\cdot 10^{10}}\ \text{W/cm}^3),$$

where Φ_{th} is the unperturbed flux density of thermal neutrons in the active zone of the research reactor; Σ_f^{th} is the macroscopic fission cross section for thermal neutrons, calculated for the composition of the fuel element under test; $R^f_{Cd}/(R^f_{Cd}-1)$ is a correction allowing for the contribution of hypercadmium neutrons to the total number of fissions; μ^f is the relative fission density on the surface of a peripheral fuel element (determined in the form of a ratio with respect to the fission density in the unperturbed part of the active zone of the reactor); $\bar{k}$ is the nonuniformity coefficient, defined as the ratio of the maximum energy evolution in the set of fuel elements to the mean value.

In view of the fact that the azimuthal nonuniformity impeded numerical integration of the fission density distributions over the cross section of the fuel-element assembly, we simply considered two extreme cases, $\bar{k} = 1$ and $\bar{k} = 1.67$ (maximum and minimum energy evolution in the assembly).

If we allow ourselves to be guided by the thermal-neutron flux density in the unperturbed region of the active zone of the VVR-M reactor $\Phi_{th} = 10^{14}$ neutrons/(cm^2 · sec) and the experimentally found values of $\mu^f = 0.053$ ± 8% and $R^f_{CD} = 12.5$ ±11%, the average specific energy evolution in the seven-element assembly of the highly-enriched fuel elements under test for a screen optical thickness of 3.6 should lie within the range 1.5-2.0 kW/cm^3.

Converting Effect of the Screen. This is illustrated in Fig. 5, which presents the experimental fast-neutron distributions over the radius of the test cell.

A comparison between curves 4 and 5 shows that the introduction of the thickest screen increases the fast-neutron flux density in the experimental region of the channel by a factor of 1.7. The fuel-element assembly increases the fast-neutron flux by a factor of 1.25.

Spectral Changes. Spectral changes in the assembly of fuel elements were studied by calculations based on the S_n method. Figure 6 shows the integrated and differential neutron spectra obtained for a screen optical thickness of 3.6. For comparison we also show the neutron spectra of the active zone of the VVR-M. On introducing the screen a hard neutron spectrum is established in the fuel-element assembly, having a median energy of about 500 keV with respect to the flux density. The differences between the spectra in the center and at the periphery of the assembly are displaced substantially in the high-energy direction. Whereas before introducing the screen the median energy in the fission spectrum in the center of the assembly equalled 100 eV, while at the periphery 86% of the fissions were caused by thermal neutrons, For $\Sigma_a \Delta l = 3.6$ the median energy equalled 465 eV. On comparing the spectrum of the converter channel with typical fast-reactor spectra we see that these are very similar to one another, only in the first case there is a low-energy "tail" which makes a considerable contribution to the total number of fissions.

Interaction of the Converter Channel with the VVR-M Critical Assembly. This interaction was studied by measuring the critical loadings and the efficiency of the peripheral fuel elements of the critical assembly. For $\Sigma_a \Delta l = 3.6$ the loading of the critical assembly fell by 0.250±0.015 kg of ^{235}U, i.e., the

gain was about 11%. We estimated the most dangerous situation in which the converter channel was filled with water. For $\Sigma_a \Delta l = 2.8$ the reactivity increased by $4\beta_{eff}$, which was reliably compensated by a system compensated by a system of emergency protection with an efficiency of (9-10) β_{eff}.

Converter Channel with a Variable-Enrichment Screen. Thermotechnical estimates based on the foregoing experimental data showed that by using liquid-metal coolants it was possible to carry off the heat generated in the converter channel under temperature conditions acceptable to the construction materials. The heating of sodium (initial temperature 250°C) should be 200°C, and the thermal fluxes in the screen $1.5 \cdot 10^6$ kcal/(m^2 · h).

A serious drawback of the converter channels is the fact that the specific energy evolution in the screen is several times greater than in the fuel-element assembly, and ten times greater than in the active zone of the VVR-M reactor. In addition to this, the radial distribution of energy evolution in the screen is distinguished by a sharp nonuniformity. The ratio of the maximum to the minimum energy evolution is 7.15.

A considerable equalization of the energy evolution over the radius of the converter cell may be achieved if the ^{235}U concentration in the screen is gradually increased on approaching the axis of the channel. We studied the characteristics of such a channel theoretically, the screen consisting of five zones with successive 10, 20, 35, 60, and 90% enrichment of the UO_2. The geometrical thickness of each layer was 0.25 cm. In this case the bias coefficient of the fission density in the screen was 1.70; the maximum specific energy evolution was altogether four times greater than the analogous quantity for the active zone of the VVR-M, and coincided with the specific energy evolution in the experimental assembly of the fuel-element models. In the loop assembly surrounded by a screen with a varying degree of enrichment the neutron energy spectrum is characterized by a median energy of 800 keV (referred to the flux density), half the fissions producing neutrons with energies of over 10 keV. In a channel of the construction under consideration there is a further equalization of the field of energy evolution in the fuel-element assembly. The radial bias coefficient falls to 1.21. An increase in the optical thickness of the screen to 6.5 reduces the average specific energy evolution in the fuel-element assembly by a factor of 1.45 compared with the analogous quantity for the channel considered, and lies at a level of 700-900 W/cm^3 for the nominal power of the VVR-M reactor. The thermal flux in the screen should not exceed $0.4 \cdot 10^6$ kcal/(m^2·h).

Thus the foregoing theoretical and experimental data lead to the conclusion that, by using loop channel converters, the representative quality of investigations into highly-enriched fuel elements in a thermal research reactor may be greatly enhanced. In a channel with a variable-enrichment screen we find extremely hopeful characteristics for an irradiating device containing a seven-element fuel-element assembly with cores made of 90%-enriched UO_2.

A serious disadvantage of channels of the construction here considered is the necessity of making a complicated liquid-metal loop system. Although the thermal fluxes should not exceed $0.4 \cdot 10^6$ kcal/(m^2·h) the creation of such a loop installation demands considerable modernization of the research reactor.

LITERATURE CITED

1. V. A. Tsykanov et al., At. Énerg., 30, No. 2, 192 (1971).
2. J. Plunkett et al., Third Geneva Conf., 1964; Belgian Paper No. 441.
3. Canad. J. Nucl. Techn., 3, 61 (1964).
4. G. Minsart and F. Motte, Fast Reactor Physics, Vol. 1, IAEA, Vienna (1968), p. 327.
5. V. B. Klimentov et al., At. Énerg., 29, No. 4, 283 (1970).
6. V. B. Klimentov et al., At. Énerg., 30, No. 3, 309 (1971).
7. G. A. Kopchinskii et al., Izv. Akad. Nauk Beloruss. SSR, Ser. Fiz.-Énerg. Nauk, No. 1, 22 (1971).
8. V. B. Klimentov et al., At. Énerg., 20, No. 1, 63 (1966).
9. L. P. Abagyan et al., Group Constants for Calculating Nuclear Reactors [in Russian], Atomizdat, Moscow (1964).

TESTS ON EXPERIMENTAL FUEL ELEMENTS CONTAINING CARBIDE FUEL, IRRADIATED IN THE BOR-60 REACTOR TO BURN-UPS OF 3 AND 7%

E. F. Davydov, A. A. Maershin,
V. N. Syuzev, Yu. K. Bibilashvili,
I. S. Golovnin, and T. S. Men'shikova

UDC 621.039.542.344

Experience in the use of the carbide zones of the BR-5 reactor and several foreign versions confirms the practical possibility of using carbide fuel in fast reactors [1-3]. However, the difficulty of producing stoichiometric uranium monocarbide (which possesses a high radiation resistance) and our insufficient knowledge of its properties are the main obstacles to the use of this type of fuel. In addition to stoichiometric uranium monocarbide there is also considerable interest in the use of the easier-to-make hypo- and hyperstoichiometric compositions. In order to realise the advantages of uranium carbide over oxide fuel and ensure optimum fuel-element construction, careful experimental investigations into a number of problems are required, especially the swelling of the fuel, gas evolution, the compatibility of the fuel with the can, and so on.

In this paper we shall present the results of material investigations into the fuel elements of two assemblies irradiated in the BOR-60 reactor of burn-ups of 3.3 and 7.1% of the heavy atoms. The maximum linear power taken from the fuel elements was no greater than 550 W/cm; the greatest can temperature was 650°C; the temperature of the center of the core was 1100-1200°C for fuel elements with helium filling and 900-950°C for sodium—potassium filling.

TABLE 1. Initial Characteristics and Observed Behavior of Fuel Elements

Number of assembly	Carbon content of fuel, wt. %	Form of core	Fuel density, g/cm³	Diametral gap, mm	Medium	Gas evolution, % of theoretical	Changes in external can diameter, %	Rate of fuel swelling, %
First (burn-up 3.3% of heavy atoms)	4,68	Bushing	12,5	0,2—0,4	He	2,3	0	0,5
	4,7	Briquette	12,4	0,2—0,4	He	8,8	0	—
	4,8	Bushing	12,9	0,15—0,25	He	4,3	0	1,2
	4,8	Briquette	12,9	0,15—0,25	He	5,8	0	1,2
	4,91—5,0	Bushing	12,6	0,2—0,4	He	2,3	0	—
	4,91	Briquette	12,6	0,2—0,4	He	10	0	—
	4,9	"	12,5	0,6	Na—K	1,7	0	—
	5,1	"	12,8	0,25	Na—K	1,2	0	—
Second (burn-up 7.1% of heavy atoms)	4,68	Bushing	12,5	0,2—0,4	He	4,0	0	0,9
	4,7	Briquette	12,4	0,2—0,4	He	6,8	0	—
	4,8	Bushing	12,9	0,15—0,25	He	4,6	0,2—0,6	1,6
	4,8	Briquette	12,9	0,15—0,25	He	6,0	0,3—0,7	
	4,91—5,0	Bushing	12,6	0,2—0,4	He	4,5	0,2—0,4	1,5
	4,91	Briquette	12,6	0,2—0,4	He	9,0	0,4	
	4,8	"	12,8	0,5	Na—K	1,0	0,4	
	4,95	"	12,8	0,25	Na—K	3,0	0,3	
	5,0	"	12,8	0,5	Na—K	1,1	0,3	

Translated from Atomnaya Énergiya, Vol. 39, No. 1, pp. 33-36, July, 1975. Original article submitted September 23, 1974.

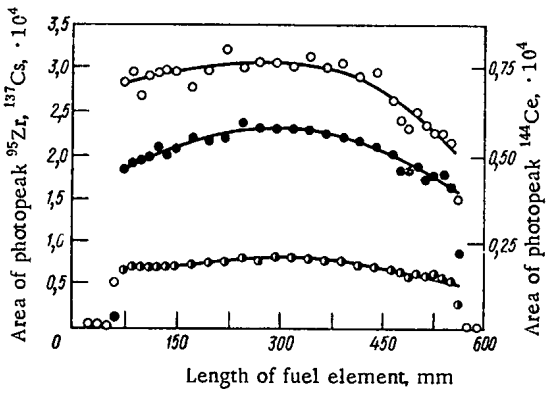

Fig. 1. Distribution of fission fragments over the height of the active part of the fuel element: ○) ^{137}Cs; ●) ^{95}Zr; ◐) ^{144}Ce.

Construction of Fuel Elements and Assembly

The assemblies contained 19 fuel elements enclosed in a hexagonal jacket (stainless steel 1Kh18N10T) with an "under-key" size of 38.0 mm and a wall thickness of 0.8 mm. The fuel element was a OKh16N15M3B stainless steel tube with an external diameter of 6.9 and a wall thickness of 0.4 mm. Fuel tablets in the form of bushings or briquettes were loaded into the tube over a length of 500 mm.

The diametral gap between the fuel and the can varied over the range 0.15-0.4 mm for fuel elements with helium filling and 0.25-0.6 mm for fuel elements with sodium—potassium filling. In the lower part of the fuel elements with helium and in the upper part of the fuel elements with sodium—potassium filling a compensation volume was provided for collecting the gaseous fission products. The amount of carbon in the fuel varied from 4.68 to 5.1 wt. %. The enrichment of the fuel with ^{235}U was 90%. The fuel density was 90-96% of theoretical.

Study of the Fuel Elements

Primary Investigations. On inspecting the assemblies no external damage was apparent; all the fuel elements were hermetic.

The external diameter of the fuel-element cans (Table 1) remained constant in the case of the first assembly; in the second assembly it remained within the range 6.88-6.94 mm. The maximum increase in diameter appeared in the center of the fuel column, i.e., in the zone of maximum burn-up, diminished toward the ends. The greatest deformation of the can was 0.8%.

The quantity of gaseous fission fragments evolved under the can was insignificant, amounting to 1-3% for a core-center temperature of ~1000°C (fuel elements with sodium—potassium filling) and 4-10% of theoretical for temperatures of ~1100-1200°C (fuel elements with helium filling). The low yield of gaseous fission products indicates a high retaining capacity of the carbide fuel for temperatures below the recrystallization point.

The results of our determinations of the gas evolution, the changes in the external can diameter, and the swelling of the fuel are presented in Table 1.

A study of the height distribution of the fission fragments with respect to the active part of the fuel elements showed that the fragments did not migrate in the direction of the axis. Typical results are presented in Fig. 1 (fuel density 12.6 g/cm^3, carbon content 5.0 wt. %, burn-up 7.1% of the heavy atoms).

Metallographic Study of the Fuel. This was carried out on samples cut from various cross sections along the height of the active zone in the fuel element. We found that during the investigation the tablets cracked (Fig. 2) as a result of thermal stresses arising in the reactor shutdown periods.

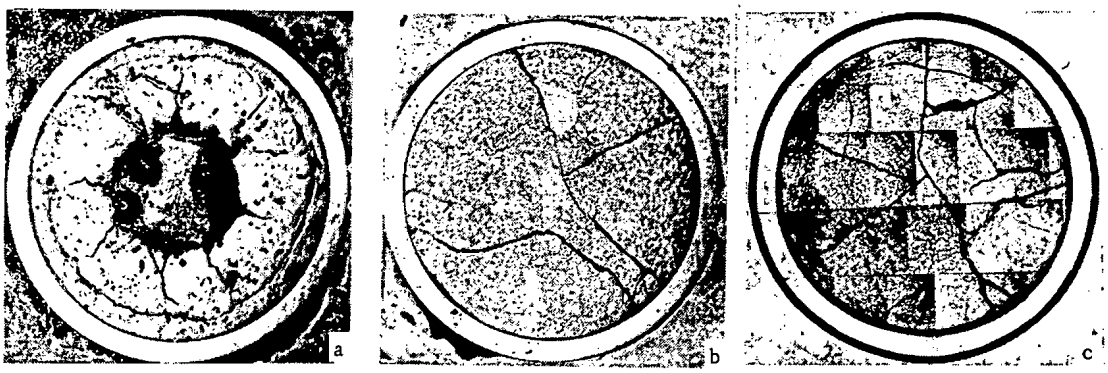

Fig. 2. Macrostructure of fuel (burn-up 7.1% of the heavy atoms; ×10): a) 4.68 wt.% C, medium He; b) 4.9 wt.% C, medium He; c) 5.0 wt.% C, medium Na—K.

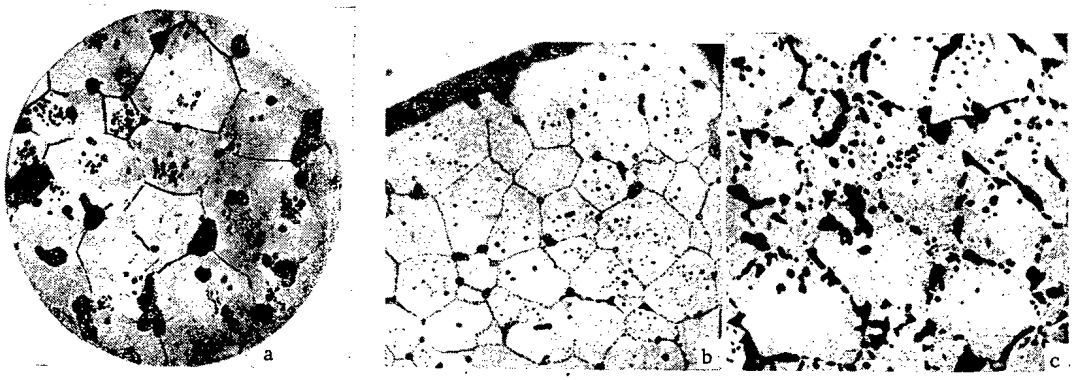

Fig. 3. Microstructure of the fuel (4.91 wt.% C, ×200): a) original; b) periphery, burn-up 7.1% of the heavy atoms; c) center, same burn-up.

The high capacity of the uranium carbide to retain the gaseous fission fragments leads to the development of preferential porosity in the central part of the core. Large pores disposed at the grain boundaries form a streak configuration, and on merging create extended cavities; small pores are located in the interior of the grain (Fig. 3).

Fuel of hypostoichiometric composition, with an initial coarsegrained structure characterized by a small number of large pores around the grain boundaries and aggregates of small pores inside the grains, undergoes additional centering for temperatures of ~1100-1200°C in the center of the core, as a result of which the size of the internal cavity of the core increases from 1.8 to 2.5 mm (Fig. 2a). This agrees with the results of other authors [4]. The swelling of this kind of fuel is no greater than 1.0% for 1% burn-up under the conditions indicated.

The behavior of hyperstoichiometric and stoichiometric fuel is practically identical in respect to changes in grain size and the mode of redistribution of the porosity. We found a certain increase in grain size in the central part of the core. In the peripheral parts fine pores lay both inside the grains and along the boundaries. At temperatures of over 1050°C the pores were enlarged [4] and the fine-grained structure was characterized by the presence of "lens-shaped" pores on the "hotter" grain boundaries (Fig. 4). The swelling of the cores made from fuel of hyperstoichiometric and stoichiometric compositions, determined hydrostatically and by quantitative metallographic analysis, averaged 1.5 ± 0.5% per 1% burn-up.

Interaction of the Can with the Fuel. It is well known that the interaction of the developing fission fragments with the fuel-element can does not play any decisive part in fuel elements made from carbide fuel. The interaction is chiefly characterized by carburization of the can on the side of the core (for a carbon content of over 4.8 wt. % in the fuel), as a result of which carbide phases are precipitated along the grain boundaries and the ductility of the can is impaired.

The use of a eutectic sodium—potassium mixture as heat-conducting interlayer between the fuel and the can also has its demerits. In particular carbon transfer causes a considerable carburization of the can for an amount of carbon in the uranium carbide exceeding 5 wt.%. The depth of the interaction zone depends on both the conditions of use, i.e., the temperature of the can and core, and the operating time in the reactor [5]. A typical picture of such interactions is shown in Fig. 5a. We see that for a can temperature of 650°C and 5.1 wt.% C in the fuel the depth of the interaction zone is 100-150 μ, while the microhardness (in principle this may serve as a criterion of the change in can-material ductility) for this zone is ~700 kg/mm^2. For parts outside the interaction zone the figure is ~300 kg/mm^2. The increase in microhardness is due to the considerable carburization (up to 0.7 wt.%) of the inner surface of the shell. Earlier it was noted [1] that such zones of interaction contained uranium and fission fragments in quantities of 10^{-4}-10^{-5} wt.% in addition to carbon.

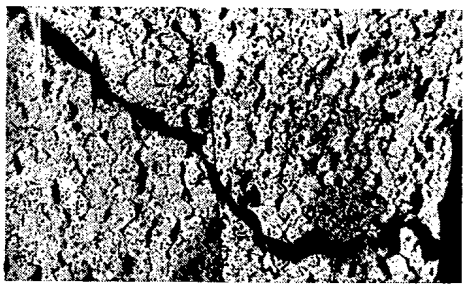

Fig. 4. Microstructure of the center of the core (burn-up 7.1% of the heavy atoms; 5.0 wt.% C, × 200).

On using uranium monocarbide with less than 5 wt.% carbon the carburization is very slight. In the middle and upper cross sections of the fuel elements with helium filling

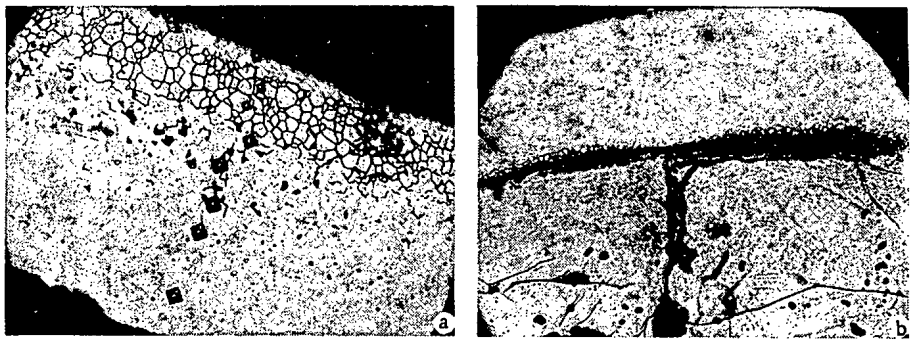

Fig. 5. Interaction between the fuel and the can: a) burn-up 3.3% of the heavy atoms, medium Na—K, × 200; b) burn-up 7.1% of the heavy atoms, medium He, × 100.

a dark zone, characterized by high etchability of the grain boundaries, appeared on the inner surface of the cans. We were unable to identify this zone (which was no more than 50 μ wide); however, other evidence suggests [6] that its carbon chromium content were some 1-2% higher than elsewhere.

Of the fifteen fuel elements studied, in only one case did we find interaction due to the direct diffusion of carbon into the can, when close contact occurred between the latter and the fuel (Fig. 5b). The depth of the interaction zone was no greater than 50 μ, while the microhardness was ~450 kg/mm^2.

Thus on the basis of these material investigations into the fuel elements of the two experimental assemblies, irradiated in the BOR-60 reactor to burn-ups of 3.3 and 7.1% of the heavy atoms with a linear power of 450-550 W/cm and can temperatures of 550-650°C, we may draw the following conclusions.

1. The fuel elements of the experimental assemblies containing an OKh16N15M3B steel can and a core in the form of bushings or briquettes were in excellent condition. The maximum increase in the external diameter of a can containing fuel elements irradiated to a burn-up of 7.1% of the heavy atoms was no greater than 0.8%.

2. The yield of gaseous fission fragments was very low, amounting to 1-10% of the theoretical value.

3. The rate of uranium monocarbide swelling equalled 1.5 ± 0.5% per 1% burn-up.

4. On using uranium monocarbide containing less than 5 wt. % carbon the can suffered decarburization to a depth of no greater than 50 μ; this had no effect on the properties of the can material.

5. An analysis of the state of the fuel elements studied in this investigation showed that these exhibited satisfactory efficiency under the irradiation conditions envisaged, and further exploitation was a real possibility.

LITERATURE CITED

1. A. Ya. Ladygin et al., in: Atomic Energy, Fuel Cycles, and the Study of Irradiated Materials [in Russian], Vol. 2, Moscow (1971), p. 314.
2. A. Ya. Ladygin et al., "Study of the fuel elements in the carbide zone of the BR-5 reactor", Contribution to the Soviet—French Symposium (Dimitrovgrad, December 12-15, 1972).
3. H. Mikailoff, "Experience in the fast-neutron irradiation of carbide fuel with sodium filling", ibid.
4. W. Chubb et al., Nucl. Techn., No. 18 (3), 231 (1973).
5. G. Nishio et al., Nucl. Engng. and Design, 22, 326 (1972).
6. A. Strasser, Trans. Amer. Nucl. Soc., 14, 40 (1971).

RECOLLECTIONS OF PROFESSOR BORIS VASIL'EVICH KURCHATOV, DOCTOR OF CHEMICAL SCIENCE, ON HIS SEVENTIETH BIRTHDAY

S. A. Baranov, A. R. Striganov,
and P. M. Chulkov

Boris Vasil'evich Kurchatov was born August 3, 1905 in the South Urals, and spent his childhood in the Sim's factory settlement, Ufimka province, now the town of Sim in the Chelyabinsk oblast. He received his secondary education in Simferopol. In 1927 he was graduated from the Kazan State University with a major in physical chemistry. In 1928 he was offered a job in the Leningrad Physicotechnical Laboratory of the Academy of Sciences of the USSR, now the A. F. Ioffe LFTI, where he was first a junior and then a senior research worker and head of the laboratory. In 1943 he moved to Laboratory No. 2 of the Academy of Sciences of the USSR, later the Institute of Atomic Energy, and worked there the rest of his life. Boris Vasil'evich died on April 13, 1972.

B. V. Kurchatov was one of the founders of Soviet radiochemistry and contributed greatly to the solution of chemical problems of the Soviet atomic industry. He was one of the first to use chemical methods to interpret nuclear reactions in the study of artificial radioactivity. Under his direction, and with his direct participation, the first trace and weighable amounts of neptunium and plutonium obtained in USSR were separated, and important radiochemical research was performed on the transplutonium elements from americium to californium. Important results were obtained on nuclear reactions with high-energy particles accelerated in a synchrocyclotron, and on the physics of the fission of heavy nuclei.

Unfortunately B. V. Kurchatov's scientific work has been very poorly dealt with in the literature. Being a very modest person he did not concern himself with the priority of his work, and many important results were not published in the open literature at the proper time. In this brief article we shall attempt to some degree to fill this gap and to shed some light on the contribution of B. V. Kurchatov to the development of radiochemistry and nuclear physics.

B. V. Kurchatov's first work, performed at LFTI under the direction of Academician A. F. Ioffe, had to do with the physics of dielectrics and semi-conductors. He obtained interesting results on the dielectric polarization of isomorphic mixtures of Rochelle salt. These crystals were found to be completely analogous to ferromagnets. They obey the Curie—Weiss law above the Curie point, the maximum flux of the electric displacement increases as the temperature decreases in the region of spontaneous orientation, and the phenomenon of hysteresis is pronounced. The data obtained, together with a study of the quantitative dependences on the concentrations of the components of the mixture, served as a basis for the development of the theory of ferroelectrics by his elder brother I. V. Kurchatov.

In his work on semiconductors he studied the dependence of electrical conductivity on temperature and impurities. These studies were designed to find new types of solid rectifiers. As a result a sulfate rectifier was developed capable of operating at larger current densities than other rectifiers of that time.

In 1938 B. V. Kurchatov was awarded the academic degree of Candidate of Physical-Mathematical Sciences for his work on dielectrics and semiconductors.

Beginning in 1934 B. V. Kurchatov took a very direct part in the work of I. V. Kurchatov on artificial radioactivity. The whole radiochemical part of this pioneering research was performed by B. V. Kurchatov. They studied nuclear reactions involving the bombardment of aluminum nuclei by neutrons

Translated from Atomnaya Énergiya, Vol. 39, No. 1, pp. 39-41, July, 1975.

with the formation of ^{27}Mg and ^{24}Na. Simultaneously a method was developed for studying nuclear reactions in a cloud chamber with vapor of a volatile boron compound. In subsequent experiments a third radioactive isotope of bromine was detected for the first time. This led to the remarkable discovery by I. V. Kurchatov, L. V. Mysovskii, and L. I. Rusinov of nuclear isomerism in artificially produced radioactive nuclei — one of the most outstanding achievements of Soviet nuclear physics.

Obtaining the first Soviet plutonium is of great scientific and historical interest. It is directly linked with the name B. V. Kurchatov. He began research in this direction in Moscow in 1943, well before the startup of the first Soviet graphite-moderated uranium reactor on December 25, 1946. The experiment was performed by mixing 2.5 kg of uranous-uranic oxide in a gelatinous precipitate of uranium peroxide deposited from 3.8 kg of uranyl nitrate and diluted with water to 7.5 liters. The flask with the mixture was placed in a vat of water. A radium-beryllium neutron source containing 1.8 g of radium was placed at the center of the flask. Irradiation was continued for 83 days until October 17, 1944. Estimates showed that the total amount of plutonium accumulated was $3.3 \cdot 10^{12}$ atoms. The plutonium was separated from five samples by various chemical processes. In each of the first three experiments 500 g of U_3O_8 were taken, in the fourth 820 g, and in the fifth 2.2 kg.

B. V. Kurchatov showed that plutonium can be separated by the so-called Cupferron sulfate scheme developed for neptunium by using the double salt potassium sulfate-lanthanum sulfate instead of potassium sulfate-cesium sulfate.

By processing 2.2 kg of irradiated uranium in the form of U_3O_8 a sample was separated with an alpha activity of 22 counts/min. This amount of material was enough to establish the chemical nature of the new alpha emitter with certainty and to estimate its half-life as 31 thousand years. This value is fairly close to the more accurate value of 24.3 thousand years now known for the half-life of ^{239}Pu.

Under the direction of I. V. Kurchatov a cyclotron with 73 cm diameter pole pieces was constructed and put into operation toward the end of 1944 in Laboratory No. 2 of the Academy of Sciences of the USSR. It was used to obtain plutonium. Deuterons accelerated to energies of 4 MeV were directed onto a lithium target. The neutrons obtained as a result of the reaction

$$^{7}_{3}\mathrm{Li} + ^{2}_{1}\mathrm{D} \rightarrow ^{8}_{4}\mathrm{Be} + ^{1}_{0}n$$

were used to bombard uranium. Uranyl nitrate was mixed with paraffin to moderate the neutrons. About ten uranium samples weighing up to 5 kg each were irradiated for 150 h.

From December 10, 1945 to September 1, 1946 B. V. Kurchatov performed many experiments on the separation of plutonium. As a result a technological laboratory scheme was developed for its separation. In all these experiments $1.8 \cdot 10^{-2}$ μg of plutonium were extracted.

In April of 1947 B. V. Kurchatov and his coworkers were the first in the USSR to separate milligram amounts of ^{239}Pu from uranium irradiated in the first experimental graphite-moderated uranium reactor. The plutonium was separated from two 5 kg samples of irradiated uranium oxide. The manganese sulfate method was used in the first experiment and the acetate-sulfate method in the second.

The plutonium was concentrated by the lanthanum sulfate method developed in detail by that time by B. V. Kurchatov and his coworkers. The essence of this method consists in the dropping of lanthanum in the form of lanthanum sulfate-potassium sulfate in an oxidizing medium and the precipitation of plutonium with a small amount of lanthanum in the form of lanthanum sulfate-potassium sulfate in a reducing medium. Decreasing the carrier content by repeated oxidation-reduction cycles diminishes the volume of the solution so much that the plutonium is precipitated in pure form without fragments. To precipitate 5-20 μg of plutonium the volume of the solution must be $\sim 10^{-4}$-10^{-3} ml. Two samples of plutonium were obtained: 6.1 μg from the first part of the uranium oxide, and after more intense and prolonged irradiation, 17.3 μg from the second.

These samples were used to study some of the properties of chemical compounds of plutonium: plutonium peroxide, plutonium fluoride, Pu(IV) hydroxide, the double salt potassium sulphate—Pu(III) and Pu(IV) sulfate, Pu(IV) hydride, Pu(III) oxalate, and Pu(III) sulfate. The solubilities of a number of difficultly soluble plutonium compounds (hydroxide, fluoride, hydride, peroxide, iodate) were determined also.

Numerous papers of B. V. Kurchatov in the field of the chemistry of the first transuranic elements, fission products, analytical procedures, and technological processes for the processing of irradiated uranium were important scientific contributions and were widely used in Soviet atomic industry.

B. V. Kurchatov's radiochemical studies of reactions of complex nuclei bombarded by high-energy particles were fruitful. Those studies were performed at Dubna during 1949-1953, directly after the startup of the high-power synchrocyclotron. The rules for the yields of various distintegration products of silver and tungsten bombarded with fast particles were studied; a number of new isotopes were found and identified; such phenomena as the escape of light nuclei from silver (sharply asymmetric fission), secondary nuclear reactions with an increase in the charge and mass of the bombarded nucleus, the fission of nuclei in excited states etc. were observed.

B. V. Kurchatov initiated research on the charge of the air and ground from radioactive isotopes formed in nuclear explosions. These experiments were for the most part of a pioneering character and were very valuable in the study of the effect of the products of atomic explosions on the biosphere.

B. V. Kurchatov devoted the latter years of his life to research on nuclear fission, mainly of heavy elements. Using radiochemical methods he found the laws of symmetric and asymmetric fission as a function of the charge and mass of the fissioning nucleus.

B. V. Kurchatov paid great attention to the training of scientific personnel. His students became highly qualified specialists who independently put into practice the scientific ideas of their teacher.

B. V. Kurchatov was a member of the communist party. He took part in the work of a number of committees on various problems of radiochemistry, was a member of the Academic Council of the Institute of Atomic Energy, a member of the committee of experts of the High Degree Commission, and a member of the editorial board of the journal Radiokhimiya.

The government of the USSR properly assessed the scientific work of B. V. Kurchatov and awarded him the honorary title of Lenin prize laureate, second laureate of the state prize, and also conferred on him the Order of Lenin and five orders of the Red Badge of Labor.

B. V. Kurchatov combined exceptional abilities, diligence, and love of science, and was a man of great erudition and culture. Boris Vasil'evich was a sensitive and sympathetic person, always very willing, ignoring time, helping everyone who turned to him for advice and assistance. Frequently he even developed and checked special procedures for obtaining and analyzing some compounds of interest to his coworkers at the Institute.

The scientific work of Boris Vasil'evich is inseparably linked with that of his brother Igor Vasil'evich. This was a sincere and business-like friendship of a talented radiochemist and a prominent experimental physicist of our day, a friendship stimulating scientific research and leading to great achievements in both radiochemistry and nuclear physics.

PROBLEMS IN SHIPMENT OF SPENT FUEL FROM NUCLEAR POWER STATIONS

Yu. I. Arkhipovskii, V. A. Burlakov, A. N. Kondrat'ev, E. D. Lyubimov, and A. P. Markovin

UDC 621.039.59:656

The projected high growth rates for nuclear power in all the countries of the world require shipment of considerable amounts of irradiated fuel from nuclear power stations to processing plants. Characteristics of spent fuel as a material for shipment include high radioactivity, considerable residual heat emission, presence of fissile materials, high cost, and the need to prevent the consequences of possible accidents during shipment.

Spent fuel from nuclear power stations is shipped by railroad, truck, and water transport in specially manufactured shipping casks. Loaded casks weigh from 30 to 110 tons with the fuel being 2-5% of the total mass and the mass of the means of transport being about the same as the mass of the cask. The time the means of transport is under way with a load is only 10-20% of the total time involved after subtracting the time taken for the return trip, for loading, for tie-down, for unloading, and for clean-up, inspection, repair, etc. One can imagine how expensive it is to ship spent fuel.

The shipping problem is an important link in the fuel cycle and requires creative participation by scientists, designers, and builders in various fields of science and technology for the succesful development of safe and economical designs for casks, for the selection of the most economical form of shipment, and for the solution of legal and organizational problems.

An increase in the specific power of reactors leads, as a rule, to an increase in the dimensions and mass of spent fuel-element assemblies and of the energy intensity and fissile material content in them. Reduction of the fuel cycle time, on the other hand, demands shipment of fuel after short holding times and consequently with greater residual heat emission and activity (Table 1). All this complicates the solution of the problems connected with shipping.

TABLE 1. Some Characteristics of Fuel from Soviet Water-Cooled, Water-Moderated Reactors and from the Reinsberg Nuclear Power Station (East Germany) [1, 2]

Reactor	Electrical power, MW	Fuel loading UO_2, tons	Depth of burn-up (mean /maximum), GW·day/ton	Number of assemblies	Size of assembly, S × L,* mm	Specific γ activity, gamma-equiv. Ra per assembly, holding time, yr				Residual heat emission of assemblies after holding, kW per assembly, holding time, yr			
						0,5	1	2	3	0,5	1	2	3
Reinsberg	70	18	10	132	144·3200	$3,4 \cdot 10^4$	$9,7 \cdot 10^3$	$4 \cdot 10^3$	$3,2 \cdot 10^3$	1,1	0,6	0,3	0,2
VVÉR-210	210	44	13/19	349/37†	144·3200	$3,7 \cdot 10^4$	$1 \cdot 10^4$	$4,4 \cdot 10^3$	$3,5 \cdot 10^3$	1,2	0,7	0,3	0,2
VVÉR-365	365	44	28/41	349/73	144·3200	$6,4 \cdot 10^4$	$1,8 \cdot 10^4$	$7,5 \cdot 10^3$	$6 \cdot 10^3$	2,1	1,1	0,5	0,3
VVÉR-440	440	44	28/42	349/73	144·3200	$6,7 \cdot 10^4$	$1,9 \cdot 10^4$	$7,9 \cdot 10^3$	$6,3 \cdot 10^3$	2,2	1,2	0,6	0,3
VVÉR-1000	1000	72	41/44	151	238·4665	$3,4 \cdot 10^5$	$9,6 \cdot 10^4$	$4 \cdot 10^4$	$3,2 \cdot 10^4$	11,1	6,0	2,8	1,7

* S, clamped dimension; L, assembly length.
† Numerator is total number of assemblies in reactor; denominator is number of control assemblies.

Translated from Atomnaya Énergiya, Vol. 39, No. 1, pp. 42-47, July, 1975. Original article submitted June 3, 1974; revision submitted January 23, 1975.

TABLE 2. Characteristics of Shipping Casks

Reactor	Shape of cask	Mass, tons	Size, m	Shield thickness, mm	Fuel weight, tons	Number of assemblies	Cavity filling (heat-transfer medium)
VVÉR-440	Vertical cylinder	90	⌀2,3; $H=4,4$	Steel; 400	3,8 (UO_2)	30	Water, inert gas
VVÉR-1000	Horizontal cylinder	110	⌀2,1; $L=6,1$	Steel; 410	3 (UO_2)	6	Water
Reinsberg power station	Vertical cylinder	80	⌀3; $H=4,3$	Steel; 350	3,9 (UO_2)	30	Nitrogen, water
KS-150 (Czechoslovakia)	Horizontal parallelopiped	78	1,68·1,2; $L=6,1$	Steel; 385	2, 7 (natural uranium)	16	Agueous solution of $KrCr_2O_7$, Water, inert gas
BWR or PWR (IE-300 cask)*	Horizontal cylinder	70	⌀1,5; $L=5,4$	Uranium; steel	Up to 4(UO_2)	18 (BWR) or 7 (PWR)	Water

* Shipment by rail and special truck.

Development of Safe and Economical Cask Design

Packaging of spent nuclear fuel is the most complex part of shipment. Shipping casks for the shipment of spent fuel must have reliable biological protection against penetrating radiations (γ, n); it must be hermetically tight, i.e., it must eliminate the possibility of escape of radioactive products into the environment at levels above permissible standards; it must provide sufficient heat removal to prevent fusion of fuel elements or spontaneous combustion of cladding and fuel and, when necessary, provide removal or combustion of hydrogen formed by radiolysis of water; it must meet the requirements for nuclear safety under normal and accident conditions [3-5].

The IAEA rules for safe shipment of radioactive materials and the shipping regulations of individual countries [6, 7] based on them impose rigid requirements on the design of shipping casks to ensure safety in case of accident.

To confirm adherence to standards for integrity and protection against ionizing radiation, it is necessary to perform tests which simulate the maximum predictable accident: dropping from a height of 9 m onto a steel plate; dropping of any point from a height of 1 m onto a solid metal rod 0.15 m in diameter; exposure to fire (800°C) for 30 min without subsequent forced cooling for three hours; submersion in water to a depth not less than 15 m for eight hours.

Biological Shield

Steel, lead, and depleted uranium are used in the manufacture of casks as contruction materials for protection against γ radiation. The lead and uranium are additionally encased in steel. Steel is used predominantly in the USSR; several casks with lead and uranium shielding have been constructed in the USA and France [8, 9].

The required thicknesses of uranium, lead, and steel shields are in the ratio 1 : 1.8 : 3.1, varying somewhat depending on the degree of irradiation of the fuel. There is a resultant difference in cask mass for a given internal volume or in internal volume for a given total mass.

The use of lead for increasing the useful volume of a cask while maintaining total mass has a number of serious deficiencies. The lead may fuse in a fire which may lead to its loss because of failure of the casing around it or to redistribution of the lead with the formation of radiation windows (voids in the shield) and the creation of extremely high radiation levels at the outer surface. What is needed is the development of external protection against fire and sufficient thickness of the outer steel casing to protect the cask in the case of an accidental drop as well as internal linings.

The use of uranium as a γ shield in the USA is explained by a trend toward maximum reduction of cask mass so that truck transport can be used because of its high level of development and the absence of railway spurs at many nuclear power stations. In casks with uranium shields, various types of porous copper or tungsten membranes are used to prevent the possible formation of eutectics with the steel shell which have a low fusion temperature and which would fail in a fire. These casks must have internal and external steel shells. The future use of steel casks with solid walls has recently been regarded as promising

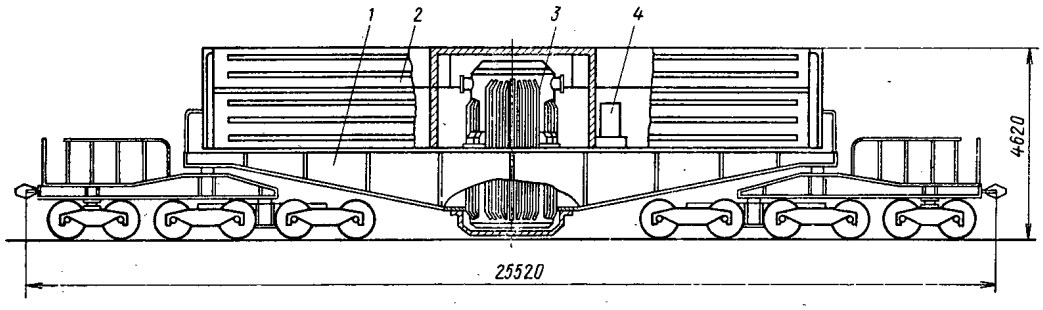

Fig. 1. Railway container car for shipment of spent fuel from a nuclear power station with VVÉR-440 reactors.

especially for spent fuel from fast reactors because of simplicity of construction, good heat removal, and structural integrity.

The external shells of casks are usually made of stainless steel or of coated carbon steel. For spent fuel from water-cooled, water-moderated reactors with a burnup of the order of 40,000 MW·day/ton and also for fuel from fast reactors, it is also necessary to provide protection against neutrons in addition to the protection against γ rays in the design of a cask because of significant amounts of heavy isotopes of plutonium and transplutonium elements which undergo spontaneous neutron emission. A composite metal shield is used for the absorption of γ rays; a shield of water or other hydrogenous material is used for moderation of neutrons and a shield of boron or cadmium is used for absorption of the moderated neutrons.

Heat Removal

In accordance with IAEA rules, the temperature of the outer surface of a cask must not exceed 82°C at an ambient air temperature of 38°C. The maximum permissible pressure in the cask must not be more than 686 kN/m^2 (7 kg/cm^2). Furthermore, it is not desirable to use a system of forced cooling in the design of a cask to provide safety since such a system inevitably fails in an accident.

As shown in numerous studies, one can remove about 250 W of heat by convection and radiation from 1 m^2 of steel plate when the ambient air temperature is 38°C and the temperature of the cask wall is 82°C if the plate is vertical and about 50 W more with a horizontal plate.

The surface of a cask for shipment of spent fuel from a VVÉR-440 reactor is about 30 m^2 which makes it possible to remove about 15 kW of heat without using fins or a system for forced cooling. The amount of heat removed can be increased by factors of 1.5-2 by the use of the fins on lateral surfaces.

Heat removal often limits the number of assemblies shipped in a single cask. To improve the conditions for heat transfer from spent fuel to the outer surface, the inner cavity of the cask is filled with water or other coolant as a rule. In principle, there are two possible methods of shipment: dry and wet. In dry shipment, the maximum permissible fuel temperature is a limiting factor; in wet shipment, the limiting factor is the pressure in the internal cavity of the cask. It has been suggested that liquid sodium would be the best coolant [10] for the shipment of spent fuel from fast reactors with short holding times and large heat emission.

In order that the temperature of fuel-element cladding and the pressure in the internal cavity of a cask be within permissible limits during a fire, the design of a cask often provides various linings which prevent transport of heat into the internal cavity during a fire and which provide the necessary heat removal under normal shipping conditions. For example, in the body of a cask for spent fuel from the Diori reactor (Switzerland) there is a lining of moist gypsum which dries out in a fire and reduces heat transfer.

For this same purpose, there has been developed in the USA thermal insulation based on aluminum and iron oxides which contain a large amount of bound water. Special structural materials with one-way conductivity are being developed.

In wet shipment (particularly of fuel with high residual activity), various measures are specified which can prevent the formation and detonation of explosive mixtures during shipment: catalytic combustion of hydrogen on platinum catalyzers, introduction of a suppressant gas into the gas cavity (for example, CO_2), filling the cask with high-purity water for marked reduction of hydrogen emission, and blow-off of released hydrogen into a special tank.

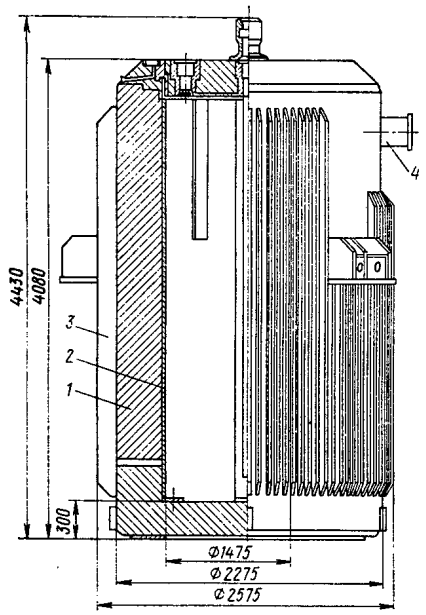

Fig. 2. Cask: 1) body; 2) internal lining; 3) fins; 4) pin.

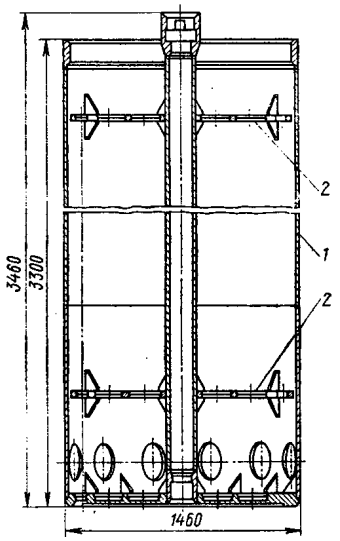

Fig. 3. Case: 1) cylindrical shell; 2) gridwork.

Nuclear Safety

In the development of a design for a shipment unit, conditions must be provided such that a spontaneous nuclear chain reaction (SCR) cannot arise under any foreseeable shipping conditions. One should particularly consider the possibility of rearrangement of materials in the cask into more reactive systems, of a loss of efficiency of built-in neutron absorbers or moderators, of an increase in reactivity because of temperature changes, or of penetration of water into the cask when it is dropped into water or snow.

For example, nuclear safety can be ensured by the inclusion in cask design of various moderators and neutron poisons, by control of possible geometries and degrees of moderation, etc.

Design of Shipment Unit

Physical, technical, and economic features of spent nuclear fuel have a great influence on the design of a shipment unit.

The creation of an acceptable design for a shipment unit for the transport of spent nuclear fuel is the solution of many contradictory problems imposed by the requirements of the "Rules for Safe Transport of Radioactive Materials" and by the economics of shipping.

Shipping rules are very strict and the design of a shipping unit must ensure the impossibility of initiation of an SCR, of weakening of the biological shield, and of uncontrolled loss of activity under any foreseeable shipping conditions including accidents; all of this entails great expense.

As a rule, a shipping unit for the transport of spent nuclear fuel consists of a cask and shipping space in the form of a container and hermetically sealed cases [11]. The cask is a thick-walled, sealable vessel which performs the function of a biological shield and which confines the activity under any foreseeable shipping conditions. The shipping container is a multiregional container which provides fixed geometric arrangement of spent fuel-element assemblies or of hermetically sealed cases containing spent assemblies under any foreseeable shipping or storage conditions and which simplifies the technical operations during loading and unloading of the cask.

The hermetically sealed cases are containers into which spent assemblies with damaged fuel-element cladding are placed. They prevent spread of activity into the internal cavity of the cask or into a storage area.

As necessary, the cask is supplied with a system for monitoring parameters in the internal cavity of the cask (temperature, pressure), with systems for neutralization or combustion of hydrogen formed in

the internal cavity of the cask because of radiolysis of water, and with other devices.

The final design of a shipment unit depends on the technical and physical characteristics of fuel-element assemblies subject to shipment, on the packing regulations of the nuclear power station and the processing plant, and on the type of transport used.

Railway transport is mainly used in the USSR for the shipment of spent nuclear fuel as the most logical for large distances. In addition, spent fuel can be shipped by rail in very massive containers and a large number of shipment units can be transported on a single trip.

In the shipment of spent fuel from SÉV member-countries to the USSR, special equipment is set up at border stations for shifting railway cars from 1520-mm track to 1435-mm track and vice versa; considerable experience has been accumulated in the performance of such operations.

The railway container car (Fig. 1) is a special railway car 1 with a body 2 in which the cask 3 is placed. The body is supplied with a heating system 4 and in it instruments are installed for monitoring technical parameters of the cask (temperature, pressure, hydrogen content) along with other special equipment. For insertion and removal of the cask, the body has a roof which opens.

Figure 2 shows a cask for the shipment of spent fuel-element assemblies. The cask material is carbon steel and the internal lining is made of stainless steel. The cask body is finned, which softens the shock from a fall and increases the surface area for hot removal. Special pins are provided on the body for moving the container.

Table 2 gives the characteristics of some shipping casks intended for rail transport which were designed and built in the USSR and SÉV member-countries. For comparison, specifications are given for the IE-300 cask of the General Electric Company (USA) [10].

Figure 3 shows the container which is a cylindrical shell with a gridwork which ensures a fixed arrangement of the cases containing spent fuel-element assemblies. Capacity of the container is 30 cases.

LITERATURE CITED

1. A. M. Petros'yants et al., At. Énerg., 31, No. 4, 315 (1971).
2. V. P. Denisov et al., idem, p. 323.
3. Rules for Safe Shipment of Radioactive Materials, Revised Edition, 1973, IAEA, Vienna (1973).
4. Radiation Safety Standards NRB-69 [in Russian], No. 821-A-69, Atomizdat, Moscow (1972).
5. Basic Health Rules for Working with Radiactive Materials and Other Sources of Ionizing Radiation [in Russian], OSP-72, No. 950-72, Atomizdat, Moscow (1973).
6. Anordnung über den Transport radioaktiver Stoffe, ATRS, DDR (1967), Vol. 10.
7. Anordnung Nr 2 über den Transport radioaktiver Stoffe, DDR, Februar 1971, Vol. 11.
8. Nucl. Engng. Intern., 19, No. 213, 104 (1974).
9. Nucl. Engng. Intern., 18, No. 204, 429 (1973).
10. B. Jenail, in: Proc. IAEA Specialists' Meeting on Handling and Transportation of Spent Fuel Elements for LMFBR's, Rome, April 26-28 (1972).
11. GOST 19541-74, Methods for Transportation of Spent Fuel-Element Assemblies for Nuclear Reactors [in Russian]. Terminology and Definitions.

TOTAL STABILITY OF A NUCLEAR REACTOR WITH CONNECTED CORES

N. A. Babkin

UDC 621.039.51

This paper, based on the second method of Lyapunov and the decomposition method [1], investigates the stability of the stationary operation of a reactor with connected cores, assuming not only a weak connection between cores as in [2] but also a strong one as in [3]. The dynamic equations for describing this reactor can be written in the form

$$\dot{n}_k = F_k(n_k, z_{1k}, \ldots, z_{M_k k}) + \sum_{j \neq k}^{M} \alpha_{kj}[n_k - n_j(t-\tau_{kj}) - \psi_{kj}(n_j(t-\tau_{kj})];$$

$$\dot{z}_{i_k k} = \phi_{i_k k}(n_k, z_{1k}, \ldots, z_{M_k k}), \quad k = 1, \ldots, M; \quad i_k = 1, \ldots, M_k. \tag{1}$$

Here n_k is the relative power displacement of the k-th reactor core from its stationary level; the variable $z_{ik}k$ characterizes the concentration of radiative delayed neutrons, the temperature of the different components of the k-th core, control effects, etc.; α_{kj} is a constant that is proportional to the neutron interaction factor between cores with numbers k and j; the τ_{kj} are the delays.

It is assumed that the necessary conditions of smoothness are satisfied for the nonlinear functions F_k, $\Phi_{ik}k$, and ψ_{kj}, which ensure the existence, uniqueness, and continuity of solutions for the connected system (1). Furthermore, the correlation:

$$|\alpha_{kj}\psi_{kj}(q_j)| \leqslant \varepsilon_{kj}|q_j|, \; k, \; j = 1, \ldots, M, \ldots j \neq k, \tag{2}$$

is satisfied for the function $\psi_{k\gamma}$, where ε_{kj} is a nonnegative number, and $q_j = n_j(t-\tau_{kj})$.

As is customary in problems of this kind, we consider $F_k(0) = \Phi_{ik}k(0) = \psi_{kj}(0) = 0$, i.e., the origin of the system of coordinates

$$n_k = z_{i_k k} = 0 \tag{3}$$

is the equilibrium state of the system (1).

It is evident that when $\alpha_{kj} = 0$, system (1) breaks down into M isolated subsystems

$$\dot{n}_k = F_k, \; \dot{z}_{i_k k} = \phi_{i_k k}, \; k = 1, \ldots, M; \; i_k = 1, \ldots M_k. \tag{4}$$

The following theorems have been proved:

THEOREM 1. For any $\alpha_{kj} > 0$ and $\tau_{kj} \geq 0$ the equilibrium state (3) of system (1) in the case of weakly connected cores ($\psi_{kj} \equiv 0$) is "totally" asymptotically stable, if there exist for each of the subsystems in Eq. (4) an infinitely large Lyapunov function which is positively defined throughout all phase space in the form $V_k = v_{1k}(n_k) + v_{2k}(z_{1k}, \ldots, z_{Mk}k)$ and in addition the inequality $0 \leq \partial v_{1k}/\partial n_k/n_k < \delta_k \leq \infty$ is satisfied.

THEOREM 2. Let the function ψ_{kj} satisfy correlation (2) and each subsystem in Eq. (4) be subject to the conditions in Theorem 1, then for any arbitrary $(\dot{V}_k)_{(4)}$ the evaluation

---

Translated from Atomnaya Énergiya, Vol. 39, No. 1, pp. 48-53, July, 1975.

$$(\dot{V}_k)_{(4)} \leqslant -\gamma_k |n_k|^2 - \sum_{i_k=1}^{M_k} \varphi_{i_k k} |z_{i_k k}|^2,$$
$$k = 1, \ldots, M,$$

will be true, in which γ_k and $\varphi_{ik}k$ are positive numbers. If the inequalities $\gamma_k/\delta_k > \sum_i \varepsilon_{kj}$, $k = 1, \ldots, M$; $j = k$ are satisfied, then for all $\alpha_{kj} > 0$ and $\tau_{kj} \geq 0$ system (1) with nonlinear delayed connections is "totally" asymptotically stable.

LITERATURE CITED

1. F. Bailey, SIAM Contr., 3, 443 (1966).
2. N. A. Babkin and V. D. Goryachenko, in: Problems of Atomic Science and Technology, Series: Dynamics of Nuclear Energy Reactors, Vol. 2, Izd. TsNIIatominform, Moscow (1972), p. 67.
3. Y. Asahi, S. An, and A. Oyama, Nucl. Sci. Technol., 4, No. 6, 49 (1967).

Original article submitted March 4, 1974.

FREQUENCY CRITERION FOR THE STABILITY OF A CIRCULATING-FUEL REACTOR

V. D. Goryachenko and V. V. Mikishev

UDC 621.039.514

Frequency criteria for reactor stability have been obtained only for fixed-fuel reactors. We propose a frequency condition for the asymptotic stability of a circulating-fuel reactor. As initial equations we take the kinetic equations of a circulating-fuel reactor from [1] and the linear feed-back equations in integral form. Proper transformations reduce the initial system to a single nonlinear integro-differential equation

$$\nu \frac{dx}{dt} = -(1+x) \int_{-\infty}^{\tau} f(\tau - u)\, x(u)\, du - \sum_i \frac{\beta_i}{\beta} \left[\xi_i x - \int_{-\infty}^{\tau} k_i (\tau - u)\, x(u)\, du \right], \quad (1)$$

in which x is the relative deviation of the reactor power, τ is the time measured in fractions of τ^*, the transit time of the fuel through the core, β_i and ξ_i are the fraction and the importance [2] of the i-th group of delayed neutron emitters, $\beta = \sum_i \beta_i$, $\nu = l/\beta\tau^*$, l is the neutron lifetime, $f(\tau)$ is the kernel for linear feedback which can be either lumped or distributed, and the $k_i(\tau)$ are the kernels generated by the equations for delayed neutron sources.

The steady state of a circulating-fuel reactor is described by the solution x = 0 of Eq. (1). We denote by $K_i(p)$ and $F(p)$ the Laplace transforms of the kernels $k_i(\tau)$ and $f(\tau)$. On the basis of the results of [2, 3] we prove the following. Suppose the function $F(p)$ has no poles for $\mathrm{Re}\, p \geq 0$ and $F(0) > 0$, and for all real values of ω the inequality

$$\mathrm{Re} \frac{F(i\omega)}{\nu p + \sum_i \frac{\beta_i}{\beta} [\xi_i - K_i(p)]} > 0 \quad (2)$$

is satisfied.

Then the zero solution of Eq. (1) is asymptotically stable for all initial conditions.

This statement is analogous to the criterion obtained in [4] for fixed-fuel reactors and lumped linear feedback.

LITERATURE CITED

1. V. D. Goryachenko and E. F. Sabaev, Atomnaya Énergiya, 23, No. 4, 295 (1967).
2. V. D. Goryachenko, Stability Theory Methods in the Dynamics of Nuclear Reactors [in Russian], Atomizdat, Moscow (1971).
3. V. D. Goryachenko, in: Problems of Atomic Science and Engineering, "Dynamics of nuclear power installations," No. 2 (6) [in Russian], TsNIIatominform, Moscow (1974), p. 75.
4. W. Baran and K. Meyer, Nucl. Sci. and Engng., 24, No. 4, 356 (1966).

Original article submitted April 3, 1974.

ESTIMATION OF THE EFFECT OF PHYSICO-GEOMETRIC FACTORS ON THE DISTRIBUTION OF DELAYED FISSION NEUTRONS IN A BOREHOLE

Yu. B. Davydov

UDC 550.835

In order to determine the uranium content by delayed neutrons, the fission reaction of natural uranium nuclei under the action of primary neutron radiation is used [1, 2]. The purpose of this paper is to estimate the effect of physico-geometric factors on the distribution of delayed fission neutrons in a borehole. A quantitative estimate of the effect of the hole diameter and the water saturation of the breeding medium on the distribution of fast and thermal delayed neutrons is obtained by a numerical method.

The problem is solved concerning the distribution of delayed fission neutrons, induced by a point source of fast neutrons in a two-layered infinite medium with a cylindrical boundary of separation.

The calculations are carried out for the case when the breeding medium is composed of porous rock of carbonate composition, the pores are filled completely with fresh water and the content of natural uranium in the rock is constant. The energy of the primary neutrons from the source is assumed equal to 14.1 MeV.

The results of the calculation allow the following conclusions to be drawn: the flux of fast delayed neutrons decreases monotonically with increase of the hole diameter for probes of any length; the nature of the effect of the hole diameter on the magnitude of the flux of thermal delayed neutrons depends on the length of the probe. In the region of small probes of $l \leq 20$ cm, an increase of the hole diameter causes a decrease of the thermal neutron flux. In the region of large probes, an increase of the hole diameter leads to the appearance of a local flux maximum of thermal delayed neutrons, which is attained when the depth of the water layer in the hole is equal to 2 to 3 cm. With further increase of the hole diameter, the buildup process is replaced by a process of absorption of thermal neutrons in the water and the flux decreases.

An increase of the moisture content of the breeding medium leads to a reduction of the flux of delayed fast fission neutrons in the hole. The nature of the effect of water-saturation of the rock on the magnitude of the thermal delayed neutron flux depends on the hole diameter and the length of the probe. In the region of small probes, the magnitude of the thermal neutron flux decreases, for large diameters, with increase of the water-saturation of the medium and has a local maximum for small hole diameters when the moisture content reaches 10-20%. For large probes of $l \geq 30$ cm, an increase of the moisture content leads to a monotonic reduction of the magnitude of the thermal delayed neutron flux for any hole diameter.

LITERATURE CITED

1. S. Amiel and M. Peisakh, Atomnaya Énergiya, 14, No. 6, 535 (1963).
2. Yu. B. Davydov, Izv. Vuzov. Gornyi Zhurn., No. 6, 8 (1972).

Original article submitted May 20, 1974.

SPATIAL DISTRIBUTION OF FISSION NEUTRONS IN A BREEDING MEDIUM, CROSSED BY A DRILL HOLE

Yu. B. Davydov

UDC 550.835

The solution is considered of the problem concerning the spatial distribution of fission neutrons, induced by a point source of fast neutrons in an infinite homogeneous uraniferous medium, crossed by a drill hole [1-4].

The numerical calculation is carried out for the case when the breeding medium is composed of a dense rock of carbonate composition containing uranium ore of natural isotopic composition and with a density of the medium of 2.7 g/cm^3. A source of primary neutron radiation is located in the hole, filled with fresh water — a borehole generator of neutrons with energy equal to 14.1 MeV. The initial energy of the prompt fission neutrons is assumed to be 2 MeV and the neutron yield 2.5 n/event.

In order to estimate the effect of the hole on the magnitude of the flux of fast $\Phi_{21k}(r, z)$ and thermal $\Phi_{22k}(r, z)$ fission neutrons, the results of the calculation are presented in units of magnitude of the fast $\Phi_{21}(0, 0)$ and thermal $\Phi_{22}(0, 0)$ fission neutron fluxes in an infinite breeding medium, in the case of a negligibly small effect of the hole.

The spatial distribution of the flux of fast and thermal fission neutrons is shown in Fig. 1. The results of the calculation confirm that the fission neutron flux reaches a maximum magnitude in the breeding medium in regions subjected to the most intense irradiation. The moderation length of the fast neutrons exceeds the diffusion length of the thermal neutrons, and therefore data concerning the moderating properties of the breeding medium are obtained from the more distant regions.

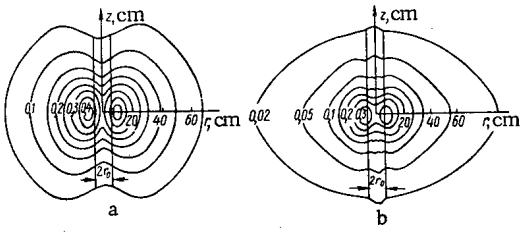

Fig. 1. Spatial distribution of the flux of fast and thermal fission neutrons in units of the maximum flux magnitude in an infinite breeding medium: a) $\Phi_{21k}(r, z)/\Phi_{21}(0, 0)$; b) $\Phi_{22k}(r, z)/\Phi_{22}(0, 0)$.

LITERATURE CITED

1. S. A. Igumnov, Izv. Vuzov. Gornyi Zhurn., 2, 3 (1966).
2. Yu. B. Davydov, Izv. Vuzov. Gornyi Zhurn., 6, 8 (1972).
3. Yu. B. Davydov and A. T. Markov, Atomnaya Énergiya, 33, No. 1, 574 (1972).
4. J. Czubek, Report N. 732/PH, Cracow Institute of Nuclear Physics (1971).

Original article submitted May 20, 1974.

VARIABLE MECHANICAL STRESSES, INDUCED IN THE FUEL ELEMENT CLADDINGS OF THE IBR-30 REACTOR BY POWER PULSES

V. S. Dmitriev, L. S. Il'inskaya,
G. N. Pogodaev, V. V. Podnebesnov,
A. D. Rogov, V. T. Rudenko,
and O. A. Shatskaya

UDC 621.039.55:621.039.526

During the development of power excursions, the active zones of pulsed fast reactors and boosters are subjected to the action of thermal shocks. This phenomenon, due to exceeding the rate of rise of temperature above the rate of expansion of the material, is accompanied by the stimulation in the fuel elements of alternating deformations and stresses, which are transmitted to the claddings and supporting structures of the core [1]. The action of the thermal shocks is aggravated by their high repetition frequency, which creates an accelerated wear of the active zone elements due to material fatigue. Damage of the fuel elements might also occur when the tensile strength is exceeded, either during a single power pulse or from wave interference from the stresses of several pulses in the case of a too high repetition frequency.

On the pulsed fast reactor (IBR) of the Joint Institute of Nuclear Research in Dubna, this phenomenon has been investigated over a number of years for the purpose of finding the optimum fuel element design and for determining the permissible pulsed loading [2, 3].

The paper describes the procedure and gives the results of measurements of the alternating mechanical stresses which are induced by power pulses in the fuel element claddings of the IBR-30 reactor. The relative deformations were determined by means of high-temperature wire tenso-resistors with a base of 10 mm. Wire with a diameter of 30 μ made of NM23 × 10 alloy is used as the material for the tenso-sensitive lattice and VN-15T organo-silicon cement is used as the binding and insulating material. The principal measurements were conducted during operation of the IBR-30 in a cycle of widely-spaced pulses at a repetition frequency of 0.2 Hz and an average reactor power of up to 15 kW. Longitudinal and transverse oscillations were detected, with a frequency of ~5000 and ~1000 Hz respectively (Fig. 1). The amplitudes of the oscillations increased with increase of the pulse energy, and the time of damping did not exceed 10 msec. With power pulse energies of $2 \cdot 10^{15}$ fissions (average rise in temperature of the plutonium fuel elements of the active zone was 20°C per pulse), the maximum stresses in the cladding, created by the longitudinal and transverse oscillations amounted to $7 \cdot 10^5$ and $5 \cdot 10^5$ N/m^2 respectively.

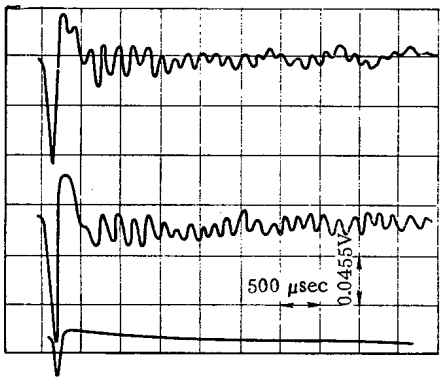

Fig. 1. Signals from the tenso-resistors installed on the cladding of a fuel element of the working fuel assembly; below: pulse power. The pulse energy was $2 \cdot 10^{15}$ fissions; pulse frequency 0.2 Hz.

LITERATURE CITED

1. I. Randles and R. Laursma, EUR-3654-1 (1967).
2. V. T. Rudenko, Preprint OIYaI 13-764, Dubna (1971).
3. V. D. Anan'ev, OIYaI 13-4395, Dubna (1969).

Original article submitted July 10, 1974.

CORRECTION OF THE GROUP CONSTANTS BY THE RESULTS OF EXPERIMENTS ON THE BFS CRITICAL ASSEMBLIES

A. A. Van'kov and A. I. Voropaev

UDC 621.039.519

The following problems are considered in the paper: correction of the group constants on the basis of integral experiments on critical assemblies (measurements of the ratio of the average cross-sections of different reactions and the ratio of the reactivity of samples at the center of the active zone for three BFS assemblies); determination of the constant error of the principal characteristics of a fast reactor of the OK-5 type (parameters of criticality and breeding, reactivity coefficients) before and after taking account of the integral experiments; determination of the bias of the numerical values of these characteristics, due to taking account of the integral experiments.

A statistical method has been used for the correction, in linear approximation, of the coefficients of sensitivity. Part of the results obtained is given in Table 1.

The conclusion consists in the following: the bias of the constants with a correction based on the integral data, depend significantly on the assumptions about the dispersions and also on the form and magnitude of the initial correlations for both the group constants and the integral data. In order to obtain physically plausible results of the correction, it is important to estimate correctly the error of the group constants and of the integral quantities associated with the approximations of the numerical model (requirement of adequacy of the conditions of the calculation and of the experiment). Taking account of correlations between the measured quantities is of considerable importance. The bias in the calculated reactor parameter is stable, if the choice of the integral quantities is sufficiently informative relative to this parameter.

TABLE 1. Bias and Error K_{eff} of the Total Coefficient of Breeding KB and of the active zone KB_{az}, the Doppler (DKR) and Sodium (NKR) Coefficients of Reactivity

	BFS-22*		BFS-23*		BFS-27†	OK-5 ‡			
	K_{eff}	KB_{az}	K_{eff}	KB_{az}	K_{eff}	K_{eff}	KB	DKR	NKR
σ_0, %	1	5,5	3,7	9,2	4,1	4,2	6,2	80	60
σ_1, %	0,9	4,4	1,4	5,3	1,5	1,6	4,4	50	55
δ, %	0,0	—4,5	1,6	—8,5	2,7	3,8	—6,0	35	15

* Model of fast reactor with uranium (BFS-22) and plutonium (BFS-23) fuel.
† Assembly without U-238, with large dilution with graphite.
‡ Breeder-reactor with oxide fuel, volume of active zone 5 m^3. Calculated values: KB = 1.39; DKR = $-4.4 \cdot 10^{-3}$ ($\Delta K_{eff}/\Delta T°$), T° from 900 to 1500°K; NKR = 1.1% ($\Delta K_{eff}/K_{eff}$) with 50% of sodium removed from the reactor.
σ_0 and σ_1 are the errors, with and without taking account of the integral experiments respectively;
δ is the bias relative to the values calculated by the BNAB-70 system of constants; BFS = Fast Physics Assembly.

Original article submitted August 23, 1974.

THE INFLUENCE OF BEAM NOISE ON THE CRITICAL CURRENT OF LINEAR ELECTRON ACCELERATORS

I. N. Mondrus

UDC 621.384.64

This paper deals with the development of the transverse beam instability in a single section of a linear electron accelerator, taking into account the fluctuations in transverse displacement $Y_1(s)$ and

transverse velocity $Y_2(s)$ of the center of mass of the beam bunch. At the section input the time-series $Y_1(s)$, $Y_2(s)$ constitute a normal stationary process and are described by the spectral density matrix $f(\omega)$. The variance $\sigma^2 n$ and the mean μ_n of the transverse displacement of the n-th bunch at the section output (Y_n) can be expressed by the elements $f_{ik}(\omega)$ of this matrix and the fundamental solutions of the transverse instability problem $\eta_1(s)$, $\eta_2(s)$ by the relation [1]

$$Y_n = \sum_{s=0}^{n} [Y_1(s)\,\eta_1(n-s) + Y_2(s)\,\eta_2(n-s)].$$

The probability that the displacement of the last (n-th) bunch in the pulse does not exceed the section aperture a at critical current is given by

$$P(|Y_n| \leqslant a) = \Psi\left(\frac{a-\mu_n}{\sigma_n}\right) + \Psi\left(\frac{a+\mu_n}{\sigma_n}\right) - 1,$$

where Ψ is the normalized Gaussian distribution function.

Assuming that the effect of the bunching part of the accelerator is to average out the shot noise of the gun over phase angle, the coefficients $f_{ik}(\omega)$ are constant over the entire frequency. If in addition the noise amplitudes $A_{ik} = f_{ik}(\omega)$ satisfy the inequality

$$\alpha\left(\sum_{i=1}^{2} \bar{Y}_i a_i\right)^2 \ll \frac{4\pi}{T_0} a_i a_k A_{ik},$$

the critical current is determined only by input noise level, in agreement with the results of Kramskoi et al. [2]. Here α is the growth increment of the instability, $\bar{Y}_i$ is the average value of Y_i; $1/T_0 = f_0$ is the bunch repetition frequency, $a_1 = 1$ and a_2 is the time of flight of a bunch through the section.

We have considered the possibility of increasing the critical current by noise suppression at the section input. It is shown that the reduction of noise in a narrow band around the resonance frequency $f_r = f_{11} - f_0$ (f_{11} is the instability frequency) increases the critical current 5 to 7%. The critical current can be increased to a larger extent by noise suppression in the entire frequency band, e.g., 45 dB noise suppression doubles the current.

LITERATURE CITED

1. Ē. L. Burshtein and G. V. Voskresenskii, Intense Beam Linear Electron Accelerators [in Russian], Atomizdat, Moscow (1970).
2. G. D. Kramskoi et al., Zh. Tekh. Fiz., 17, No. 3, 553 (1973).

Original article submitted September 4, 1974.

MODEL OF GROUPING OF LOW ENERGY TRANSFERS IN CALCULATING ELECTRON FIELDS BY THE MONTE CARLO METHOD

A. V. Plyasheshnikov and A. M. Kol'chuzhkin

UDC 539.121.72

The calculation of electron fields by the Monte Carlo method is now most frequently carried out in the fragment of catastrophic-collision models [1, 2]. The scheme suggested in the present article is based on a synthesis of these two models. The generation of fast secondary electrons and the emission of high-energy bremsstrahlung quanta are simulated as in the catastrophic-collision model, whereas collisions

involving low energy transfers are grouped. Too large paths between catastrophic collisions are treated as in the fragment model, i.e., are fragmented into smaller parts to which the regular multiple-scattering theories can be applied.

To speed up calculations, the fluctuations of electron energy loss in noncatastrophic collisions are taken into account. This is done in accordance with the Vavilov distribution [3] obtained and tabulated in [4]. The fact that electron paths between nodes of the enclosed trajectory are not straight as a result of multiple scattering is allowed for with greater precision. The longitudinal component of the radius vector joining adjacent nodes of the enclosed trajectory is drawn from the Jang—Spenser distribution [5, 6] tabulated in [4], whereas the transverse component is taken from the Fermi distribution [7] in which the exact second moment [8] is used.

The Goudsmit—Saunderson distribution [9] is used for drawing the electron multiple scattering angle.

Application of more precise distributions of the multiple scattering theory and high calculations speed made it possible to carry out the calculations in three-dimensional geometry. Similar calculations have been carried out before in a continuous-deceleration approximation only [10, 11]. The analysis proved that the continuous-deceleration approximation is applicable to depths less than one half of the total electron range.

LITERATURE CITED

1. M. Berger, in: Proc. Methods in Computational Phys., Vol. 1, Acad. Press, New York—London (1963), p. 135.
2. A. F. Akkerman, Yu. M. Nikitushev, and V. A. Botvin, Application of Monte Carlo Method to Problems of Fast Electron Transport in Matter [in Russian], Nauka, Alma-Ata (1972).
3. P. V. Vavilov, Zh. Éksper. Teor. Fiz., 32, 920 (1957).
4. A. V. Plyasheshnikov and A. M. Kol'chuzhkin, Izv. Vuz. Fiz., No. 1, 81 (1975).
5. C. Jang, Phys. Rev., 84, 599 (1951).
6. L. Spenser and J. Coune, Phys. Rev., 128, 2230 (1962).
7. B. Rossi, High-Energy Particles [Russian translation], Gostekhteorizdat, Moscow (1955).
8. H. Lewis, Phys. Rev., 78, 526 (1950).
9. G. Goudsmit and J. Saunderson, Phys. Rev., 57, 24 (1940); 58, 36 (1940).
10. H. Kessaris, Phys. Rev., 145, 164 (1966).
11. B. Ya. Narkevich, V. S. Endovitskii, and I. S. Konstantinov, At. Énerg., 26, No. 5, 473 (1969).

Original article submitted October 1, 1974.

USE OF A ^{252}Cf FISSION CHAMBER IN CERTAIN PHYSICAL MEASUREMENTS

V. F. Efimenko, V. K. Mozhaev, and V. A. Dulin

UDC 621.039.51

In recent years californium neutron sources have been more and more widely used in experimental reactor physics. A number of useful quantities can be measured using fission chambers with a layer of ^{252}Cf.

The block diagram of the experiment (Fig. 1a) is described in [1, 2]. When the fission chamber and detector are outside any medium the distribution observed in the analyzer (Fig. 2a) can be written in the form:

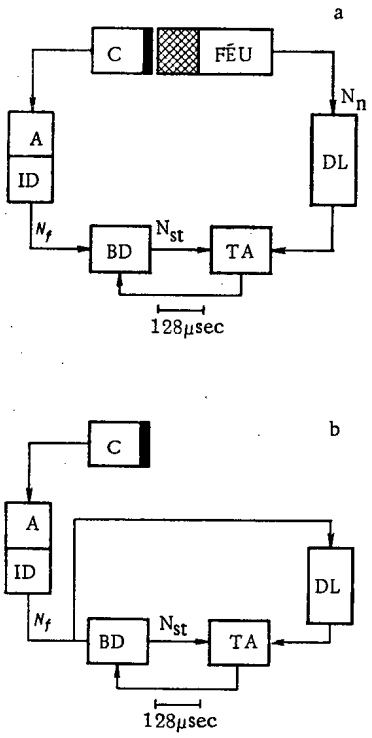

Fig. 1

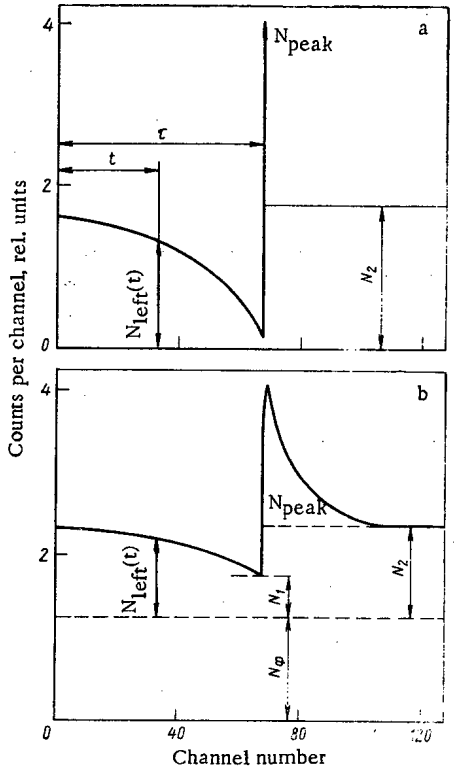

Fig. 2

Fig. 1. Block diagram of experiment: C) fission chamber with a layer of ^{252}Cf; FÉU) neutron detector; A) amplifier; ID) integral discriminator; DL) delay line (passive); TA) time analyzer; BD) blocking device ensuring that the interval between starts of the TA is not less than the time scale of the analyzer (controlled from TA).

Fig. 2. Time distribution of neutrons: a) chamber and detector outside any medium; b) chamber and detector in reactor.

Translated from Atomnaya Énergiya, Vol. 39, No. 1, pp. 54-56, July, 1975. Original article submitted July 1, 1974; revision submitted January 24, 1975.

TABLE 1. Experimental Values of ε_f and Q, Fissions/sec

Measured quantity	Value	Method of measurement
ε_f	0,946±0,003	n-f coincidences [2]
ε_f	0,948±0,0018	Eq. (3) [1]
ε_f	0,947±0,002	Eq. (4)
Q	(3,213±0,008)·10³	Eq. (6)

TABLE 2. Experimental Values of ρ/β, ε_d, and l

Method of measuring ρ/β			$\varepsilon_d \cdot 10^5$	l, μsec
Rod drop	^{252}Cf chamber: α-method	^{252}Cf chamber: integral method		
0,418±0,008	—	0,42±0,008	1,51±0,05	0,294±0,01
1,15±0,1	1,1±0,03	1,09±0,05	1,380±0,036	0,290±0,01
2,80±0,1	2,63±0,03	2,66±0,11	1,50±0,05	0,296±0,01
—	2,96±0,09	2,90±0,12	0,553±0,017	0,293±0,01
—	3,90±0,12	3,96±0,15	1,60±0,05	0,291±0,01

$$N(t)=\begin{cases}\dfrac{QN_f\varepsilon_n}{(1+TN_f)}\Delta t\nu_n(1-\varepsilon_f+\varepsilon_f\times\\ \times\{1-\exp[-N_f(\tau-t)]\})\,t_{meas}\\ t<\tau;\\ \dfrac{N_f\varepsilon_n}{(1+TN_f)}\nu_n[\delta(\tau-t)+\Delta tQ]\,t_{meas},\\ t\geqslant\tau,\end{cases}\qquad(1)$$

where $\delta(\tau-t)$ is the Dirac delta function, Q is the activity of the ^{252}Cf layer in fissions/sec, ε_f is the efficiency of recording fissions, N_f is the rate of counting recorded fissions, ε_n is the neutron counting efficiency of the detector, taking account of geometry; T is the time scale of the analyzer TA (Fig. 1), Δt is the width of a TA channel, ν_n is the average number of neutrons per fission of ^{252}Cf, τ is the delay time, t_{meas} is the time of the measurement, $N_{st}=N_f/(1+TN_f)$. We neglect the delay neutrons emitted by ^{252}Cf. If the apparatus is connected as shown in Fig. 1b, then after correcting counting errors in the analyzer

$$N'_{peak}=\frac{N_f}{(1+TN_f)}t'_{meas},N'_2=\frac{N_f^2\Delta t}{(1+TN_f)}t'_{meas}.\qquad(2)$$

A number of quantities can be determined from the measured distribution (1): a) the efficiency of the fission chamber ε_f when it is close to unity

$$1-\varepsilon_f=\lim_{t\to\tau_0}\frac{N_{left}(t)}{N_2}\qquad(3)$$

or

$$\varepsilon_f=\frac{N_{peak}N'_2}{N_2N'_{peak}};\qquad(4)$$

b) the width of the time analyzer channel

$$\Delta t=\frac{N'_2}{N'_{peak}N_f};\qquad(5)$$

c) the absolute fission rate in the chamber

$$Q=\frac{N_2}{N_{peak}\Delta t}.\qquad(6)$$

Table 1 shows the results of measuring ε_f and Q by various methods. The measured value of the channel width of the AI-256 analyzer is Δt = 1.0010 ± 0.0012 μsec.

The ^{252}Cf fission chamber placed in the reactor and connected as shown in Fig. 1a gives the distribution shown in Fig. 2b on the analyzer. Within the framework of the elementary point model of reactor kinetics with a single effective group of delayed neutrons this distribution can be found by substituting the expression for the external neutron source S(t) obtained from Eq. (1) into the kinetic equations [3]

$$S(t)=\begin{cases}\nu_nQ\{1-\varepsilon_f\exp[-N_f(\tau-t)]\},\\ t<\tau;\\ \nu_n[\delta(\tau-t)+Q],\\ t\geqslant\tau.\end{cases}\qquad(7)$$

Solving the kinetic equations we find that after subtracting the steady background from the spontaneous reactor sources N_φ (Fig. 2b) the distribution has the form

$$N(t)=\begin{cases}\dfrac{QN_f\nu_n\varepsilon_d}{(1+TN_f)}\left\{\dfrac{1}{k\rho}-\dfrac{\varepsilon_f}{k(\rho+\beta)+lN_f}\exp[-N_f(\tau-t)]\right\}\Delta tt_{meas},t<\tau;\\ \dfrac{N_f\nu_n\varepsilon_d}{(1+TN_f)}\left\{\dfrac{\alpha}{k(\rho+\beta)+lN_f}\exp[-\alpha(t-\tau)]+\dfrac{Q}{k\rho}\right\}\Delta tt_{meas};\qquad t\geqslant\tau,\end{cases}\qquad(8)$$

where k is the effective neutron multiplication constant, β is the effective fraction of delayed neutrons, l is the prompt neutron lifetime in the reactor, ε_d is the efficiency of the detector when located in the reactor, determined by the ratio of the detector counting rate to the rate of production of neutrons in the reactor, $\rho = (1-k)/k$; $\alpha = [1-k(1-\beta)]/l$. The extrapolated background to the left of the peak for $t \to \tau_{-0}$ is

$$N_1 = \frac{Q^2 \varepsilon_f \nu_n \varepsilon_d}{(1+TN_f)} \left[\frac{1}{k\rho} - \frac{\varepsilon_f}{k(\rho+\beta)+lN_f} \right] \Delta t t_{\text{meas}} \tag{9}$$

The background to the right of the peak for $t \to \infty$ is

$$N_2 = \frac{Q^2 \varepsilon_f \nu_n \varepsilon_d}{(1+TN_f)\, k\rho} \Delta t t_{\text{meas}}. \tag{10}$$

The area in the peak over the background on the right is

$$N_{\text{peak}} = \int_{\tau}^{\infty} [N(t) - N_2]\, dt = \frac{Q \varepsilon_f \nu_n \varepsilon_d t_{\text{meas}}}{(1+TN_f)\, k\,(\rho+\beta)\,[1+(N_f/\alpha)]}. \tag{11}$$

Combinations of the quantities N_1, N_2, N_{peak}, and α obtained from the experimental distribution N(t) give a number of physical quantities: a) the reactivity in units of β

$$\rho/\beta = 1 \Big/ \left[\frac{N_2}{QN_{\text{peak}}[1+(N_f/\alpha)]\,\Delta t} - 1 \right] \text{ or}$$

$$\rho/\beta = 1 \Big/ \left[\frac{\varepsilon_f}{[1-(N_1/N_2)]\,[1+(N_f/\alpha)]} - 1 \right]; \tag{12}$$

b) the neutron lifetime in the reactor is determined from the decay constant α, the value found for the reactivity ρ/β, and the calculated value of β; c) the efficiency of the neutron detector

$$\varepsilon_d = \frac{(N_2 - N_1)\,(1+TN_f)\, l\,(\alpha+N_f)}{N_f^2 \nu_n \Delta t t_{\text{meas}}} \text{ or}$$

$$\varepsilon_d = \frac{N_{\text{peak}}(1+TN_f)\, l\,(\alpha+N_f)}{N_f \nu_n t_{\text{meas}}}. \tag{13}$$

Table 2 lists the experimental values of ρ/β measured by various methods and also the values of l and ε_d obtained with the ^{252}Cf chamber for various conditions of the BFS-30 fast critical assembly [4]. The errors listed in Table 2 are determined from the dispersion of the results obtained in series of several measurements, and do not take account of the error in using the simple reactor kinetics model. The value of k_{eff} was established by the position of the regular controls. The subcritical 2.9β state was established by placing absorbing boron rods in a row with the SNM-11 neutron detectors at a reactivity of 1.1.

In conclusion the authors thank Yu. A. Kazanskii, S. P. Belov, A. G. Shokod'ko, and V. G. Kulebyakin for their interest in the work and for helpful discussions.

LITERATURE CITED

1. V. Dulin and V. Mozhaev, Nucl. Instrum. and Methods, 105, 277 (1972).
2. V. A. Dulin and V. K. Mozhaev, Preprint FÉI-309 [in Russian], Obninsk (1972).
3. G. Keepin, Physics of Nuclear Kinetics, Addison—Wesley, Reading (1965).
4. V. Dulin et al., Paper A-26 presented at a Symposium on the Physics of Fast Reactors. Tokyo, October 16-21, 1973.

ENERGY DISTRIBUTION OF NEUTRONS EMERGING FROM BR-10 REACTOR CHANNELS

L. A. Trykov, V. P. Semenov and A. N. Nikolaev

UDC 621.039.512

During construction of the BR-10 reactor it becomes necessary to measure the spectra of neutrons $\Phi(E)$ emerging from the core through channels B-3, B-2, and P-2, and the thermal neutron flux from channels T-4 and K-5. The measurements were made at low reactor power in a relatively small γ-flux, due mainly to the residual activity of the reflector.

In the reconstruction of the BR-5 reactor into the BR-10 the core was modified to use ^{239}Pu as fissionable material instead of ^{235}U. In addition, the biological reactor shield was made thicker, and this lengthened the B-3, P-2, and T-4 channels.

The geometry of the experiment is shown in Fig. 1. The measurements were made with the center of the detector 10-20 cm from the end of the channels. The neutron spectrum of the B-3 beam was measured also at a distance of 3.7 m from the end of the channel.

$\Phi(E)$ was measured with a scintillation spectrometer having a 10 × 10 mm stilbene crystal [1] in the neutron energy range above 0.2 MeV, an SÉN2-02 neutron spectrometer with an SNM-38 counter operating in the 10-20 to 700 keV energy range, and a multisphere neutron spectrometer consisting of five

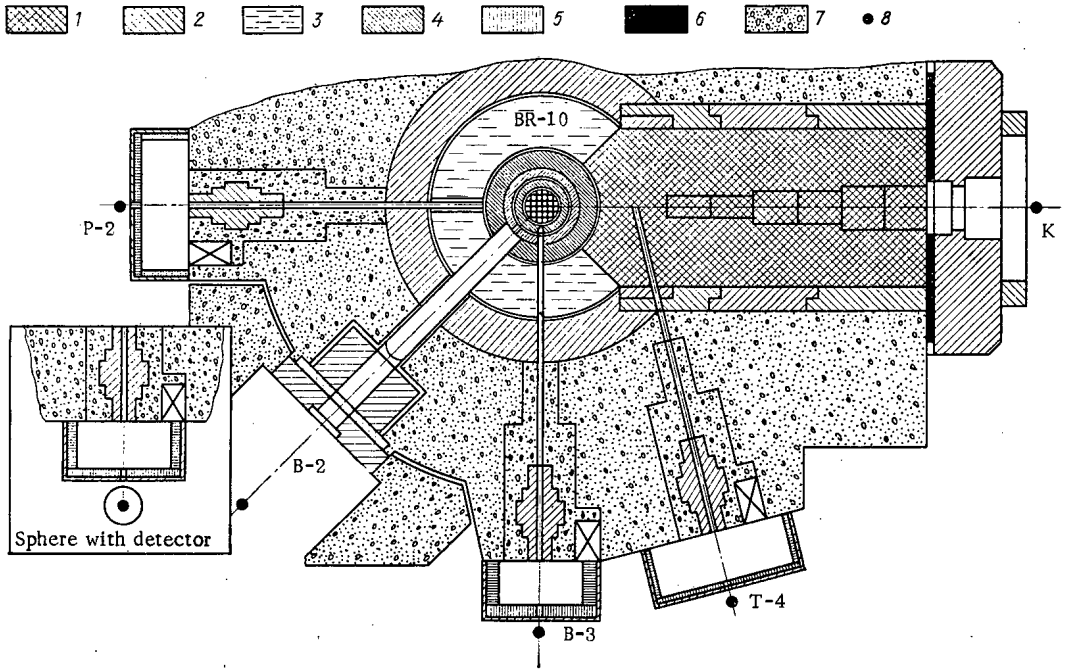

Fig. 1. Schematic diagram of experiment. 1) graphite; 2) iron; 3) water; 4) nickel; 5) polyethylene; 6) boron carbide; 7) concrete; 8) detector.

Translated from Atomnaya Énergiya, Vol. 39, No. 1, pp. 56-60, July, 1975. Original article submitted April 9, 1974.

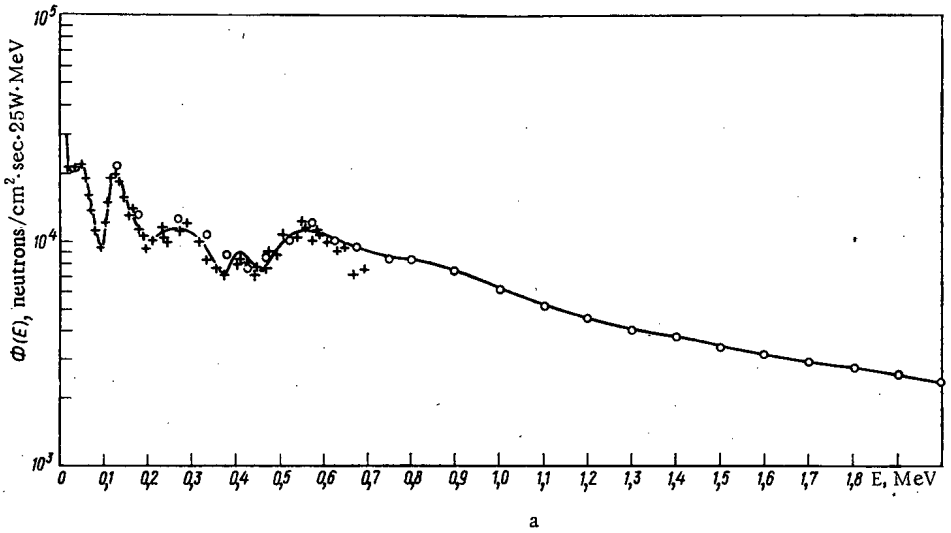

a

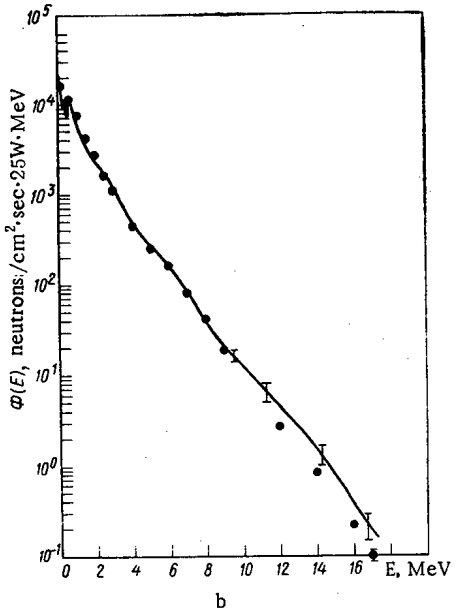

b

Fig. 2. Energy distribution of neutrons: a) emerging from B-3 channel of BR-10 reactor measured by an SĒN2-02 spectrometer (+) and a spectrometer with a stilbene crystal (○); b) emerging from the B-3 channel of the BR-10 reactor (–) and from the BR-5 (●).

TABLE 1. Values of Functions $F_{E_{thr}}$ for Fluxes of Neutrons Emerging from Channels at a Power of 1000 kW with the Detector 380 cm from the Core Center

E_{thr}, MeV	E_{thr}, neutrons/cm²·sec						
	P-2	B-2		B-3		T-4	K-5
	BR-10	BR-10	BR-5	BR-10	BR-5	BR-10	BR-10
10^{-6}	6,1·10⁷	6,7·10⁹	3,64·10⁹	7,7·10⁸	—	4,0·10⁷	2,4·10⁶
10^{-2}	5,36·10⁷	6,4·10⁹	3,5·10⁹	7,2·10⁸	—	—	—
$5\cdot10^{-2}$	4,56·10⁷	6,1·10⁹	3,36·10⁹	6,8·10⁸	—	—	—
10^{-1}	3,96·10⁷	5,4·10⁹	2,96·10⁹	6,5·10⁸	4,1·10⁸	—	—
$5\cdot10^{-1}$	1,72·10⁷	3,04·10⁹	1,66·10⁹	4,8·10⁸	2,8·10⁸	—	—
1	0,42·10⁷	1,32·10⁹	0,72·10⁹	2,8·10⁸	1,74·10⁸	—	—
2	0;204·10⁷	0,40·10⁹	0,22·10⁹	1,4·10⁸	0,71·10⁸	—	—
3	0,106·10⁷	0,132·10⁹	0,072·10⁹	0·66·10⁸	0,32·10⁸	—	—
6	0,005·10⁷	0,0164·10⁹	0,009·10⁹	0,10·10⁸	0,046·10⁸	—	—

Note 1. The error in $F_{E_{thr}}$ is generally no more than 10-15 %. 2. The error in the fluxes of thermal neutrons emerging from the T-4 and K-5 channels is 50—100%. The thermal neutron fluxes were measured with a DTN-1 detector.

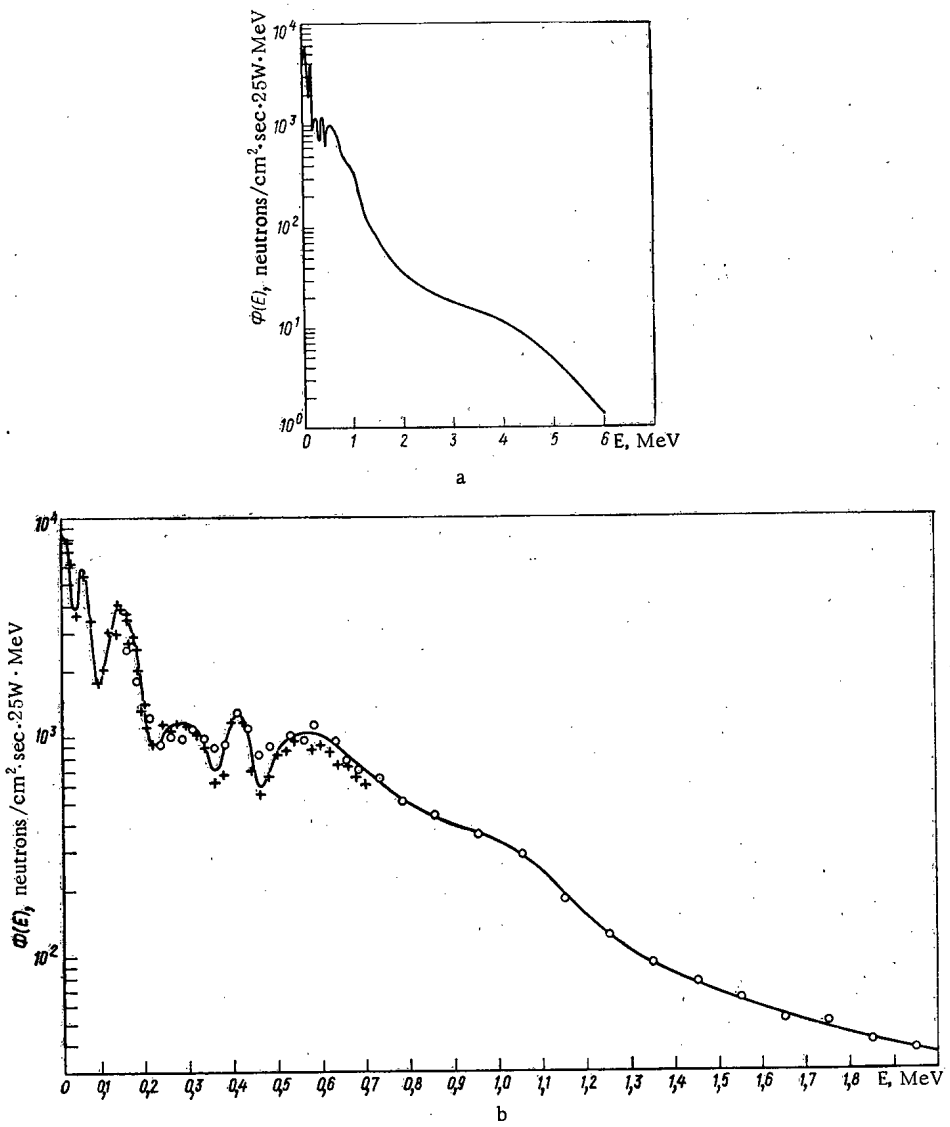

Fig. 3. Energy distribution of neutrons emerging from P-2 channel of BR-10 reactor: a) general form; b) measured by SÉN2-02 (+) and stilbene crystal spectrometers (○).

polyethylene spheres with a DTN-1 thermal neutron detector [2] operating in the range from thermal energies to several MeV.

Since the B-3, P-2, and T-4 channels are 50 mm in diameter at exit, measurements with the large spheres were made by successively displacing them relative to the opening of the collimator with a subsequent integration of the number of counts over the whole volume of the sphere.

During the measurements the reactor operated at a power of 20-50 W. The energy distributions obtained were normalized to a power of 25 W. The energy distributions of neutrons $\Phi(E)$ are shown in Figs. 2-4. Table 1 lists the functions $F_{E_{thr}} = \int_{E_{thr}}^{E_{max}} \Phi(E)\,dE$ for various values of E_{thr}.

The absolute neutron fluxes obtained with the stilbene crystal spectrometer are in error by 10-20% for various neutron energy ranges, due mainly to inaccurate knowledge of the reactor power.*

*The errors in the neutron spectra are no more than 10-20% for E > 10 keV, and no more than 50-100% for E < 10 keV.

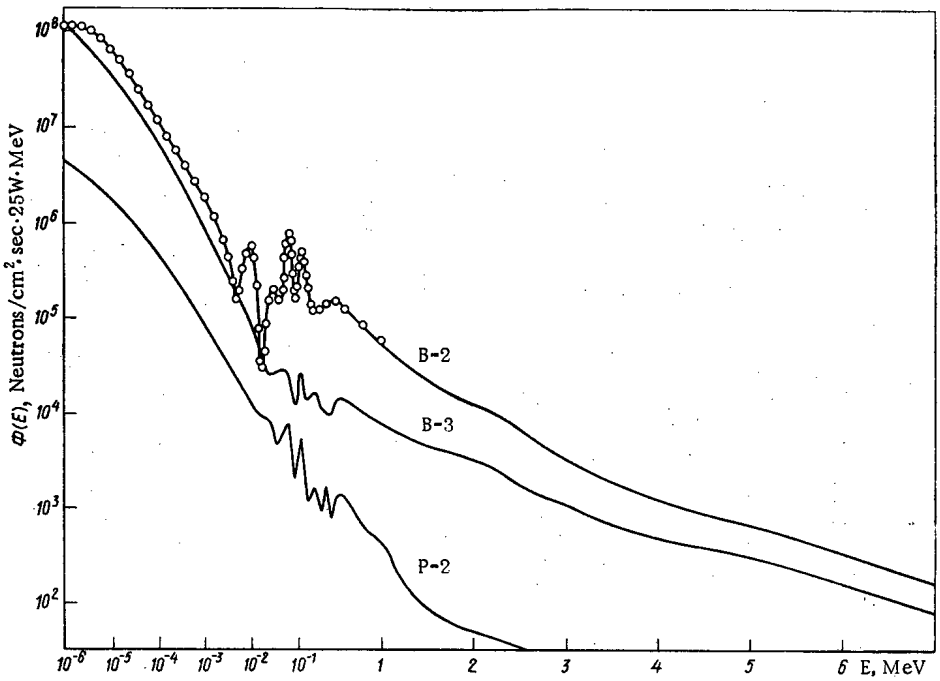

Fig. 4. Energy distribution of neutrons emerging from B-2, B-3, and P-2 channels of BR-10 reactor: ○) data from [3]; —) our data.

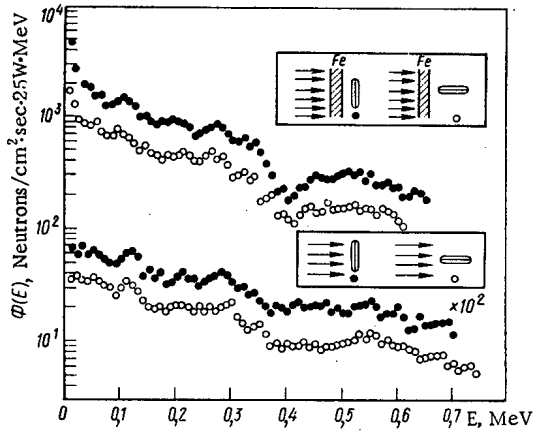

Fig. 5. Energy distribution of neutrons measured with an SĒN2-02 spectrometer with an SNM-38 hydrogen counter placed with its axis perpendicular to (●) and parallel to (○) the neutron flux.

The Φ'(E) spectra measured with the SĒN2-02 spectrometer were calculated in relative units and matched with the Φ(E) spectra measured with the stilbene crystal spectrometer in the 0.3-0.7 MeV energy range by integral count. In this case the condition

$$\int_{0.3}^{0.7} \Phi'(E)\,dE = \int_{0.3}^{0.7} \Phi(E)\,dE. \qquad (1)$$

is satisfied.

The functions Φ'(E) and Φ(E) for the P-2 neutron beam agreed to better than 5% for ΔF = 0.3-0.7 MeV.

The functions Φ'(E) calculated from the expression [1]

$$\Phi'(E) = C\left[\frac{d}{dE}N(E)\right] \times K(E)\ [\text{neutrons/cm}^2\cdot\text{sec}\cdot\text{MeV}] \qquad (2)$$

were somewhat lower than Φ(E).

The spectrum of neutrons emerging from the reflector of the reactor at zero power was measured with an SNM-38 counter placed with its axis parallel to the perpendicular to the neutron flux. Similar measurements were made behind a 30 cm iron shield. The results are shown in Fig. 5, from which it is clear that the functions Φ'(E) measured at two counter positions have the same character but differ in magnitude by about a factor of two. Hence it follows that the form of the function Φ'(E) is obtained correctly for any position of the counter, but the absolute neutron flux calculated from these data may be underestimated. This is accounted for by the following way. The values of the efficiency functions of the hydrogen counter are calculated from the total number of hydrogen nuclei in the SNM-38 counter volume. If the circuit for identifying protons and electrons by pulse shape is turned on, as it was in our experiments, and the beam of particles is incident along the axis of the counter, a fraction of the pulses formed close to the wall of the proton counter has a longer rise time and is not recorded with the pulses from γ-rays.

The shapes of the neutron spectra $\Phi(E)$ for the B-3 beam from the BR-5 and BR-10 reactors joining in the neutron energy range $E_n = 6$ MeV were compared (Fig. 2b). The slight differences in the spectra for $E_n > 10$ MeV can be accounted for by experimental errors and the difference in fissionable material in the reactor cores.

Because of the good agreement in the shapes of the $\Phi(E)$ functions for the B-3 channel of both reactors, the $\Phi(E)$ distribution for the B-2 channel of the BR-10 reactor was obtained from the $\Phi(E)$ data for the BR-5 reactor by a simple scale factor determined from the B-3 neutron beam data [1].

Table 1 also lists the B-2 and B-3 neutron beam data for the BR-5 reactor scaled to the distances at which the BR-10 measurements were made.

The authors thank Yu. V. Fadeev for help in performing the measurements.

LITERATURE CITED

1. V. I. Kukhtevich, L. A. Trykov, and O. A. Trykov, The Single Crystal Scintillation Spectrometer [in Russian], Atomizdat, Moscow (1971).
2. V. P. Semenov, L. A. Trykov, and N. D. Tyufyakov, in: Program and Abstracts of Papers of the Twenty Third Annual Conference on Nuclear Spectroscopy and the Structure of the Atomic Nucleus [in Russian], Nauka, Leningrad (1973), p. 385.
3. I. I. Bondarenko et al., At. Énerg., 18, No. 6, 593 (1965).

TRACK DETECTORS WITH AN EXTENDED RANGE OF MEASUREMENTS

L. P. Roginets, O. I. Yaroshevich, A. P. Malykhin, and I. V. Zhuk

UDC 539.107:621.039.564

The range of measurable track densities on the surface of a solid track detector is two orders of magnitude or a little more, and is limited at low track densities by the deterioration of the counting statistics, and at high densities by the overlapping of tracks.

In order to encompass a broader range for measuring neutron doses or nuclear fission densities people generally use a set of fissionable foils with various enrichments in contact with the detectors, or process the detectors by a stepwise chemical procedure.

We have studied the possibility of broadening the range of measurements for one source, one detector, and one chemical processing. To do this we propose to use a track detector with a thickness less than the maximim range of the fission fragments of the fissionable nuclei in the detector material. If the radiation dose is large and the tracks on the front side of the detector facing the source overlap, the required value is found by determining the track density on the back face, where it is very much lower, and multiplying it by the attenuation factor K, numerically equal to the ratio of the track density on the front of the detector T' to that on the back T''. The value of K does not depend on the neutron flux density or the irradiation time, and can be measured beforehand with good accuracy for a given source and detector and a given processing procedure.

We used a rose polycarbonate film of the Makrofol type $(\sim C_{19}H_{14}O_3)_n$ 1.73 mg/cm^2 ($\sim 15\,\mu$) thick with a recording efficiency of ~95% for fragments [1]. K was determined by placing a 5 × 5 mm Makrofol detector in close contact with a 4 × 4 × 0.1 mm uranium foil enriched 6.5% in ^{235}U and irradiating it with neutrons from the critical assembly of the Institute of Nuclear Power of the Academy of Sciences of the Belorussian SSR. The detector was then processed for 30 minutes in 6.25 N NaOH at 60°C. The value obtained was 11.0 ± 0.3, which corresponds to a broadening of the range of measurable fission densities (neutron dose) by approximately an order of magnitude. After additional etching of the detector in ten minute steps in the same solution (Fig. 1) the value of K fell, mainly, apparently, as a result of the decrease of the thickness of the detector.

The value of K can be estimated beforehand in the following way. Let d_1 and d_2 be the thicknesses of the source and detector, R_1 and R_2 the average initial ranges of fragments in the source and detector, and ε' and ε'' the recording efficiencies for fragments on the front and back faces of the detector respectively.

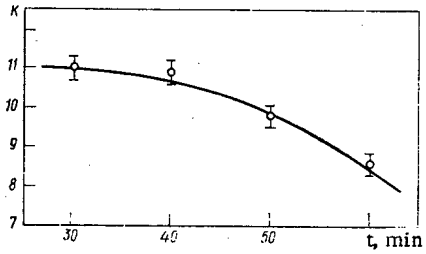

Fig. 1. Dependence of attenuation factor on time of etching of detector.

Translated from Atomnaya Énergiya, Vol. 39, No. 1, pp. 60-62, July, 1975. Original article submitted September 23, 1974.

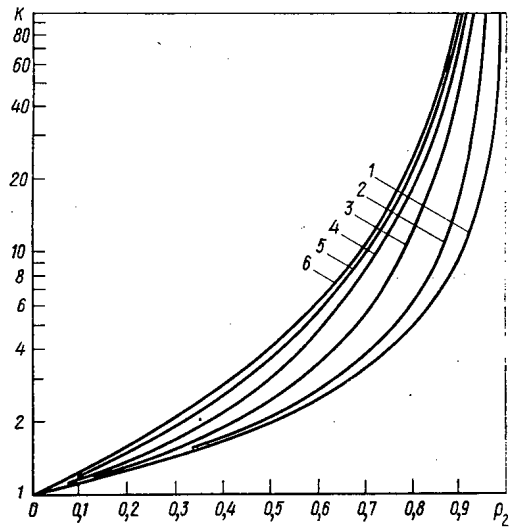

Fig. 2. Attenuation factor as a function of the thickness of track detector ($p_2 = d_2/R_2$) for various source thicknesses p_1 when $\varepsilon'/\varepsilon'' = 1$: 1-6) $p_1 = 0.001$, 0.1, 0.3, 0.5, 0.7, and $\geq 1{,}0$ respectively.

Then $K = (T'/T'') = (N'\varepsilon'/N''\varepsilon'')$, where N' and N'' are respectively the numbers of fission fragments incident on the detector and passing through it.

If the recording efficiency is high ($\varepsilon' \approx \varepsilon'' \approx 1$) or the detector is very thin ($d_2 \ll R_2$), $\varepsilon'/\varepsilon'' \approx 1$. In this case using the notation $p_1 = d_1/R_1$ and $p_2 = d_2/R_2$ and the relations from [2] for calculating N' and N'' we obtain for $p_2 < 1$:

for a thin source ($d_1 \leq R_1$)

$$K = \begin{cases} \dfrac{1-0.5p_1}{1-0.5p_1-p_2} & \text{for} \quad p_1+p_2 \leqslant 1; \\ \dfrac{(2-p_1)\,p_1}{(2-p_2)^2} & \text{for} \quad p_1+p_2 \geqslant 1, \end{cases}$$

for a thick source ($d_1 \geq R_1$), $K = 1/(1-p_2)^2$.

Since the spectrum of the fragments incident on the detector is harder than the spectrum of fragments passing through it, $\varepsilon' > \varepsilon''$, and therefore the true K must be somewhat larger than the calculated value. However, for long etching times the decrease in the thickness of the detector can lead to a decrease in K to the calculated value or even lower (Fig. 2).

The average range of unattenuated fragments in Makrofol calculated for our case according to [3] is 2.49 mg/cm^2 ($\sim$22.2μ), and the value of K calculated by the above formulas is 10.8 for $d_1 > R_1$, which is in good agreement with experiment. It is important that in using a thick source K does not depend on d_1 and R_1.

It is clear from Figs. 1 and 2 that K can be varied by choosing the thickness of the detector, and to a lesser degree by the chemical processing procedure. The recommended values of K are from 3-5 to 30-50. For $K < 3$ the detectors are too thin for convenience and the effect is rather small; for $K > 50$ variations in the thickness of the detector have a large effect on K.

For $K > 10^2$ a discontinuity can exist between the two subregions of the sensitivity of the detector on the front and back faces with the width of each slightly more than two orders of magnitude in track densities.

Such detectors and dosimeters with an overlapping range of measurable nuclear fission densities of 3-4 orders of magnitude for the same processing procedure or 5-6 orders of magnitude for stepwise etching may turn out to be useful in measuring the spatial distribution of neutron flux density in recording events from an a priori unknown radiation dose as, for example, in the role of emergency dosimeters etc.

LITERATURE CITED

1. R. Gold, R. Armani, and J. Roberts, Nucl. Sci. and Engng., 34, No. 1, 13 (1968).
2. A. P. Malykhin et al., Izv. AN BSSR, Ser. Fiz.-Énerg. Nauk, No. 2, 16 (1970).
3. A. K. Krasin (Editor), Physical Foundations of the Use of the Kinetic Energy of Fission Fragments in Radiation Chemistry [in Russian], Nauka i Tekhnika, Minsk (1972).

γ-DETECTORS OF THE RADIATION TYPE BASED ON "PURE" GERMANIUM

V. K. Eremin, E. P. Dudnik,
D. I. Levinzon, N. B. Strokan,
N. I. Tisnek, and O. P. Chikalova

UDC 621.315.592

The recent development of semiconductor radiation detectors has increased the interest in materials with concentrations of uncompensated impurities $|N_D - N_A| \leq 10^{10}$ cm^{-3}. Such small concentrations can be achieved by extremely high purity of the material or by using various compensation methods. The first way was used in [1, 2] to obtain germanium with $|N_D - N_A| \approx 10^{10}$ cm^{-3}. Among the compensation methods doping with Li^+ ions [3] and "cold doping" [4] lead to detectors which do not require continuous cooling even in storage. We describe the possibilities of cold doping by the example of germanium with $N_D - N_A \approx 10^{11}$ cm^{-3}.

To obtain a detector with a large sensitive volume and a high resolving power by cold doping the impurity composition of the starting material must be such that in the compensation radiation defects are produced with rather deep acceptor levels, and the undesirable decompensation in a strong field region must be eliminated [5, 6]. If levels arise which can give decompensation it is necessary to achieve concentrations of radiation defects in which they are not filled by electrons. In addition the material must be very homogeneous to eliminate np conversions during compensation in certain regions leading to a sharp inhomogeneity of the field [7].

Since the resolving power of a detector depends on the lifetime of nonequilibrium carriers, a certain condition is imposed on the production of concentrations of centers introduced in the compensation (i.e. the initial $N_D - N_A$) and the capture cross sections of carriers. The system of radiation defects in germanium irradiated by γ-rays satisfies these requirements in principle [8].

We illustrate the above by the example of the use of sufficiently "pure" n-type germanium with a concentration of $3 \cdot 10^{11}$ cm^{-3}. The material was obtained by the Chokhral'skii method in a "Redmet-4M"

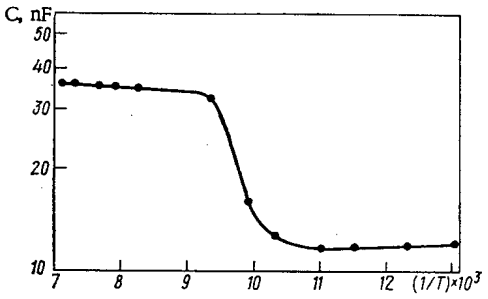

Fig. 1

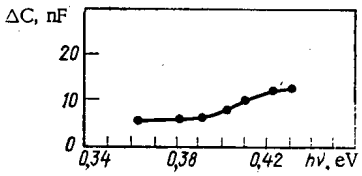

Fig. 2

Fig. 1. Temperature dependence of detector capacitance. Grid bias 30 V, frequency of probe signal 330 Hz.

Fig. 2. Change of capacitance of detector under external irradiation as a function of γ-energy. Grid bias 15 V, frequency of probe signal 1 kHz, temperature 78°K, irradiation time 15 min.

Translated from Atomnaya Énergiya, Vol. 39, No. 1, pp. 62-63, July, 1975. Original article submitted September 24, 1974.

furnace using turbomolecular (TMN-200) and titanium (GVN-0.2) pumps ensuring a vacuum of 10^{-6} mm Hg in the furnace.

Zone-purified germanium with a resistivity at −78°C of more than 500Ω·cm was used as starting material. This was obtained from the regulus and had a resistivity at room temperature of more than 20 Ω·cm. In the zone-melting process the starting germanium was further purified of admixtures of Si, C, B, Al, etc. by the action of argon containing 0.02% oxygen on the melt [9].

The choice of crucible material is important. Sintered silicon dioxide turned out to be the best. Single crystals were grown at the rate of 2 mm/min for rotations of the seed crystals at 60 rpm. The germanium melt was degassed at 1200°C for 30 min, and then the temperature was lowered and the crystal was grown under dislocation-free conditions; i.e. seeding was performed by the Dash method, and the growth angle of the crystal did not exceed 60°.

In compensating the conductivity the sample was irradiated with such a dose of γ-rays that a concentration of $\sim 10^{10}$ cm^{-3} remained in the conduction band. In principle this permits a domain of the field ~5 mm with dislocations of about 300 eV, analogous to the case of superpure germanium.

To investigate the levels arising in the forbidden zone during compensation, studies were made of the changes in capacitance with temperature C(T) and with external irradiation C(hν). The behavior of C(T) shows the presence of a level E_c = 0.27 eV for a concentration of $1.15 \cdot 10^{11}$ cm^{-3} (Fig. 1). The photocapacitive measurements show the presence of still another deeper level E_v+ + 0.33 eV (Fig. 2). The positions of the observed levels are such that they cannot give decomposition at the operating temperature of the detector.

The stepwise behavior of C(T) shows also that during compensation a p-type domain was not produced in the sample, since the presence of a domain with n—p conversions would require C(T) to have a maximum.

The spectrometric characteristics of the detector are rather high. The resolution at the ^{60}Co line (1.33 MeV) is 0.24% for a 5 mm thick sensitive region. This resolution is only twice the limiting resolution determined by ionization fluctuations.

The effective capture cross section of holes determined from the collective component of the resolution is rather large ($\sigma_{eff} = 3 \cdot 10^{13}$ cm^2) but the concentration $N_D - N_A$ ensured retention of a rather long lifetime.

The spectrometry of low-energy radiation in the 5-50 keV range has recently acquired special significance in connection with the rapid chemical analysis of materials. The resolution of 0.24% is unconditionally sufficient for these purposes since in the range indicated electronics noise contributes more than 1% to the resolution.

It can be expected that the purification of material up to $N_D - N_A \approx 10^{11}$ cm^{-3} for subsequent application of cold doping is sufficient to obtain detectors with high spectrometric characteristics, at least for soft radiation.

LITERATURE CITED

1. R. Hall and T. Soltys, IEEE Trans., NS-18, No. 1, 160 (1971).
2. W. Hansen, Nucl. Instrum. and Methods, 94, No. 2, 377 (1971).
3. E. Pell, J. Appl. Phys., 31, 291 (1961).
4. S. M. Ryvkin et al., Zh. Tekh. Fiz., 34, 1535 (1964).
5. S. Ryvkin et al., IEEE Trans., NS-15, No. 3, 226 (1968).
6. L. L. Makovskii et al, in: Physics of Electron—Hole Transitions and Semiconductor Devices [in Russian], Nauka, Moscow—Leningrad (1969).
7. S. M. Ryvkin et al., Physics and Technology of Semiconductors, Vol. 4 [in Russian], (1970), p. 1303.
8. Abstracts of All-Union Symposium on "Radiation defects in solids" [in Russian], BGU, Minsk (1972).
9. D. I. Levinzon and V. N. Nefedov, Izv. AN SSSR, Neorganicheskie Materialy, 10, No. 1, 9 (1974).

COMPARATIVE CHARACTERISTICS OF NaI(Tl) AND CsI(Tl) DETECTORS

O. P. Sobornov and O. P. Shcheglov

UDC 539.1.074

By comparing the characteristics and spectrometric parameters of similar sized detectors we have determined the possibility of using CsI(Tl) detectors in research where NaI(Tl) detectors are ordinarily used. Figure 1 shows the general characteristics of the temperature dependence of the light output (signal amplitude) of detectors and scintillation blocks with NaI(Tl), CsI(Tl), and CsI(Na) crystals obtained from research [1] and an analysis of data [2-7].

TABLE 1. Spectrometric Parameters and Relative Photoefficiencies of NaI(Tl) and CsI(Tl) Detectors

Crystal size, mm		Parameters of assembly			Relative photoefficiencies for gamma rays of energy Eγ, MeV					
					0,66		1,46		2,62	
		R	R'	V_{NaI}/V_{CsI}	F_1	F_2	F_1	F_2	F_1	F_2
NaI (Tl)	40×40	8,1	8,7	2,0	1,0	1,00	1,0	1,00	1,0	1,00
CsI (Tl)	40×40	9,0	9,8		1,4	1,40	1,5	1,50	1,6	1,60
NaI (Tl)	63×63*	7,5	8,3	2,6	4,6	1,00	6,0	1,00	6,4	1,00
CsI (Tl)	63×63*	8,6	9,4		6,1	1,32	8,4	1,40	9,0	1,41
NaI (Tl)	76×76*	8,6	9,1	—	8,8	1,00	12,2	1,00	11,9	1,00
CsI (Tl)	76×76*	10,3	11,5		11,2	1,25	16,4	1,34	16,6	1,38
NaI (Tl)	80×80	8,3	8,5	2,3	9,2	1,00	13,0	1,00	—	—
CsI (Tl)	80×80	12,5	13,2		11,7	1,25	16,8	1,29	—	—

*Scintillation blocks; explanations given in text.

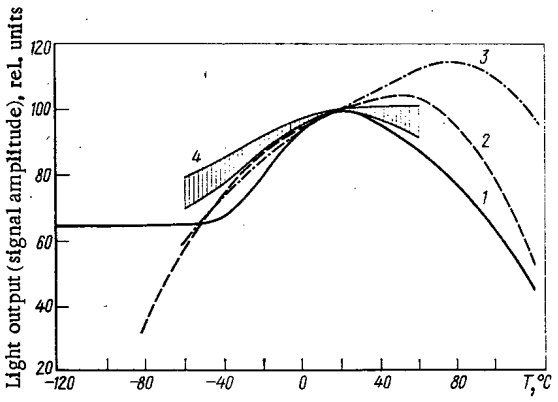

Fig. 1

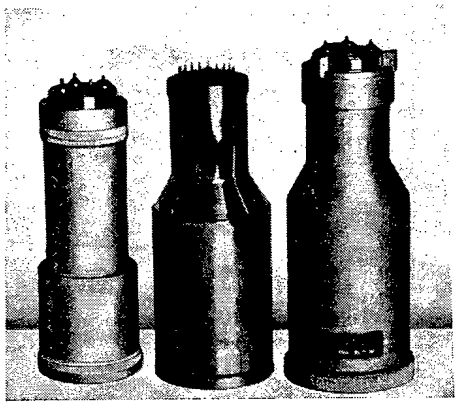

Fig. 2

Fig. 1. Temperature dependence of light output of detectors and signal amplitude of scintillators: 1) NaI(Tl) [3, 4, 5, 7]; 2) CsI(Tl) [2-5]; 3) CsI(Na) [2, 6]; 4) scintillation blocks with NaI(Tl) crystals showing limits of variation of characteristics [1].

Fig. 2. Scintillators with NaI(Tl) and CsI(Tl) crystals.

Translated from Atomnaya Énergiya, Vol. 39, No. 1, pp. 63-65, July, 1975. Original article submitted October 11, 1974.

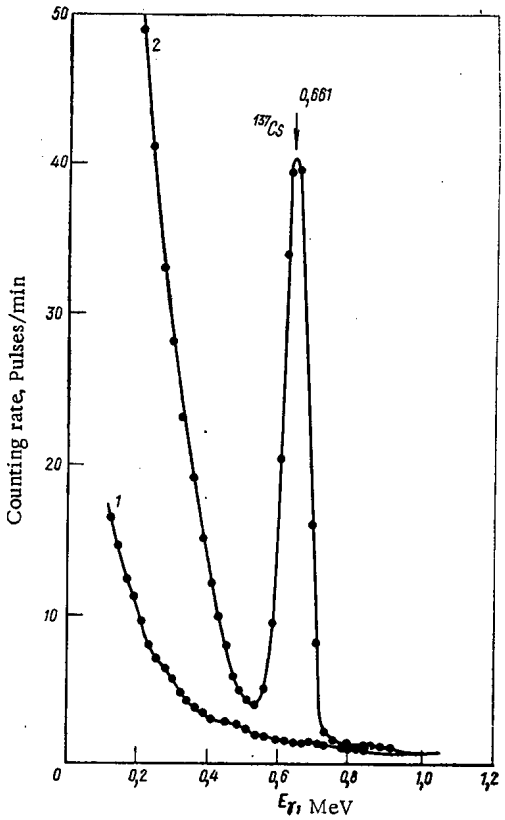

Fig. 3. Spectra of the background of the γ-spectrometer with scintillation blocks using 76 × 76 mm NaI(Tl) (1) and CsI(Tl) crystals (2) and an FÉU-110.

TABLE 2. Background Counting Rate (counts/min) in Various Energy Intervals ΔE_γ

Block	ΔE_γ, MeV					
	0.1—3.0	0.1—0.75	0.55—0.75	1.35—1.55	1.7—2.0	2.5—3.0
S_1	1116	1076,6	162,0	4,40	2,80	2,30
S_2	202	154,0	12,5	3,13	2,62	1,85
S_1/S_2	5,52	7,0	13,0	1,40	1,07	1,24

The photoefficiencies of the spectrometric detectors were compared for NaI(Tl) and CsI(Tl) crystals of the commonest sizes 40 × 40, 63 × 63, and 80 × 80 mm. In addition scintillation blocks were used with 76 × 76, 63 × 63, and 40 × 40 mm NaI(Tl), CsI(Tl), and CsI(Na) crystals and an FÉU-110, FÉU-93, and FÉU "Comet" with a 40 mm multialkaline cathode. Figure 2 shows the external appearance of the scintillation blocks. All the measurements were made on a low-background arrangement attenuating the radiation of the external medium by as much as a factor of 100 [8]. The spectrometric parameters of all the detectors were determined on one FÉU-110. The energy range of the investigation was 0.6-3.0 MeV. A point ^{137}Cs γ-source and distributed sources of ^{137}Cs, ^{40}K, and ^{232}Th were used. In the latter case the containers with the sources surrounded the detector being studied in a layer ~12 mm thick, producing a nearly 4π radiation geometry. This enabled us to determine the performance figures of the detectors under conditions which closely resemble those in many geophysical and cosmophysical investigations. Table 1 lists the basic spectrometric parameters of the detectors being compared and their relative photoefficiencies obtained by measuring the same distributed γ-sources under identical conditions. The errors in determining the photoefficiencies are due mainly to tolerances in the crystal sizes (—1 mm for 40 × 40 crystals and —2 mm for 80 × 80 mm crystals) and are estimated as 10%. The errors in measurements using scintillation blocks are no more than 3%. Since the detector parameters depend on the radiation geometry [9], Table 1 lists the resolution R determined by the standard method (point source of γ-rays) and under "isotropic" radiation conditions (R'). The ratios of the signal amplitudes V_{NaI}/V_{CsI} show how much the signal amplitude from a CsI(Tl) detector falls below that from a NaI(Tl) detector of similar size. The photoefficiencies were compared in the same energy intervals, including the characteristic peaks of total absorption of γ-radiation. The values of F_1 given in Table 1 represent the sensitivities of detectors of various sizes and types relative to the 40 × 40 mm NaI(Tl) detector, and the values of F_2 characterize the photoefficiency of CsI(Tl) detectors relative to an NaI(Tl) detector of the same size.

In measurements of low concentrations of radioactive elements one of the basic factors limiting the sensitivity of the method is the intrinsic background of the γ-spectrometer. Figure 3 shows spectra of the background of the scintillation γ-spectrometer using 76 × 76 mm NaI(Tl) and CsI(Tl) crystals. Radiation pure materials were used in constructing the blocks; the housing was made of oxygen-free copper. The elimination of glass used in ordinary detectors significantly decreases the background by lowering the contribution of ^{40}K. In addition to the contribution of direct and scattered radiation from natural radioactive elements the background spectrum of the CsI(Tl) crystal scintillator shows the clearly separated peak of the ^{137}Cs radioisotope. Table 2 gives the background counting rate with a CsI(Tl) crystal (S_1) and a NaI(Tl) crystal (S_2), and the ratio S_1/S_2 for selected energy intervals.

Table 2 shows that the measured and intrinsic background of the block with the CsI(Tl) crystal are higher over the whole range of energies, particularly in the region below 0.75 MeV which includes the ^{137}Cs peak. Studies showed that ^{137}Cs is present in various amounts in all CsI crystals of both domestic and foreign manufacture. The ^{134}Cs isotope was not identified in the background spectra of unwrapped CsI

crystals. These measurements were made using a block with NaI(Tl) on which the crystal under investigation was mounted. However, the relatively high cross section for the capture of thermal neutrons (of cosmic origin) with the formation of ^{134}Cs (28b) and ^{134m}Cs (2.6b) [10] for the 76 × 76 mm CsI(Tl) crystal may cause a saturated activity of the order of 10 decays/min. The relatively high ^{137}Cs content can be accounted for only by the contamination of the raw material by fission products. This limits the use of CsI detectors in low-ground γ-spectrometry in the energy range below 0.75 MeV. In some studies the ^{137}Cs peak (661.6 MeV) can be used as a reference point for γ-spectrometer stabilization systems.

The use of CsI(Tl) detectors in the 0.75-3.0 MeV energy range can be assessed by the criterion [11]

$$M = k\varepsilon^2/N_b R,$$

where k is a coefficient of proportionality, ε is the counting efficiency, R is the resolution, and N_b is the background counting rate. Comparing the average data obtained for 76 × 76 mm NaI(Tl) and CsI(Tl) crystals we find that the value of M is 15% larger for CsI(Tl) crystals than for NaI(Tl). Therefore, in spite of the somewhat worse resolution and larger measured and intrinsic backgrounds the CsI(Tl) detector should be preferred to the NaI(Tl), particularly in analyzing a mixture with a simple isotopic composition (^{40}K, U—Ra, ^{232}Th). The advantages of CsI(Tl) detectors increase as their size is decreased. The spectrometric parameters of CsI(Na) detectors for the same counting efficiency are better than the spectrometric parameters of CsI(Tl) detectors.

The authors thank L. L. Nagornaya, Ya. A. Zakharin, and A. L. Lifits for constructing the high-quality detectors.

LITERATURE CITED

1. O. P. Sobornov, S. P. Shcheglov, and N. M. Balugina, in: Single Crystals, Scintillators, and Organic Luminophors, No. 6, Part 2 [in Russian], Cherkassy (1972), p. 249.
2. I. Arens and B. Taylor, Nucl. Instrum. and Methods, 108, No. 1, 147 (1973).
3. A. F. Vedekhin et al., Pribory i Tekh. Éksperim., No. 1, 75 (1967).
4. A. Werkheiser and T. Miller, Nucl. Instrum. and Methods, 75, 167 (1969).
5. M. N. Nazarova and N. K. Pereyaslova, Pribory i Tekh. Éksperim., No. 6, 49 (1962).
6. J. Toshinobu, Bull. Japan Petr. Inst., 13, No. 1, 97 (1971).
7. G. I. Yakhnis et al., in: Single Crystals, Scintillators, and Organic Luminophors, No. 5 [in Russian], Khar'kov (1970), p. 302.
8. Yu. A. Surkov and O. P. Sobornov, At. Énerg., 34, 125 (1973).
9. O. P. Sobornov and O. P. Shcheglov, Pribory i Tekh. Éksperim., 6, 67 (1974).
10. C. Lederer, J. Hollander, and I. Perlman, Table of Isotopes, 6th edition., Wiley, New York (1967).
12. G. G. Ménov, in: Metrology of Ionizing Radiations [in Russian], Gosatomizdat, Moscow (1962), p. 192.

CALCULATION OF BREMSSTRAHLUNG SPECTRA AT VARIOUS ANGLES IN THE 1-30 MeV RANGE

V. E. Zhuchko and Yu. M. Tsipenyuk

UDC 539.124.17

The analysis of most experiments in which bremsstrahlung is used requires a knowledge of the γ-spectrum as a function of the energy of the incident electrons, the observation angle, and the target thickness and material. A number of experiments have shown that the yield of forward bremsstrahlung is largest for targets ~0.3 radiation lengths in thickness. The spectrum of the radiation from such a target cannot be considered equivalent to the commonly used Schiff spectrum for thin targets, and in this case special calculations are required. The radiation spectrum must be known not only in the forward direction, but also at various angles, since a certain range of angles is included in an actual experiment. Thus, for example, it is shown in [1] that the calculation of spectra using only slightly different photonuclear reaction cross sections leads to a broadening and displacement of the resonances, and to the appearance of fraudulent peaks.

A formula is obtained in [2] for the forward bremsstrahlung spectrum from a thick target:

$$\frac{d^2Y}{dk\,d\Omega} = \sum_{i=1}^{n} \alpha_i \tau_i N_i \frac{d\sigma}{dk} B_i, \quad 1/(\text{MeV} \cdot \text{sr}). \tag{1}$$

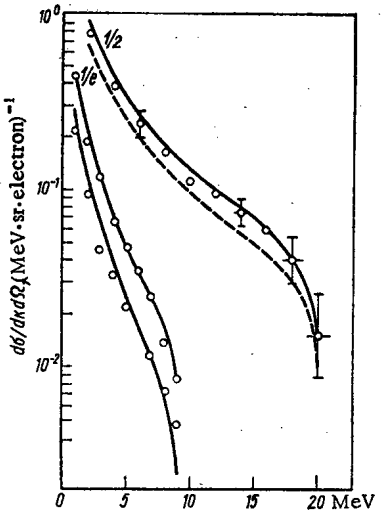

Fig. 1

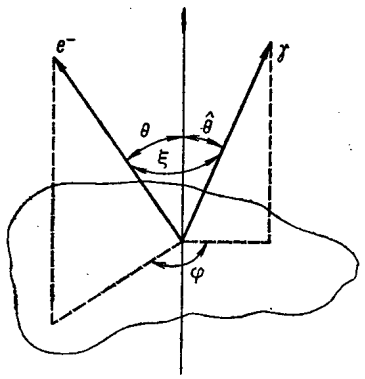

Fig. 2

Fig. 1. Bremsstrahlung spectra at 0° from 20.9 MeV electrons on a target of 0.735 g/cm^2 W + 7.72 g/cm^2 Al [6], and at angles of 0 and 12° from 9.66 MeV electrons on a target of 5.8 g/cm^2 W [8]. ○) experiment; ——) calculated; ----) calculated by approximating the Molière distribution by a Gaussian with the same 1/e width.

Fig. 2. Schematic representation of angles between directions of motion of the electron, the emitted photon, and the primary beam.

Translated from Atomnaya Énergiya, Vol. 39, No. 1, pp. 66-68, July, 1975. Original article submitted October 18, 1974; revision submitted February 10, 1975.

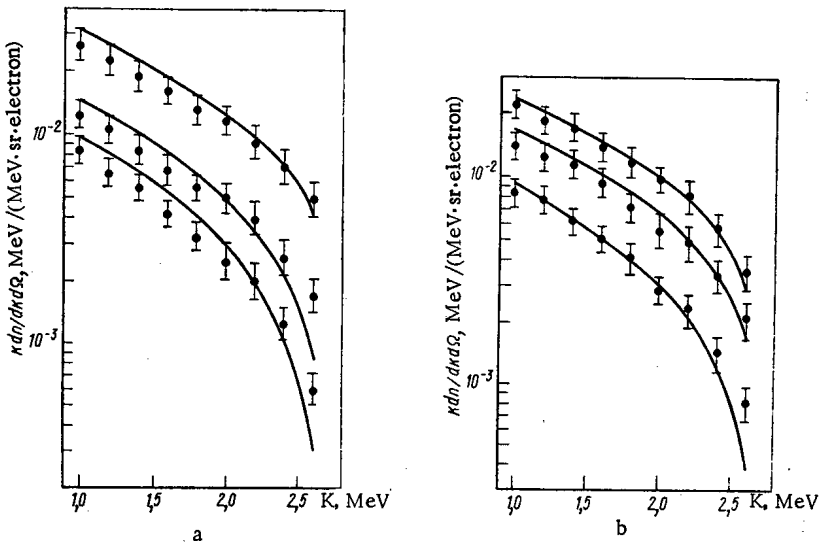

Fig. 3. Comparison of calculated (solid curve) and experimental [7] bremsstrahlung spectra at angles of 0, 10, and 20° for 2.8 MeV electrons on targets of a) iron (2.31 g/cm^2) and b) aluminum (1.73 g/cm^2).

Here n is the number of layers of the target, each layer assumed to have a thickness ~0.001 radiation lengths; i is the number of the layer, α_i is the absorption coefficient for photons in the target material, $\tau_i(T_e, \alpha_i)$ is the transport coefficient, i.e. the fraction of the electrons reaching the i-th layer, T_e is the initial energy of the electrons, N_i is the number of atoms along the path of an electron after the i-th layer (cm^{-2}), $d\sigma/dk\,[(T_e)_i, d_i]$ is the elementary (inner) bremsstrahlung spectrum, where $(T_e)_i$ is the energy of the electrons in the i-th layer and d_i is the coordinate of the i-th layer. The angular dependence of the elementary spectrum and the angular distribution of electrons after penetrating the i-th layer are assumed Gaussian with mean square angles $(\langle\theta_b^2\rangle)^{1/2}$ and $(\langle\theta_e^2\rangle)^{1/2}$ respectively. The number of photons emitted from the i-th layer per unit solid angle at 0° i.e. the coefficient B_i, is

$$B_i = \frac{1}{\pi \langle\theta_b^2\rangle_i \langle\theta_e^2\rangle_i} \int_0^{2\pi} \int_0^{\pi} \exp\left(\frac{-\theta^2}{\langle\theta_e^2\rangle_i}\right) \exp\left(\frac{-\theta^2}{\langle\theta_b^2\rangle_i}\right) \theta\, d\theta\, d\varphi \approx \frac{1}{\pi\,(\langle\theta_e^2\rangle_i + \langle\theta_b^2\rangle)} .$$

In contrast with [2] we used the Schiff integral spectrum [3] as the elementary spectrum since it seems to agree best with experiment, and we approximated the Molière distribution by Gaussians having the same 1/e width and the same half width [4]. According to Frank [5], starting with angles $(\langle\theta_e^2\rangle)^{1/2} = 30°$ replacing the Gaussian by $\cos^2\theta$ gives a better description of the angular distribution of electrons in the diffusion domain. The spectrum of the forward radiation turned out to be insensitive to the choice of the elementary spectrum. Approximating the Molière distribution by a Gaussian with the same half width rather than the same 1/e width gives better agreement with experiment (Fig. 1), and therefore we used it in all the calculations. The calculated spectra agree with experiment to within ~10-15% over the whole range of E_γ values and for electron energies from 1 to 30 MeV.

We modified this procedure for calculating the angular dependences of bremsstrahlung spectra. In going to nonzero angles in Eq. (1) only the coefficients α_i and B_i change; they depend on the angle of observation $\hat{\theta}$ with respect to the axis of the electron beam. Since after the emission of a γ-photon its path length depends on the angle $\hat{\theta}$, the absorption of γ-energy must be taken into account as follows:

$$\alpha_i = \exp \frac{[-\mu(k)]\,(D - d_i)}{\cos\hat{\theta}} ,$$

where k is the energy of the γ-photon, $\mu(k)$ is the γ-absorption coefficient, D is the target thickness and d_i is the length of the path traversed by the electron before the emission of a photon.

We now find the coefficient $B_i(\hat{\theta})$. Suppose the electron moves at an angle θ with the axis of the beam and the photon is emitted at an angle $\hat{\theta}$ (Fig. 2). Then the angle ξ between the direction of emission of the photon and the direction of motion of the electron is

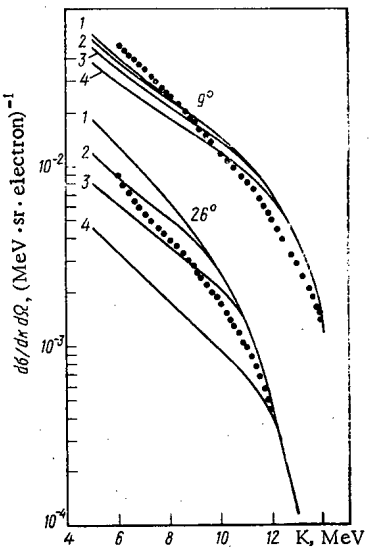

Fig. 4. Dependence of shapes of bremsstrahlung spectra at angles of 9 and 26° from 15 MeV electrons on a 10.2 g/cm^2 iron target on boundary of diffusion domain. 1-4 correspond to 45, 30, 25, and 20° respectively. The points are values from [9] increased by a factor of three.

$$\xi = \arccos(\sin\hat{\theta}\sin\theta\cos\varphi + \cos\theta\cdot\cos\hat{\theta}). \quad (2)$$

By integrating over the angles φ and θ we obtain the fraction of photons emitted per unit solid angle at an angle $\hat{\theta}$ with the axis of the incident beam:

$$B_i(\hat{\theta}) = A\int_0^{2\pi}\int_0^{\pi}\exp\left(\frac{-\xi^2}{\langle\theta_e^2\rangle_i}\right) f(\theta)\sin\theta\, d\theta\, d\varphi, \quad (3)$$

where for $(\langle\theta_e^2\rangle_i)^{1/2} < 30°$ $1/A = \pi^2\langle\theta_e^2\rangle_i\langle\theta_b^2\rangle_i$ and $f(\theta) = \exp(-\theta^2/\langle\theta_e^2\rangle_i)$, and for $(\langle\theta_e^2\rangle_i)^{1/2} > 30°$ $1/A = (3/4)\pi^2 \cdot \langle\theta_b^2\rangle_i$ and $f(\theta) = \cos^2\theta$.

Unfortunately there is much less experimental information on bremsstrahlung spectra at nonzero angles from the forward radiation. In the 1-30 MeV range which interests us we know of only a few papers [7-9] with which the calculations can be compared. As an example Fig. 3 compares calculated and experimental data for aluminum and iron targets for electron energies of 2.8 MeV [7], and Fig. 1 shows bremsstrahlung spectra at 0 and 12° from a tungsten target for 9.66 MeV electrons [8]. Clearly, the calculation gives an adequate description of the spectral shape at various angles.

Measurements of angular distributions of bremsstrahlung were recently reported in [9]. Unfortunately these data were obtained by complicated processing of the activities of threshold detectors and therefore are not certain enough. Our calculations give a good description of the shapes of the spectra obtained in [9] (Fig. 4), but for all angles the calculated results are systematically about three times higher than the experimental values. Since the radiation spectrum in the forward direction is not given in [9] it is impossible to find the reason for these differences.

While the angle at which electron diffusion is taken into account has little effect on the results for forward radiation, the spectrum of the radiation at nonzero angles depends strongly on the choice of the boundary of the diffusion domain, and this difference increases with increasing angle (Fig. 4). It appears that the best agreement between calculation and experiment is obtained by taking account of diffusion beginning with angles $(\langle\theta_e^2\rangle_i)^{1/2} = 30°$ as was done in calculating the forward radiation.

LITERATURE CITED

1. H. Dahmen et al., Nucl. Instrum. and Methods, 107, 329 (1973).
2. H. Ferdinande et al., Nucl. Instrum. and Methods, 91, 135 (1971).
3. L. Schiff, Phys. Rev., 83, 252 (1951).
4. W. Scott, Phys. Rev., 85, 245 (1952).
5. H. Frank, Zeit. Naturforsch., 14a, 247 (1959).
6. A. O'Dell et al., Nucl. Instrum. and Methods, 61, 340 (1968).
7. W. Dance et al., J. Appl. Phys., 39, 2881 (1968).
8. N. Starfelt and H. Koch, Phys. Rev., 102, 1598 (1956).
9. H. Hirayama and T. Nakamura, Nucl. Sci. and Engng., 50, 248 (1973).

MONOCRYSTALLINE FILMS OF GaAs AS SPECTRAL DETECTORS OF X-RAYS AND SOFT γ-RADIATION

V. M. Zaletin, I. I. Protasov,
O. A. Matveev, P. I. Skorokhodov,
and A. Kh. Khusainov

UDC 539.107.45

The successes of recent years in growing relatively large, pure monocrystalline layers of gallium arsenide have given reason to hope that this material might be used in spectral semiconductor detectors of x- and soft γ-radiation [1-5]. The basic advantage of these semiconductors over the presently widely used germanium and silicon is due to the fact that, because of the wide forbidden zone (E_{gCdTl} = 1.5 eV, E_{gGaAs} = 1.42 eV at 300°K), gallium arsenide and cadmium telluride detectors can be used without extreme cooling.

In order to manufacture practical GaAs detectors it will be necessary to obtain epitaxial layers of thickness 1-2 mm with concentrations of residual electrically active impurities of less than 10^{12} cm^{-3}.

In the present article we describe the results of a study of pure gallium arsenide layers obtained by gaseous epitaxy and of the detectors made from them.

The epitaxial layers were grown in a Ga—$AsCl_3$—H_2 system with high purity components. n^+-GaAs, doped with tin, tellurium, or silicon to a concentration of $2\text{-}4 \cdot 10^{18}$ cm^{-3}, was mainly used as a substrate. A series of test layers were made on disks of semiinsulating gallium arsenide. In all cases the substrates were oriented parallel to a plane inclined 5° from (100) toward (111). The surface of the substrate was carefully prepared by chemical and mechanical processing and gaseous etching [4]. By using purified materials and optimizing the growth regimes it is possible to obtain layers 50-150 microns thick with electron concentrations of 10^{14} to 10^{13} cm^{-3}. The electron mobility was 6000-9000 cm^2/sec at room temperature and 80,000-160,000 cm^2/sec at liquid nitrogen temperature. The level of compensation in the layers was 0.5-0.9 and the overall concentration of ionized impurities (upper and lower) was less than $5 \cdot 10^{14}$ cm^{-3}.

Mass spectroscopy of similar samples showed that the content of such impurities as Cu, Fe, C, S, Cr, and Si is much larger (by about two orders of magnitude) than the concentration of the impurities as determined by physical electronic measurements. This means that the majority of the impurities in the layers are in electrically inactive, bound states, perhaps in the form of complexes, clusters, or the like.

Examination of the structural defects in pure epitaxial layers of GaAs with a type JEM-150 transmission electron microscope showed that there is an almost complete lack of dislocations, packing defects, or dislocation rings in them. The principal type of structural defect was rhomboidal laminar precipitates oriented parallel to the (100) direction. The visible dimensions of these sheets were 500-5000 Å as determined by contrast. In this regard, it was noted that an improvement in the electronic properties of the crystal corresponded to greater ordering of defects (with their number remaining roughly constant).

For layers 50 to 150 microns thick the transition region (the region with a nonequilibrium distribution of impurities between the layer and the substrate) was 5 to 15 microns thick and was determined primarily by the nature of the impurities in the substrate and by the gaseous etching arrangement. Figure 1 shows a profile of the carrier distribution in a layer grown on a tin doped substrate. The doping level of the substrate was $2 \cdot 10^{18}$ cm^{-3}.

Translated from Atomnaya Énergiya, Vol. 39, No. 1, pp. 68-69, July, 1975. Original article submitted October 24, 1974.

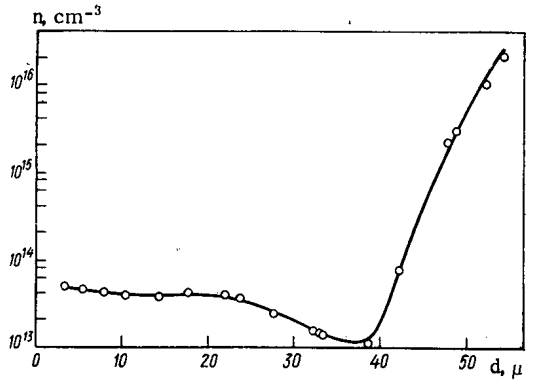

Fig. 1

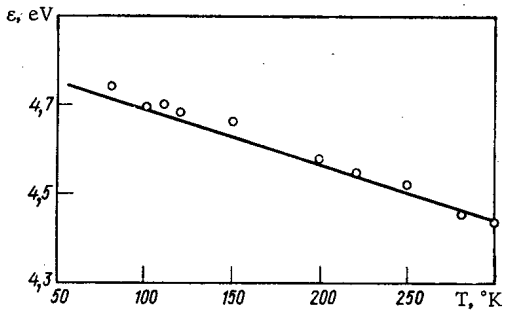

Fig. 2

Fig. 1. The distribution of the differential concentration of ionized impurities in a pure layer of gallium arsenide (sample 216.2 I).

Fig. 2. Temperature dependence of the average energy of formation of electron-hole pairs in gallium arsenide: The solid line corresponds to the calculated value according to the formula $\varepsilon = (14/5)E_g + r(1/h)\omega_{\phi}$, where $rh\omega_{\phi} = 0.5$ eV. The relation $E_g(T) = (1.54 - 36.7 \cdot 10^{-4} T)$ eV [7] was used for the temperature dependence of the width of the forbidden zone, ○ are experimental values of the temperature dependence of the pulse amplitude from ^{57}Co gammas obtained with detector 242.2 I.

Detectors were made out of layers with carrier concentrations of $0.8 \cdot 10^{13}$ to $5 \cdot 10^{13}$ cm^{-3}. The working element was a p—n—n^+ system in which the n—n^+ transition was made by growing a pure epitaxial layer (n) onto a doped substrate (n^+) and the p—n transition was made by vapor depositing a gold film. With a working detector area of 3 mm^2 the reverse current was less than $2 \cdot 10^{-8}$ A for voltages up to 100 V. The resolution for γ-emission from the isotopes ^{57}Co (122 keV) and ^{241}Am (59.6 keV) was 4.3 keV and was determined by current noise in the detector. As the working temperature of the detector was decreased the half width of the lines was reduced and at a temperature of 260°K reached a plateau of 2.4 keV which lasted down to 77°K. Measurements of the average energy of formation of electron-hole pairs showed that the temperature dependence of this quantity (Fig. 2) fits well the dependence calculated using Klein's model [5] and is determined by the temperature dependence of the width of the forbidden zone in gallium arsenide. In this case good agreement with experiment is observed if we take the minimum value (equal to 0.5 eV) for the phonon losses. We may assume that in GaAs detectors minimum values of the Fano factor and limiting resolution will be realized [6].

Our results show that over the temperature interval 77-300°K the role of charge losses in the resolving capacity and average pair formation energy is not appreciable. This is an indication of the high purity of the films obtained here with respect to recombination centers. The electron lifetime, as determined by the amount of charge loss when detecting alpha particles, was $\geq 1\,\mu$sec. An investigation of the γ (^{57}Co) count rate as a function of temperature showed that the working volume of the detectors increases substantially as the temperature is reduced. This is due to the presence of compensating lower levels. If the measurements are made when the working volume of the detector is in the space charge region of the surface barrier transition then the concentration of the compensating lower levels can be evaluated as:

$$S_1/S_2 = \sqrt{(N_d - N_a'')/(N_d - N_a')},$$

where S_1 and S_2 are the counting rates at two temperatures, N_d is the concentration of ionized gases, N_a' and N_a'' are the concentration of ionized acceptors at the corresponding temperatures.

For the films studied here, the concentration of the lower impurity levels, which are filled in the space charge region at temperatures below 220°K, were equal to half the differences in the impurity concentrations at room temperature.

In their physical electronic properties monocrystalline GaAs films grown by gaseous epitaxy are as good as the best layers obtained by liquid epitaxy.

The authors thank S. M. Ryvkin for his interest in this work.

LITERATURE CITED

1. J. Eberhardt, D. Ryan, and A. Tavendale, Nucl. Instrum. and Methods, 94, No. 3, 463 (1971).
2. T. Kabayashi, et al., IEEE Trans., NS-19, No. 3, 324 (1972).
3. P. Gibbons and J. Hawes, ibid., p. 353.
4. V. M. Zaletin and V. I. Zerkalov, in: Proceedings of VNIIGAK, Vol. 28 [in Russian], Novosibirsk (1972), p. 69.
5. C. Klein, J. Appl. Phys., 39, No. 4, 2029 (1968).
6. G. D. Alkhazov, A. A. Vorob'ev, and A. P. Komar, Izv. AN SSSR, Ser. Fizika, 29, 1227 (1966).
7. O. Madelung, The Physics of A^3B^5 Semiconducting Compounds [Russian translation], Mir, Moscow (1967).

DENSITY, SURFACE TENSION, AND VISCOSITY OF URANIUM TRICHLORIDE–SODIUM CHLORIDE MELTS

V. N. Desyatnik, S. F. Katyshev,
S. P. Raspopin, and Yu. F. Chervinskii

UDC 531.756:532.61.133

Fused salts are now finding increasing use in metallurgy, power engineering, etc. Information on the properties of uranium trichloride–sodium chloride melts is scant [1,2]. We have investigated the temperature dependence of the density (ρ), surface tension (σ), and kinematic viscosity (ν) throughout the range of UCl_3 concentrations of the system $NaCl–UCl_3$.

The density and surface tension were determined by the method of maximum pressure in a gas (argon) bubble [3]. The viscosity was measured by a method based on an investigation of the damped oscillations of a cylindrical crucible filled with the liquid under investigation and suspended from an elastic filament [4]. This is currently one of the best methods for investigating fused salts. The experimental procedure and

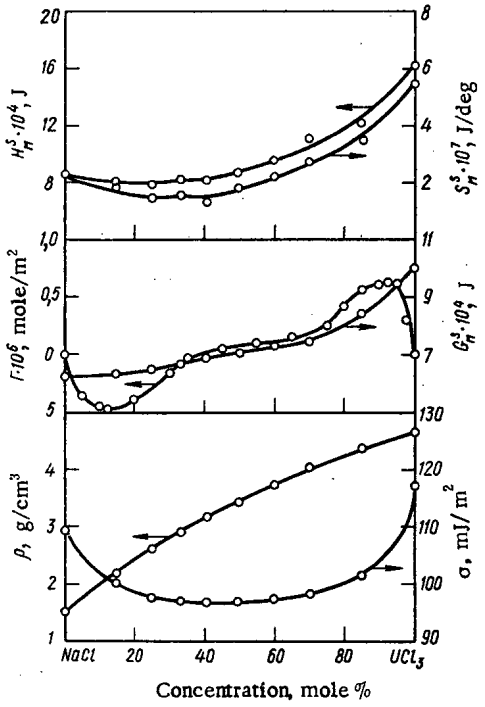

Fig. 1

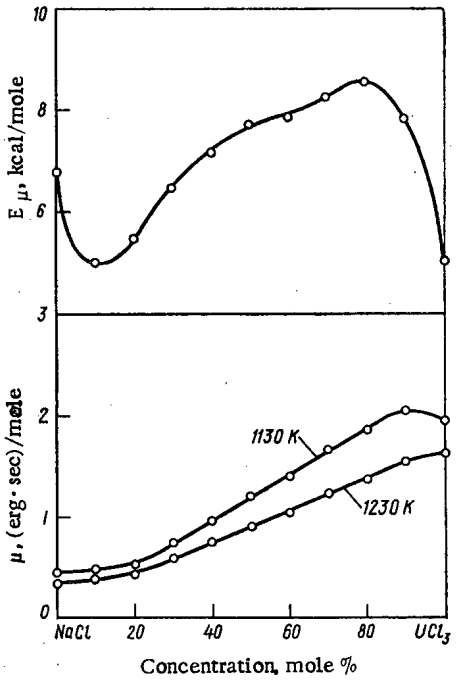

Fig. 2

Fig. 1. Density, surface tension, and adsorption isotherms and excess thermodynamic functions of melts of the system UCl_3–NaCl at 1123°K.

Fig. 2. Molar viscosity isotherms and activation energy of viscous flow of the system UCl_3–NaCl.

Translated from Atomnaya Énergiya, Vol. 39, No. 1, pp. 70-72, July, 1975. Original article submitted October 30, 1974.

TABLE 1. Density, Surface Tension, Molar Volumes and Their Deviation from Additivity in the System UCl_3—NaCl

UCl_3, mole%	$\rho = a - bT$, g/cm³		Standard deviation, g/cm³	$\sigma = \sigma - cT$, mJ/m²		Standard deviation, mJ/m²	Temperature range, °K	1123 °K		
	a	b·10³		σ_0	c·10³			V, cm³/mole	V_{ad}, cm³/mole	$\Delta V/V_{ad}$, %
0,0	2,1352	0,5405	0,001	193,63	74,03	0,02	1076—1273	38,30	38,30	0,00
14,4	2,9598	0,6673	0,001	165,34	58,17	0,03	998—1167	45,08	43,41	3,85
24,9	3,4938	0,7821	0,002	143,24	40,64	0,05	900—1141	49,56	47,14	5,13
33,3	3,8604	0,8371	0,001	143,22	41,28	0,03	892—1142	52,62	50,13	4,97
40,6	4,1966	0,9072	0,002	138,35	37,03	0,04	898—1137	54,92	52,72	4,17
49,5	4,4738	0,9304	0,003	146,75	44,24	0,03	951—1943	58,32	55,88	4,37
59,9	4,8964	1,0470	0,001	154,99	51,14	0,05	998—1148	61,74	59,58	3,62
70,0	5,2035	1,0504	0,003	160,34	55,43	0,04	1041—1195	64,27	63,17	1,74
85,0	5,5847	1,0869	0,002	171,06	62,06	0,02	1096—1218	69,09	68,50	0,86
100,0	6,3747	1,5222	0,002	224,70	95,70	0,11	1138—1296	73,82	73,82	0,00

the apparatus for viscosity measurement were described in a previous communication [5]. The measurement accuracy was 1, 1.5, and 3.7% for ρ, σ, and ν respectively.

For these investigations we obtained pure initial salts by known procedures [1]. The density and surface tension were determined in pyrographite crucibles. The capillaries were beryllium oxide tubes with sharpened ends. The viscosity was measured in beryllium oxide crucibles in purified argon. The experimental data were processed by the method of least squares. For all melts of the system UCl_3—NaCl we obtained linear temperature dependences of ρ and σ, and an exponential temperature dependence of ν (in °K). The ρ, σ, and ν values of pure sodium chloride agree well with the literature [6, 7].

The molar volumes of the melts and their relative deviations from additivity were calculated from the density measurements. Table 1 lists the results of calculations for 1123°K. Figure 1 shows the density isotherm for the same temperature. Throughout the UCl_3 concentration range the molar volumes deviate toward higher values, which indicates that UCl_3—NaCl mixtures have a "looser" structure than the pure components. The deviations are maximal for melts containing 25-33 mole% UCl_3. The "loosening-up" effect is probably due to formation of complex aggregates of uranium groups of the UCl_5^{2-} type.

Figure 1 shows the surface tension isotherm for 1123°K. The σ values of UCl_3 and NaCl are much the same. The minimum on the isotherm at 30-40 mole % UCl_3 indicates reaction of the initial components in the surface layer. This is confirmed by calculation from the Zhukovitskii—Guggenheim equation of ideal mixing [8, 9]. The surface tension of a melt of equimolar composition for 1123°K is 14.67% lower than the calculated value. The adsorption of sodium chloride in the surface layer was calculated from the experimental data [10]. The adsorption isotherm for 1123°K (Fig. 1) has a complex form. The curve intersects the zero line in the concentration range corresponding to maximum "loosening-up" of the melt.

The density and surface tension data were used to calculate the excess thermodynamic functions (the free energy G_M^S, the enthalpy H_M^S, and the entropy S_M^S) of the surface of the molar volume sphere. Figure 1 shows their compositional dependences. For all the compositions investigated the excess thermodynamic functions exhibit negative deviation from additivity. It is known that the G_M^S values of compounds

TABLE 2. Viscosity and Activation Energy of Viscous Flow in the System UCl_3—NaCl

UCl_3, mole %	$\lg \nu = A_\nu + \frac{B_\nu}{T}$ (ν, cS)		Standard deviation, cS	$\lg \eta = A_\eta + \frac{B_\eta}{T}$ (η, cP)		Standard deviation, cP	$\lg \mu = A_\mu + \frac{B_\mu}{T}$ [μ, (erg·sec)/mole]			Standard deviation, (erg·sec)/mole	Temperature range, °K
	$-A_\nu$	B_ν		$-A_\eta$	B_η		$-A_\mu$	B_μ	$E\mu$, cal/mole		
0,0	1,4291	1478	0,009	1,4357	1691	0,014	1,6624	1478	6761	0,005	1090—1254
10,0	1,2343	1097	0,008	1,0927	1275	0,016	1,2946	1097	5019	0,007	1052—1248
20,0	1,4086	1193	0,012	1,1630	1348	0,030	1,3455	1193	5457	0,014	960—1238
30,0	1,5370	1415	0,012	1,2179	1557	0,037	1,3779	1415	6475	0,017	894—1249
40,0	1,6404	1564	0,004	1,2675	1704	0,014	1,4028	1564	7154	0,007	888—1254
50,0	1,7181	1683	0,012	1,3057	1821	0,046	1,4140	1683	7700	0,024	945—1251
60,0	1,7404	1719	0,008	1,3073	1873	0,034	1,3786	1719	7866	0,019	991—1258
70,0	1,7837	1797	0,004	1,3106	1944	0,019	1,3717	1797	8224	0,011	1030—1254
80,0	1,8446	1867	0,005	1,3481	2015	0,026	1,3865	1867	8545	0,016	1072—1252
90,0	1,6992	1706	0,017	1,2006	1876	0,075	1,1998	1706	7808	0,052	1114—1252
100,0	1,2213	1100	0,003	0,7387	1310	0,012	0,6843	1100	5035	0,009	1128—1278

with an ionic reaction character are higher than those of compounds with a high proportion of covalence [11]. Therefore the excess free energy of the surface of the molar volume reflects to some extent the energy of the bond between the particles. The negative deviation of G_M^S from additivity is apparently due to an increase in the proportion of the covalent bond when the components are mixed, i.e., to complexing.

The dynamic viscosity (η) for all the compositions investigated was calculated from the results of the kinematic viscosity measurements. However, the values of η cannot be strictly related to the melt structure because the number of particles per unit volume differs for different compositions. This difficulty is overcome if we use the molar viscosity μ, equal to the product of the kinematic viscosity and the molecular weight. The extent of the structural changes in the mixtures investigated can be assessed from the deviations of the μ isotherms from additivity. The calculated values of η and μ depend exponentially on temperature. Table 2 lists the coefficients of the viscosity equations, calculated by the method of least squares. It also gives the activation energies of viscous flow (E_μ) for all the compositions investigated. Figure 2 shows the molar viscosity isotherms and the variation of the activation energy of viscous flow with the composition of the fused mixtures. Assuming that chloride melts contain complex ionic groups, in mixtures with a very low UCl_3 content the following structural units are involved in viscous flow: elementary sodium cations in the second coodination sphere, complex ions $NaCl_4^{3-}$ and UCl_5^{2-}, and a very small amount of UCl_6^{3-} [12]. With an increase in the uranium trichloride content, $NaCl_4^{3-}$ is replaced by complex uranium ions. This is accompanied by a slight change in the melt viscosity, largely as a result of the relative decrease in the number of readily displaceable sodium cations. In melts containing more than 25-33 mole% UCl_3, the Na^+ cations in the second coordination sphere are replaced by complex cations UCl_2^+. This is accompanied by a much greater increase in the viscosity. The change in the viscosity and activation energy of viscous flow in melts containing from 80-90 to 100 mole% UCl_3 indicates that the complex uranium ionic groups in the system break down into simpler groups.

LITERATURE CITED

1. V. N. Desyatnik, B. V. Dubinin, and S. P. Raspopin, Zh. Fiz. Khim., 47, No. 10, 2726 (1973).
2. J. Mochinaga, K. Cho, and R. Takagi, Denki Kagaku, 37, No. 9, 658 (1969).
3. S. I. Filippov et al., Physicochemical Methods for the Investigation of Metallurgical Processes [in Russian], Metallurgiya, Moscow (1968).
4. E. G. Shvidkovskii, Some Problems of the Viscosity of Fused Metals [in Russian], Gostekhteorizdat, Moscow (1956).
5. V. N. Desyatnik et al., in: Proc. of Universities of the Russian Federation. 2. Physicochemical Investigations of Metallurgical Processes [in Russian], Izd. UPI im. S. M. Kirova, Sverdlovsk (1974).
6. Handbook of Fused Salts [Russian translation], edited by A. G. Morachevskii, Vol. 1, Khimiya, Leningrad (1971).
7. ibid, Vol. 2, Khimiya, Leningrad (1972).
8. A. A. Zhukovitskii, Zh. Fiz. Khim., 17, 313 (1943); 18, 214 (1944).
9. E. Guggenheim, Trans. Farad. Soc., 3, 150 (1945).
10. V. K. Semenchenko, Surface Phenomena in Melts and Alloys [in Russian], Gostekhteorizdat, Moscow (1957), p. 147.
11. M. V. Smirnov and V. P. Stepanov, in: Trudy Instituta Élektrokhimii UFAN SSSR, 16, 21 (1970) (Sverdlovsk).
12. M. V. Smirnov, Electrode Potentials in Fused Chlorides [in Russian], Nauka, Moscow (1973), pp. 201-210.

INFORMATION

ON THE SO-CALLED COSMION

N. A. Vlasov

The name "cosmion" was proposed by a group of Greek physicists for the $\tilde{p}p$ pair (antiproton plus proton) in a state bound by nuclear forces. They consider that this state has been recorded in their experiments.

In the study of the annihilation of slow antiprotons $\tilde{p}$ with deuterons the Greek physicists observed [1] that the annihilation products, charged pions, carry away on the average, an energy of 1169 ± 10 MeV, which is 72 ± 10 MeV less than follows from the charge independence of nuclear forces. According to charge independence three kinds of pions (π^+, π^-, π^0) are equally probable. A special study of γ-radiation [2] showed that the average number of γ-photons is 3.77 ± 0.08, which is 0.73 ± 0.08 larger than the average number of charged pions (3.04 ± 0.02). For identical numbers of π^+, π^-, and π^0 mesons the indicated values should be equal, since each neutral pion decays into a pair of γ-photons.

Peaks were observed in the γ-spectrum correlating with certain variants of the decay, absent, for example, in $\tilde{p}n$ annihilation, particularly when four charged pions are formed. The authors assume that together with the photons of the $\pi^0 \to 2\gamma$ decay they have observed photons from a preannihilation radiative transition of the $\tilde{p}p$ pair between quasistationary states in the field of nuclear forces.

The possibility of bound states of an antinucleon with a nucleon was suggested long ago by E. Fermi, considering a pion as such a state. Even the first experiments on the $\tilde{p}p$ interaction showed that nuclear forces between an antinucleon and a nucleon are larger than the forces between a pair of nucleons, and therefore instead of a single bound state (deuteron) the $\tilde{p}p$ ($\tilde{p}n$) pair can have a large number of such states. Experiment [3] showed that states with nonzero angular momenta play an important role in annihilation. A bound state with a binding energy of ~80 MeV was observed [4] for the $\tilde{p}n$ pair. A theoretical analysis of the interaction of antinucleons with nucleons [5] showed that a whole series of both bound and unbound resonance states is possible. Therefore their observation cannot be considered unexpected. It is remarkable that a radiative transition turned out to be more probable than annihilation.

It is known that the electromagnetic interaction giving rise to a radiative transition is considerably weaker than the nuclear interaction leading to annihilation. Annihilation must be strongly forbidden to make it less probable than a radiative transition. It is possible that such a prohibition is already contained in the conclusion of the theoreticians that annihilation occurs at very small distances of the order of 0.1-0.2 F and its probability decreases rapidly with orbital angular momentum because of the centrifugal barrier. It would be interesting if it would become necessary to introduce new rules similar to those proposed in many theoretical papers to explain the recently observed [6] rather narrow resonances in the interaction of positrons with electrons at energies of 3.1 and 3.7 GeV. But the conclusion of a preannihilation radiative transition does not follow unambiguously from the observed results. They are easily accounted for by assuming the existence of a state of the $\tilde{p}p$ pair from which decay into neutral pions is relatively more probable. Kalogeropoulos et al. [2] consider that such an explanation does not agree with the spectral observations.

The γ-spectra presented [2] require refinement and confirmation, particularly since the authors did not cite the energies of the observed lines or discuss their relation to the observed excesses of photons and their total energy.

The name "cosmion" proposed in [2] replaces the old word "protonium." Protonium is a $\tilde{p}p$ pair bound by electromagnetic forces. Ordinarily protonium is formed in highly excited states [7] in which the nuclear interaction is important, but as a result of radiative transitions to less excited states the pair

Translated from Atomnaya Énergiya, Vol. 39, No. 1, p. 73, July, 1975.

converges, the role of nuclear interaction is increased and finally predominates. After this the pair is either annihilated or forms first one or more quasistationary states. Therefore it is clear that a cosmion is nothing more than dying protonium.

The proposal of the authors to use cosmion γ-radiation to search for antimatter is reminiscent of a similar proposal to use protonium radiation made ten years ago [8]. We hope that these proposals can be successfully realized.

LITERATURE CITED

1. T. Kalogeropoulos et al., Phys. Rev. Lett., 33, 1631 (1974).
2. Ibid., p. 1635.
3. D. Cline et al., Phys. Rev. Lett., 27, 71 (1971).
4. L. Gray et al., Phys. Rev. Lett., 26, 1491 (1971).
5. I. S. Shapiro, Usp. Fiz. Nauk, 109, 431 (1973).
6. J. Aubert et al., Phys. Rev. Lett., 33, 1404 (1974); J. Augustin et al., Phys. Rev. Lett., 33, 1406 (1974).
7. N. A. Vlasov, Antimatter [in Russian], Atomizdat, Moscow (1966).
8. N. A. Vlasov, Astronom. Zh., 49, 893 (1964).

THIRTY-SEVENTH SESSION OF THE ACADEMIC COUNCIL OF THE JOINT INSTITUTE OF NUCLEAR RESEARCH (JINR)

V. A. Biryukov

The thirty-seventh session of the JINR Academic Council was held in Dubna from January 14 to 17, 1975. Leading scientists of the Institute member countries took part in the work. In opening the session the JINR director, Academician N. N. Bogolyubov, reported on implementing decisions taken by the Academic Council in previous sessions. The directors spoke of the work of the various Institute laboratories.

D. I. Blokhintsev reported on the work done at the Laboratory of Theoretical Physics. In studies of power series self-similar asymptotic forms in the interaction of particles at large momentum transfer, based on the principle of self-similarity and the rules of generalized dimensional analysis of quark amplitudes, the exact angular dependence of the differential cross sections for large-angle scattering was found. It was shown that the use of renormalization invariance in nonrenormalizable quantum theories leads to nonanalyticity in the binding constant and restrictions on the subtraction constants. On examining a number of fields in nonlocal quantum theory it was established that fields can be simply classified according to their renormalizability. Physical phenomena related to strong, weak, and electromagnetic interactions of pions at low energies were successfully described within the framework of the quantum chiral theory of fields with good agreement with experiment: the scattering length and phases of $\pi\pi$ scattering, the electromagnetic radius and the form factor of the pion, the polarizability of the pion, and the weak and electromagnetic decays of pions. Based on a model of the collision of hadrons consisting of stable quarks, and in comparison with the multiplicity distribution of particles created in collisions of high-energy protons it was shown that the most probable number of quarks comprising a proton is three.

Institute theoreticians have completed direct semimicroscopic calculations of level densities in spherical and deformed nuclei. Fragmentation was considered within the framework of a model taking account of the interaction of quasi particles with phonons, leading to a complication of the structure of states with increasing excitation energy. A model of the preequilibrium decay of nuclei was constructed. Nuclear experiments showing the structure of neutral currents were reported.

The work of scientists at the High Energy Laboratory was described in a paper by A. M. Baldin. In accord with a Soviet-American agreement a group of JINR research workers took part in work at the Batavia accelerator. Processing of the measurements in an experiment on elastic pp scattering in the 9-400 GeV energy range has been completed. It was well established experimentally that the sign of the ratio α_{pp} of the real to the imaginary part of the forward scattering amplitude changes from negative to positive at high energies. The scattering cross section increases above 100 GeV; the ratio of the elastic pp scattering cross section to the total cross section is practically independent of energy. Diffraction elastic pp scattering was studied at momenta in the 50-385 GeV/sec range by using a gas jet deuterium target. The energy dependence of the slope parameter and the excitation characteristics of a nucleon were established.

The analysis of the study of the forward scattering of 50 GeV pions on electrons was completed. A magnetic spark chamber spectrometer at the Serpukhov accelerator was used in this work which was performed in collaboration with University of California physicists. The electromagnetic radius of a pion was found to be $\langle r_\pi^2 \rangle^{1/2} = 0.78 \pm 0.10$ F. This value does not contradict the result expected from the vector dominance model and agrees with other experimental data. Small-angle elastic π^-p scattering at pion momenta of 40 and 50 GeV/sec was studied. Differential cross sections were found as a function of the

Translated from Atomnaya Énergiya, Vol. 39, No. 1, pp. 74-77, July, 1975.

momentum transfer and the ratio $\alpha_{\pi p}$. This work was performed by a group of scientists from JINR, IFVÉ, and the University of California.

Cumulative meson production in the interaction of protons and deuterons of momenta 4.2, 6, and 8.4 GeV/sec per nucleon with D, Li, C, Al, Cu, Sm, W, and Pb nuclei was studied on the JINR synchrophasotron. The effect of the transfer of the energy of three or four nucleons to one particle was observed. A recoil particle spectrometer operating on-line with a computer was built to study elastic dd scattering. The first physical results for deuteron energies from 6 to 10 GeV have been obtained.

A. M. Baldin reported on improvements of the synchrophasotron. A new LU-20 injector — a linear proton accelerator giving particle energies of 20 MeV and a beam current of 20 mA — has been put into operation. With the LU-20 and a system of corrections the intensity of the internal beam in the synchrophasotron was increased to $9 \cdot 10^{11}$ protons, $7 \cdot 10^{10}$ deuterons, and $2 \cdot 10^{8}$ alpha particles per cycle. A control system was built involving the slow withdrawal of the beam from the synchrophasotron using a computer. The "Krion" ion source mounted on the LU-9M linear accelerator was started up. Helium and nitrogen nuclei were accelerated with this system.

A complex multiple-purpose device — the 90 channel Cerenkov mass spectrometer "Photon" — was put into operation on a beam of negative pions. The device consists of six proportional chambers on-line with a computer, 32 spark magnetostriction chambers, scintillation counters, 90 Cerenkov spectrometers, a liquid hydrogen target, and other systems. Proportional and drift chambers, cryogenic systems, and various electronic devices were developed further.

V. P. Dzhelepov reported on new research at the Laboratory of Nuclear Problems. Precision measurements of the positive muon lifetime have been made in experiments at the synchrocyclotron. The target for muon production was the radiator of a Cerenkov detector which recorded μ-decay positrons in 4π geometry. The apparatus operated on-line with a computer. The measured value $\tau_{\mu^+} = 2.19711 \pm 0.00008\,\mu$sec is several times more accurate than other known measurements. A new phenomenon was observed — the emission of electrons and x-rays with the formation of muonic atoms of heavy elements (U, Th, Ir, Ta) — and this opened up a new approach to the study of the dynamics of mesic atom formation. The experiments were performed in collaboration with CERN physicists on the muon beam of the JINR synchrocyclotron.

The fission of nuclei of heavy elements in interactions with negative muons was investigated. Measurements showed that the fission probabilities of isotopes of Th, U, Np, and Pu decrease significantly in the presence of a muon in the 1S orbit of a mesic atom. Institute scientists together with physicists from Moscow, Bucharest, Turin, Sofia, Plovdiv, and Rzhezh made a detailed study of the elastic scattering of pions by ^{3}He and ^{4}He nuclei in the (3/2, 3/2) resonance region. Experiments were performed on a magnetic spectrometer with a helium streamer chamber. The energy dependence of the phases of pion-nuclear scattering was found; the value of the electromagnetic radius of a pion, $\langle r_\pi^2 \rangle^{1/2} = 0.83 \pm 0.17$ F, determined by a new independent method, agrees with the results of other measurements. Experiment showed an intense formation of neutron-deficient isotopes up to 12-13 mass units from the β-stable band in reactions involving the capture of negative pions by nuclei of heavy elements. High-spin nuclear states are efficiently excited in these processes.

An international group of scientists from IFVÉ, Saclay, JINR, and ITÉF completed the processing of data obtained in experiments at the Serpukhov accelerator. Differential cross sections and polarizations in π^-p, K$^-$p, and $\bar{p}$p elastic scattering at a momentum of 4 GeV/sec were determined. Information was obtained for the first time on the polarization in pp scattering. On the whole the results of the investigations show the important role of spin dependence in hadron interactions at high energies. The construction of the five-meter JINR spark chamber spectrometer was completed on the beam of the Serpukhov accelerator. Research was begun on the diffraction of 40 GeV pions on carbon nuclei. Seventy thousand pictures were obtained on the spectrometer; they are being processed.

A high-intensity beam for medical, biological, and physical research was produced at the synchrocyclotron. Pions produced by a proton beam in a target are focused by a wide-angle magnetic lens with an axially symmetric field configuration. The electron tracks obtained in a hydrogen streamer chamber are of adequate brightness for the relatively low field intensity of 27 kV/cm at hydrogen pressures up to 1 atm.

The expansion of closed orbits in sectional magnetic field structures of cyclic accelerators, discovered earlier at JINR, was confirmed experimentally. The use of this effect in principle solves the problem of ensuring close to 100% yield of the proton beam in superhigh-current accelerators with a stationary magnetic field.

G. N. Flërov presented a paper on experiments at the Laboratory of Nuclear Reactions. A new method was proposed for the synthesis of heavy elements, based on the use of targets of stable elements and accelerated ions having masses of 40 atomic units and more. In reactions involving the bombardment of lead nuclei with Ar, Ti, Cr, and other ions accelerated in the U-300 cyclotron the isotopes ^{244,246}Fm and element No. 102, ^{254,255,256}Ku, were synthesized. This permitted the construction of a new systematics of spontaneous fission. The use of lead as a target instead of highly fissionable isotopes of Pu, Cm, and Cf eliminates the background of spontaneous fission and permits the use of the highly sensitive rapid method of observing nuclei by spontaneous fission. By irradiating the isotopes ^{207}Pb and ^{208}Pb with ^{54}Cr ions in reactions with the emission of two and three neutrons from the compound nucleus JINR scientists synthesized an isotope of a new element ^{259}106 which fissions spontaneously with a half-life of ~0.01 sec.

The search for superheavy elements in various meteorites was completed. The Efremovka, Allende, and Saratov meteorites were investigated. According to the existing hypothesis an excess of heavy xenon isotopes is related to the possible spontaneous fission of superheavy elements. Methods of analysis sensitive to 10^{-16} weight fractions failed to identify the possible radiator reliably.

The previously discovered delayed proton emitters ^{116}Cs, ^{119}Ba, and ^{121}Ba were investigated with the new BĒMS-2 mass separator on a beam of heavy ions. The decay of the lighest rubidium isotopes was studied and preliminary data were obtained on the delayed proton emitter ^{133}Sm. The method of studying neutron-rich isotopes of light nuclei was improved; the experiments used a combination of magnetic analysis, the ΔE and E methods, and the time of flight technique. Experiments showing the nuclear stability of ^{14}Be, ^{19}C, and ^{20}C (a new isotope) were completed.

Using a mass separator brought over from Orsay mounted on the beam of the U-300 a group of JINR physicists and French scientists obtained fundamental physical data on reactions which occur with the formation of compound nuclei (reactions with the evaporation of nucleons, fission) for a broad range of masses of the interacting nuclei (target nuclei and heavy ion nuclei) and energies. Level lifetimes and reduced electromagnetic transition probabilities for the neutron-deficient isotopes of ytterbium and hafnium were measured by the Doppler shift method. The experimental study of the interaction of Nb, La, and Xe ions with nuclei showed that characteristic K x-rays are radiated by quasimolecules with a total nuclear charge in the range $74 \leq Z \leq 114$.

A four-meter isochronous cyclotron is under construction at the Institute, designed to accelerate ions from neodymium to xenon to a maximum energy of 625 Z^2/A^2 MeV/nucleon with a beam intensity from 10^{14} particles/sec for Nd to 10^{11} particles/sec for Xe. G. N. Flërov also reported on the use of beams of heavy ions to solve scientific-technical problems. The technology of producing nuclear filters has been improved; experimental sample filters have been made using beams of xenon ions. Work is continuing on the use of activation analysis methods.

I. M. Frank spoke of the work of scientists at the Neutron Physics Laboratory. The processing of measurements of magnetic momenta of compound states of dysprosium excited in the capture of resonance neutrons has been completed. The experiments were performed on the JINR IBR-30 pulsed reactor. The neutron energy was measured by time of flight. The method used was the shift of neutron resonance by targets whose nuclei are oriented at extremely low temperatures. The experimental results agree with theoretical estimates. Preliminary data on holmium and terbium resonances were obtained also.

Research on very cold neutrons (VCN) continued to seek the most efficient converter-sources of VCN. Measurements of the yields of VCN from a number of gaseous and frozen converters established that frozen water at the temperature of liquid nitrogen ensures maximum yield, exceeding the yield of VCN from aluminum by a factor of 25.

Work continued on the search for the $n\alpha$ reaction with resonance neutrons. The alpha decay of neutron resonances of the isotopes ^{157}Gd and ^{171}Yb was observed experimentally. The measured values of the total alpha widths of these nuclei turned out to be close to the values predicted by a variant of the optical model in theoretical papers of Institute scientists. The first version of a spectrometer for small-angle scattering of thermal neutrons using time of flight was built. In an experimental test of the new device the radius of hemoglobin was measured as 24.5 ± 0.6 Å; the possibility of determining the dimensions of biological macromolecules and polymers was demonstrated. A theoretical analysis shows the advantages of the new instrument over installations on stationary reactors.

Measurements were concluded on the inelastic scattering of neutrons from a sample of PrF_3 at various temperatures, including 77 and 4.2°K. They were performed by the method of inversive geometry

with a beryllium filter. The parameters of the crystal field and the splitting scheme of the principal multiplet of the trivalent praseodymium ion were obtained.

Construction was continued on the complex new IBR-2 power reactor; the assembly of the technological equipment was begun. Work was continued on the construction of new experimental installations and apparatus for the IBR-2 measurement-computing center.

The paper of M. G. Meshcheryakov was devoted to work of the Laboratory of Computational Techniques and Automation. Work was continued on the JINR measurement-computing complex. Four standard magnetic tape memory units of the ES-5012 type were put into operation on the BÉSM-6. These permit the exchange of information with computing centers in other countries. A new variation of the mathematical check of the BÉSM-6 has been developed in connection with the use of such memory units. To ensure compatibility of the BÉSM-6 and CDC-6200 programs most of the library of BÉSM-6 general purpose programs has been transferred to the CDC-6200. A new variation of the translator from FORTRAN-4 was written for machines of the BÉSM-4 class, which to a large measure ensures compatability with the input language of BÉSM-4, BÉSM-6, and CDC-6200 machines. Apparatus is being developed for visual communication with a computer. Graphical displays were made on a cathode-ray storage tube with a grid potential carrier. Construction was begun on small computer displays developed at the Institute. A mathematical check of the display stations is being made.

The tuning of the "Spiral Meter" scanning system was finished and the massive processing of the pictures from the meter hydrogen bubble chamber was begun. The pictures from the track chambers were processed on the HPD and AÉLT-1 automatic machines also. The system of coupling the semiautomatic PUOS and BÉSM-4 was extended; ES-5012 magnetic recorders attached to them tripled the rate of recording and reproducing information. The standard magnetic tape memory units were introduced into the AÉLT-1 and BÉSM-4 system also. The design of the universal BPS-3U-M2 scanning—measuring table was completed; the technical documents have been transmitted to the factory for production according to statements of the physics institutes.

The development of mathematical programs for experimental installations operating on-line with computers was continued. Programs were written for "Photon" and "Alpha" which are devices operating on beams of the synchrophasotron, and the BIS-2 and the equipment for seeking new particles and nuclei used in experiments at the Serpukhov accelerator. The system of programs for processing the bubble chamber pictures on the BÉSM-6 was extended by new more efficient programs. Programs have been written for processing pictures from the five-meter spark chamber spectrometer and the two-meter streamer chamber.

In studying methods for applied calculations, criteria have been developed for the global convergence of a continuous analog of Newton's method, and the application of this method to the Sturm—Liouville problem has been justified. The influence of nonlinear effects on the radiation instability of relativistic electron rings in a collective accelerator has been investigated.

The SILUND electron accelerator has been put into experimental operation in the Division of New Methods of Acceleration. This is part of a system for accelerating heavy ions. V. P. Sarantsev spoke of this work. A fifth accelerating section was constructed to increase the particle energy. The accelerator tubes were reconstructed, the focusing magnetic field was corrected, and the currents of the accelerator pulse system were stabilized and checked. The test system permits the measurement of 32 electrical parameters of the accelerator. SILUND furnishes a beam with energies of 2 MeV, a current of 600 A, and a pulse duration of 15 nsec.

A four-step pulse system was constructed for forming the magnetic field in the adherer. It ensures the necessary field during the whole ring compression cycle. Pulsed jets of nitrogen and xenon ~30 μsec in duration have been obtained with the mock-up of the gas dynamic gun. An arrangement was developed for determining the basic parameters of the beam in the adherer, operating on-line with an M-6000 computer. The assembly of the measuring center equipment based on an M-6000 with a 32K word working memory has been completed. This was used to make magnetic and beam measurements in the heavy ion accelerator. The complex tuning of this accelerator with a beam was begun.

Systems of high-energy proton collective accelerators were studied in order to prepare a sketchy technical plan for such an accelerator. The "Kol'tsetron," a model of the basic system of the accelerator was started up several times. The main solenoid was tested under operating conditions. The results of the magnetic measurements of the field of the main solenoid and the gradients of the coil showed that the magnetic field can be shaped to the prescribed accuracy.

Specialized sections of the Academic Council have been functioning successfully at JINR. A vice-director of the Institute, K. Lanius, spoke of the work of the section of high-energy physics, vice-director Ch. Shimane spoke on the work of the section on low-energy physics, and D. I. Blokhintsev on the work of the section on theoretical physics. These sections discussed reports on the progress of research in the laboratories and research plans for next year.

K. Lanius reported on international cooperation and the development of scientific relations of the Institute. In the past year the JINR laboratories cooperated with scientific research organizations of the JINR member countries on 160 subjects. Almost 900 foreign specialists arrived at Dubna to perform such work and to solve other problems. More than 400 Institute research workers took part in conferences and joint projects in JINR member countries. 17 scientific conferences and 21 scientific organization conferences were conducted. JINR scientists took part in 84 international and national conferences, symposia, seminars etc. The 1975 plan provides for the participation of Institute research workers in 56 conferences. The Joint Institute will organize seven symposia and seminars, three schools, and 15 working and other conferences. The most important of these will be the International School of JINR and CERN Physicists in Alushta, the School of the Physics of Heavy Ions at Dubna, the Eighth International Symposium on Nuclear Electronics at Dubna, and the Fifth International Symposium on High-Energy Physics and the Physics of Elementary Particles in Warsaw.

There was a detailed discussion of the JINR Five-Year Plan (1976-1980) in connection with the paper presented by the Institute Director N. N. Bogolyubov.

The Acadamic Council chose the following laboratory directors for the new four year period: V. P. Dzhelepov (Laboratory of Nuclear Problems), G. N. Flërov (Laboratory of Nuclear Reactions), and I. M. Frank (Laboratory of Neutron Physics).

THE EUROPEAN CONFERENCE ON THE EFFECT OF RADIATION ON MATERIALS FOR FUEL ELEMENT CLADDING AND CORES

Yu. N. Sokurskii

On December 3 to 5, 1974, a European conference took place in Karlsruhe (Federal German Republic), devoted to the behavior of materials for fuel element cladding and cores under irradiation. It was organized by the Nuclear-Technical Society of Atomforum of the Federal German Republic and the British Atomic Energy Authority. About 200 representatives from 24 countries participated in the work of the conference.

Reports and communications were presented (more than 50 reports) on the following principal trend: radiation swelling after irradiation by heavy ions and electrons; radiation swelling during reactor irradiation; structural and phase stability of materials under irradiation; mechanical properties during testing in a reactor. The reports mainly considered the materials used for cladding of fuel elements, assemblies and structural cores of nuclear reactors, and also materials which it is proposed to use for these purposes.

Approximately one-half of the reports presented at the conference was devoted to the problem of radiation swelling. It was shown that the accelerated formation of defects in materials by irradiation with heavy ions and electrons with high energies (1 MeV) allowed a comparison to be made of the resistance of a number of structural materials in relation to radiation swelling.

Data were discussed also concerning the swelling as a result of neutron irradiation of austenitic steels M316, FV-548, 1.4970; 1.4981; 1.4988, Nimonic RE-16, etc. Swelling of claddings and samples of various austenitic steels were compared as a function of the type of thermomechanical processing. Some reports were concerned with the effects of swelling on the composition of the alloys, impurities, in particular carbon, and the irradiation conditions.

In the reports devoted to structural (phase) stability of alloys under irradiation, attention was paid to the fact that under the action of irradiation, because of the high concentration of defects, metastable states are formed which differ strongly from the equilibrium states. The theory of the phenomenon is discussed and experimental data are given about the dissolution and precipitation under irradiation of the γ-phase in Inconel 625 and in Nimonic RE-16.

In the investigations of the mechanical properties under irradiation, particular attention was paid to radiation creep. Austenitic steels and Nimonic RE-16, stabilized with niobium, were studied over the range 250-450°C, i.e., in the absence of thermal creep. The opinion was expressed that radiation creep may be one of the principal factors which limits the time of operation of fuel element bundles in fast reactors. A number of reports was devoted to the effect of irradiation on the creep of zirconium alloys.

In several reports, data were presented on the change of tensile and plastic properties of certain austenitic steels, hasteloya-X and other materials after irradiation. The majority of authors associate the reduction of elongation at elevated temperatures with the effect of helium formed in the materials by the action of irradiation.

At the conclusion of the conference, the Soviet delegation was afforded the possibility of becoming acquainted with the laboratories of a number of Institutes of the Center for Nuclear Research in Karlsruhe.

Translated from Atomnaya Énergiya, Vol. 39, No. 1, p. 77, July, 1975.

SEMINAR ON THE USE OF THERMAL NUCLEAR REACTORS IN FERROUS METALLURGY

E. F. Ratnikov

A seminar on the use of thermal nuclear reactors in high-temperature processes in ferrous metallurgy was held in Sverdlovsk on February 15, 1975. It was sponsored by the Section of Atomic Power Engineering of the Sverdlovsk Regional Society of Power Engineers and the power engineering industry. The seminar was held at the S. M. Kirov Ural Polytechnical Institute. The seminar was attended by representatives of scientific-research and educational institutions of the Sverdlovsk and Beloretsk nuclear power installations.

V. V. Mikhailov presented a report on several technological processes of ferrous metallurgy using thermal nuclear reactors. E. F. Ratnikov discussed nuclear power engineering for metallurgical production. Interest is increasing in the use of thermal nuclear reactors in high-temperature processes of ferrous metallurgy. Stimulating factors are the increasingly scarce (and also costly) fossil fuels presently used in ferrous metallurgy (coking coals, natural gas), atmospheric pollution in the vicinity of metallurgical plants, the advances in high-temperature gas-cooled nuclear reactors, and the possibility of lowering the cost per ton of steel by use of thermal nuclear reactors.

Metallurgists B. I. Kitaev, S. G. Bratchikov, and Yu. G. Yaroshenko discussed the logical use of thermal nuclear reactors for heating and coking of coals, heating of blast furnaces, methods of obtaining sponge iron with use of carbon monoxide and hydrogen as reducing agents, and also high-temperature heat exchangers. Power engineers A. P. Baskakov, A. G. Sheinkman, et al. reported achievements in the development and operation of high-temperature nuclear reactors. The costs per unit heat and per ton of steel in using nuclear power engineering in metallurgical plants with a capacity of five million tons of steel per year were discussed (with thermal power of 2500 MW and electrical power of 300 MW).

Those attending the seminar recommended that a council be created to consider the use of thermal nuclear reactors in ferrous metallurgy, with participation of leading power engineers and economists of the Ural Scientific Center of the Academy of Sciences USSR, the Ural Polytechnical Institute, and other scientific-research and planning organizations in Sverdlovsk.

Translated from Atomnaya Énergiya, Vol. 39, No. 1, pp. 77-78, July, 1975.

SELF-CONTAINED RADIOISOTOPE POWER UNITS FOR NAVIGATION EQUIPMENT SYSTEMS

Yu. B. Flekel', B. S. Sukov,
and A. I. Ragozinskii

A wide network of automatic radio- and light-beacons extends over the sea routes and coasts of the Soviet Union. Information obtained from these systems is the basis for navigation safety.

At present, diesel- and wind-electric plants charging accumulator batteries or batteries of dry galvanic elements are used as sources for the beacons and signal lights. The drawbacks of these electric power sources are due mainly to the necessity for their constant servicing, small operating resources, low reliability and dependence on climatic conditions.

The most promising sources of power for automatic navigation systems are radioisotope power units which are being developed both in the USSR and abroad [1]. The All-Union Scientific Research Institute of Radiation Technology, together with specialized organizations, have developed several modifications of radioisotope power units for automatic radio- and light-beacons and illuminated navigation signs. In 1970, the "Granit-1" experimental radioisotope power unit was brought into operation in the Kronstadt beacon, made on the basis of a radioisotope thermoelectrical generator with a power of 8-10 W at a potential of 14 V. The radioactive isotope Cs-137 is used in the generator. In conjunction with a buffer accumulator battery, the generator has provided round-the-clock operation of the beacon in a pulsed cycle. Operation of the radioisotope power unit has enabled several principles, fixed during its development, to be verified: the feasibility of long term operation of accumulator batteries under conditions of continuous recharging with low currents, the stability of the generator—storage element system over a wide range of temperatures, etc.

In 1969-1974, the "Éfir" radioisotope power unit was brought into operation, supplying electric power to type ANRM-1 radiobeacons with a range of operation of 100 miles [2]. The "Ēfir" radioisotope power unit was manufactured on the basis of a generator with an electric power of 30 W at output voltages of 12 and 32 V. Sr-90 is used in the generator. "Éfir"-type units are located on the coast and islands of the Arctic Ocean and provide reliable navigation on the most important sections of the Northern sea route in severe climatic conditions.

In 1973-1974, "Granit-2" and "Granit-3"-type radioisotope power units were installed, developed on the basis of the series-produced "Beta-S" radioisotope generator with Sr-90 (electric power output 10 W and potential 6 V). They feed signal lights located in the most dangerous places of the Barents and Okhotsk seas and the Sea of Japan.

In June 1974, a radioisotope power unit was brought into operation in one of the most important beacons in the Baltic Sea, "Tallin," and consisted of two radioisotope thermoelectric generators with an electric power of 60 W at a potential of 40 V, provided with an electric power storage system and voltage converters. The radioisotope power unit of the Tallin beacon has four output channels for supplying the navigation equipment, which consists of a light beacon with a power of 250 W at a supply voltage of 34 V, operating up to 19 h per day with an off-duty factor of 6; a radiobeacon, with a power of 11 W at a supply voltage of 12.6 V, operating round-the-clock with an off-duty factor of 4; an automatic unit with an average round-the-clock requirement of ~2 W at 12.6 V; remote control systems and navigation equipment monitoring systems with an average round-the-clock requirement of ~5 W at a potential of 24 V.

Translated from Atomnaya Énergiya, Vol. 39, No. 1, pp. 78-79, July, 1975.

The radioactive isotope Sr-90 is used in the generators. The combination of an isotope with a long half-life and low temperature thermoelectric converters based on ternary alloys of bismuth—tellurium—antimony and selenium allows a long-term duty (up to 10 years) of the radioisotope power unit. The generator is provided with a system for regulating the thermal current reaching the thermoelectric converter, which enables the efficiency of the generator to be increased because of optimization of the operating conditions of the thermoelectric converter, and enables the output parameters of the generator to be maintained constant during operation.

The radioisotope "fuel" with an activity of 240,000 Ci is enclosed in three hermetically-sealed ampoules which, together with the combined radiation shielding of alloys of depleted uranium and tungsten, form the thermal unit. It is mounted in the casing by means of a cylindrical sheath. A gas-screened thermal insulator with a xenon filling is used in the generator and this ensures a generator thermal efficiency of more than 0.85. The radiation shielding of the generator reduces the γ-radiation exposed dose intensity to 10 mR/h at 1 m, which allows transportation, assembly and operation of the generator without special limitations.

The electric power storage element, operating under buffer conditions, is manufactured on the basis of nickel—cadmium accumulators of the NKG-30S type and consists of four (according to the number of consumer channels required) batteries. It is provided with a special electronic device which protects the accumulators from both over-discharging and overcharging. In order to ensure the necessary operating temperatures of the accumulators over a wide range of temperature variation of the ambient air, the storage element is installed in a thermostatically controlled jacket.

The voltage converters installed in the radioisotope power unit match the output voltage of the generators (40 V) with the consumer channel feed voltage. They are made in semiconductor elements according to a push-pull circuit with a switching transformer.

The experience of operating radioisotope power units has shown the long-term prospects for their application to power systems for navigation facilities and for various self-contained systems intended for long-term operation without servicing. In the near future, tens of these systems with radioisotope power units will be installed in various regions of the Soviet Union.

LITERATURE CITED

1. G. M. Fradkin and V. M. Kodyukov, At. Énerg., 26, No. 2, 169 (1969).
2. G. M. Fradkin, A. I. Ragozinskii, and A. I. Dmitriev, At. Énerg.; 28, No. 4, 367 (1970).
3. G. M. Fradkin et al., Fourth Geneva Conference, Report No. 721 [in Russian] (1971).

TOR-3 REFLECTING GAMMA THICKNESS GAGE

P. G. Lakhmanov, Yu. A. Skoblo,
and V. B. Timofeev

The TOR-3 reflecting gamma thickness gage (see Fig. 1) has been developed at the All-Union Scientific-Research Institute of Radiation Technology to measure the thickness of carbon steel plates. The instrument can be used for measuring the wall thickness of carbon steel pipe and also plates and wall thicknesses of other materials after recalibration. It can also be used to determine the level of liquids and dry materials in various containers.

The operating principle and block diagram are the same as those of the TOR-1 instrument. The basic characteristics of the TOR-3 instrument are as follows:

Range of thickness measured, mm (steel)	0.5-16
Basic error in measurements on plates	
0.5-3 mm thick	not over 0.15 mm
3.0-16.0 mm thick	not over 4.0%
Measuring time, sec	not over 60
Operating temperature, °C	−30 to +50
Operating time per battery, h	at least 50
Weight, kg	not over 5

The instrument was designed to be compatible with the TOR-1 instrument.

The duty factor of the new instrument exceeds 60%. The TOR-3 is superior not only to the TOR-1 but also to foreign instruments of the same type.

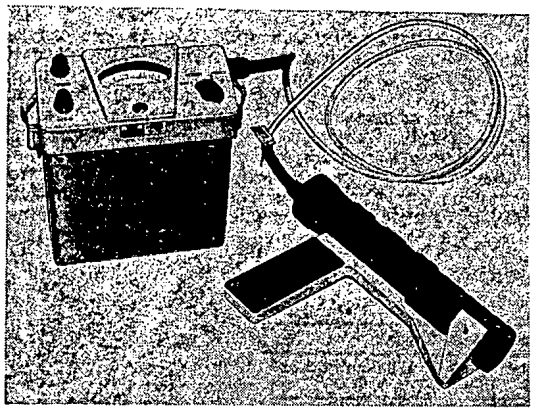

Fig. 1. TOR-3 reflecting gamma thickness gage.

Translated from Atomnaya Energiya, Vol. 39, No. 1, p. 79, July, 1975.

S. M. Gorodinskii and D. S. Gol'dshtein

DECONTAMINATION OF POLYMER MATERIALS*

Reviewed by É. Ê. Finkel'

One of the first tasks in the overall complex of problems of the radiation safety of the personnel of laboratories and industrial plants relates to the decontamination of polymer materials. They have acquired a wide range of application as protective coverings for building structures and plants in nuclear power and radioisotope technology and also as elements of individual protective agents.

The publication of the monograph "Decontamination of Polymer Materials," written by well-known specialists in the field of radiation hygiene, S. M. Gorodinskii and D. S. Gol'dshtein, is extremely opportune.

Despite the comparatively small bulk, a wide range of problems is covered in the book, including current theoretical representations and practical recommendations.

In the first chapter, general data are systematized on the sources of surface contamination and the means of individual protection against radioactive substances. Together with a description of the principal sources of radioactive contamination, associated with the operation of nuclear reactors, reprocessing of nuclear fuel, the production and application of natural and artificial radioactive isotopes, the Soviet scientists reveal the important role of a surface contaminated with radioactive substances as an additional source for the entry of radioactive substances into the air of rooms. Unfortunately, the authors have evaded with silence the industrial and combined laboratory radiation-chemical facilities, which differ in defined special properties.

In the second chapter, the principal characteristics of adhesion and sorption of radioactive contamination by polymer materials are given and the effect of the chemical structure of the chain and the state of the surface of the polymers on the strength of fixation of the radioactive contamination is analyzed briefly. The discussion is of a descriptive nature, intelligible for a wide circle of specialists of different cross-section, but simplifies somewhat this important theoretical material.

The principal material of the monograph is considered in four chapters (3 to 7).

The third chapter is devoted to the basic principles of decontamination of polymer materials. Together with an account of the permissible levels of radioactive contamination, the authors introduce a suitable classification of decontamination methods, formulate the general requirements on decontaminating solutions, by specific examples show the role of the principal components of the decontaminating solutions and also make recommendations on the choice of an efficient decontamination cycle. The possibilities are considered for the preliminary treatment of the surface for the purposes of facilitating subsequent decontamination and the necessity is emphasized for the complex solution of the problem of selection and optimization of the method of decontaminating polymer materials, as not one of the existing methods is an all-purpose method.

The fourth chapter is devoted to estimating the "decontaminability" of polymer materials. Based on the analysis of foreign and Soviet publications, the authors show every complexity of founding a methodical approach to this problem, taking into account the dependence of the sorption—desorption properties of the radioactive isotopes of various elements on the structure and composition of the polymer material. By drawing on extensive experimental data, the authors have stated the principal results of investigation of the decontaminability of polymer materials and the development of easy decontaminating formulas. They have

*Atomizdat, Moscow, 1975.

Translated from Atomnaya Énergiya, Vol. 39, No. 1, p. 80, July, 1975.

paid great attention to the effect of a mixture of tributyl phosphate with kerosene, widely used in extraction methods of nuclear fuel reprocessing, on the decontaminability of polymer materials.

The fifth chapter is of considerable interest and great practical value and is devoted to a consideration of the specific characteristics of the removal of different radioactive elements from polymer materials. Vast experimental data on the decontamination of polymer substances contaminated with radioactive products of the fission of uranium, activation products of the corrosion of structural elements of nuclear reactors, and contaminated also by α-emitters, are classified in this chapter. A comparison is given of the efficiency of removal of various contaminants, on the basis of which is introduced a 4-group classification, depending on the difficulty of removal, and also the efficiency of simple and complex decontaminating solutions is assessed.

In the sixth and seventh chapters, recommendations are made for the decontamination of protective coverings and means of individual protection where, for each method, the sphere of application, advantages and disadvantages are recounted.

The last and eighth chapter is devoted to an account of the principal requirements of safety techniques for the decontamination of protective coverings and means of individual protection.

It should be emphasized that the range of problems covered, the level of explanation and the practical value of the actual data of the monograph has no equal and is the first publication of this type; it can be used for familiarization with the essence of a problem and for obtaining reference data. The book will be useful for a wide circle of specialists — researchers, technologists, designers and operators, for whom problems of decontamination and radiation safety are of first-degree importance.

The Plenum/China Program

Research in the medical, life, environmental, chemical, physical, and geological sciences from the People's Republic of China

The 15 major scientific journals published in China since the Cultural Revolution are being made available by Plenum in authoritative, cover-to-cover English translations under the Plenum/China Program imprint.

These important journals contain papers prepared by China's leading scholars and present original research from prestigious Chinese institutes and universities. Their editorial boards are affiliated with such organizations as the Chinese Chemical Society, the Academia Sinica in Peking and its Institutes, and the Chinese Microbiological Society.

The English editions are prepared by scientists and researchers, and all translations are reviewed by experts in each field.

Journal Title	No. of Issues	Subscription Price
Acta Astronomica Sinica	2	$65
Acta Botanica Sinica	4	$95
Acta Entomologica Sinica	4	$95
Acta Genetica Sinica	2	$65
Acta Geologica Sinica	2	$75
Acta Geophysica Sinica	4	$95
Acta Mathematica Sinica	4	$75
Acta Microbiologica Sinica	2	$55
Acta Phytotaxonomica Sinica	4	$125
Acta Zoologica Sinica	4	$125
Geochimica	4	$110
Huaxue Tongbao — Chemical Bulletin	6	$95
Kexue Tongbao — Science Bulletin	12	$175
Scientia Geologica Sinica	4	$125
Vertebrata PalAsiatica	4	$95

For further information, please contact the Publishers.

SEND FOR YOUR FREE EXAMINATION COPIES

plenum

PLENUM PUBLISHING CORPORATION
227 West 17 Street, New York, N.Y. 10011
In United Kingdom 8 Scrubs Lane, Harlesden, London, NW10 6SE, England

Declassified and Approved For Release 2013/09/24 : CIA-RDP10-02196R000400060001-4